5-2023

Synaptic properties of parabigeminal circuits.

Kyle Whyland
University of Louisville

SYNAPTIC PROPERTIES OF PARABIGEMINAL CIRCUITS

By Kyle Whyland

B.S., Indiana University, 2013

M.S., University of Louisville, 2018

A Dissertation

Submitted to the Faculty of the

School of Medicine

In Partial Fulfillment of the Requirements

For the Degree of

Doctor of Philosophy

in Anatomical Science and Neurobiology

Department of Anatomical Science and Neurobiology

University of Louisville

Louisville, KY

May 2023

SYNAPTIC PROPERTIES OF PARABIGEMINAL CIRCUITS

By

Kyle Whyland

B.S., Indiana University, 2013

M.S., University of Louisville, 2018

A Dissertation Approved on

February 16, 2023

by the following Dissertation Committee:

_____

Dr. Martha Bickford

_____

Dr. William Guido

_____

Dr. Aaron McGee

_____

Dr. David Magnuson

_____

Dr. Bart Borghuis

ABSTRACT

SYNAPTIC PROPERTIES OF PARABIMEINAL CIRCUITS

Kyle L. Whyland

February 16, 2023

Subcortical structures of the visual system have been the subject of intense study in recent years, but there remain some important unanswered questions regarding the synaptic relationships linking the nuclei that comprise this important sensory network within the brain. In these studies, we use several modern and traditional approaches, including viral tract tracing, *in vitro* slice physiology, immunohistochemistry, optogenetics, and electron microscopy to characterize the circuits linking the superior colliculus (SC), parabigeminal nucleus (PBG), and lateral geniculate nucleus (LGN), with particular focus on GABAergic and cholinergic cell types. We found that the SC, an important visuomotor structure with connections to the LGN, PBG, pretectum, and pulvinar nucleus (among others), hosts a large and diverse population of GABAergic neurons that is composed primarily of interneurons labeled in the GAD67-GFP reporter mouse. Among these GABAergic cells residing within stratum griseum superficiale (SGS) of the SC, we found that GABAergic projection cells targeting the PBG exhibit unique characteristics, distinguishing them from other GABAergic projection populations as well as parvalbumin positive SC-PBG cells

that exert opposing effects on postsynaptic cells in the PBG. Utilizing optogenetics in conjunction with whole-cell patch-clamp slice physiology, we additionally demonstrate a high degree of convergence between these opposing tectal inputs onto PBG neurons. Our electron microscopy experiments and light-level immunohistochemistry in GAD67 reporter mice also revealed a previously unidentified extra-tectal souce of GABAergic input to the PBG, where these inhibitory synapses were observed to account for almost half of its inputs. Finally, using MATH5$^{-/-}$ mutant mice that lack retinofugal projections, we identify the largely cholinergic inputs from the PBG as the likely source of “retinal replacement terminals” observed in the LGN in previous studies utilizing animal models of retinofugal input loss.

TABLE OF CONTENTS

PAGE

ABSTRACT……..iii

LIST OF FIGURES……vi

CHAPTER I……1

CHAPTER II……...13

Methods……...15

Results……23

Discussion……...30

CHAPTER III……...49

Methods……52

Results……..62

Discussion……72

CHAPTER IV……91

Methods……93

Results……..99

Discussion……105

CHAPTER V……122

REFERENCES……129

CURRICULUM VITA……..143

LIST OF FIGURES

FIGURE PAGE

1.1……10
1.2……11
1.3……12
2.1……38
2.2……39
2.3……40
2.4……41
2.5……43
2.6……44
2.7……45
2.8……46
2.9……48
3.1……80
3.2……82
3.3……84
3.4……86
3.5……88
3.6……89
4.1……111
4.2……112
4.3……113
4.4……114
4.5……116
4.6……117

4.7……118
4.8……119
4.9……120
4.10……121
5.1……126
5.2……127
5.3……128

CHAPTER I: INTRODUCTION

The inner workings of the human brain have long mystified scientists and philosophers alike, but recent advances in biology and technology have fostered a new understanding of this bewilderingly complex organ that has both enlightened and further intrigued investigators. Although we typically think of consciousness and cognition when contemplating our brains' role in our lives, much of its processing resources are devoted to the coordination of two mostly involuntary functions that can feel elementary but are often far more complex in their execution: sensation and movement. An organism has little chance of survival if it cannot quickly make sense of its environment and move or respond accordingly. These processes and how they are coordinated with one another is a great place to begin to unravel the mysteries of our nervous system for two reasons: 1) these functions are common to almost all organisms with a nervous system, providing a model that might reveal the fundamental organizing principles of the brain 2) sensorimotor functions have measurable inputs and outputs, especially visuomotor systems, usually making the interpretation of their empirical study more straightforward.

With these ideas in mind, it is no surprise that sensory systems have become the subject of intense study for neuroscientists in recent decades. Th superior colliculus (SC), or optic tectum in non-mammals, is one such sensorimotor structure that receives the majority of the retinas' output via the optic tract (Ellis et al., 2016; Hofbauer & Dräger, 1985; Linden & Perry, 1983; Vaney et al., 1981). Interestingly, although the SC receives the bulk of the retina's afferents, it is not thought to be involved in visual perception itself like its thalamic counterpart, the dorsal lateral geniculate nucleus (dLGN). It turns out, there's a lot more to "seeing" than just our perception of an image itself. The SC is organized in such a way as to coordinate and execute critical motor responses to salient visual stimuli. The SC is a laminar structure; its superficial layers receive inputs from the retina as well as higher-order visual structures while its deep layers have both inputs from higher-order motor areas as well as outputs to premotor nuclei (Basso et al., 2021; Ellis et al., 2016; Masullo et al., 2019; Sahibzada et al., 1986). Making matters more complex, the SC's visual layers have their own projections to several brainstem and thalamic structures, including the ventral lateral geniculate nucleus (vLGN), dLGN, pulvinar nucleus, pretectum, and parabigeminal nucleus (PBG), among others. Some of these output targets, like the pulvinar nucleus and dLGN, transmit their signals to the visual cortex (V1), which in turn sends feedback projections to the visual layers of the SC. This is just one example of how complex circuit loops are formed by the nuclei comprising the visual system. Perhaps inconveniently for researchers but adaptive for organisms, the myriad of structures involved in visuomotor

processing allows for contextual modulation of sensory signals and their associated motor responses that would be more difficult to achieve in a more segregated, linear system. Key to the nervous system's adaptability is a certain level of both seeming redundancy and surprising plasticity.

To parse a complex visual environment more efficiently, especially for visually inclined organisms like primates and birds, neurons throughout the visual system, from the retina to the cortex had to assume morphologies that made them more adaptive to the processing demands of the visual world. The SC hosts a diverse population of neurons that developed very specific morphologies and physiology to fulfill their respective roles in sensorimotor processing. Neurons in the SC's superficial layers show varying degrees of direction selectivity as well as motion contrast enhancement; that is, they are sensitive to motion in particular directions and their activity is often boosted by motion opposite to their preferred direction in areas that surround their receptive fields (Barchini et al., 2018). This motion contrast enhancement is thought to help organisms better comprehend relative motion, or put another way, to distinguish focal (moving in the scene) from global (moving through the scene) motion. Additionally, neurons sensitive to specific types of moving stimuli, like wide field vertical cells (which are sensitive to looming and sweeping stimuli) are also found in the SC's visual laminae (Gale & Murphy, 2014, 2016). These stimuli are particularly salient to many organisms because they often signal the presence of predators or prey.

The retinal inputs to these specialized cell populations within the SC create a topographic representation of the visual space in the SC, where the spatial relationship between retinal ganglion cells that tile the retina is preserved by the spatial organization of their efferent synapses in the SC (Chandrasekaran et al., 2005; Sparks & Mays, 1980). Often in order for neurons to develop their particular receptive field properties, it is not enough for them to simply adopt a specific dendritic morphology to sample their retinal afferents in a way that biases their responses to a particular portion of the visual space or the orientation of a stimulus within it. Neurons frequently need inhibitory partners to facilitate the development of more specific or complex receptive field properties. It is thought that the large and diverse population of GABAergic neurons within the SC's superficial layers exist in part for this reason. GABAergic neurons with horizontal morphology are believed to be partially responsible for the unique receptive field properties of the wide field vertical cell for example (Gale & Murphy, 2014, 2016). These horizontal cells have receptive field properties opposite to those of the wide field vertical cell, further pushing their partner populations' preferred stimulus towards a particular set of characteristics through inhibition (Gale & Murphy, 2014, 2016). Other neurons' signals are sculpted by GABAergic neurons in a temporal fashion via the feedforward inhibitory circuits that narrow the window in which a neuron can be maximally excited (del Bene et al., 2010; Kardamakis et al., 2015)

Most of the GABAergic neurons of the SC are thought to be interneurons, or neurons that form synapses locally or within the SC rather that send axon

projections to make efferent synapses in other nuclei. However, extrinsic or projection cells form a significant subpopulation of GABAergic SC neurons and their axons project to many of the same targets as their excitatory counterparts residing in the same layers of the SC (Whyland et al., 2020). In the first data chapter, I used transgenic mice as well as viral and traditional tracers to better characterize the genetic and/or morphological subpopulations that comprise the GABAergic neurons of the SC and how those subpopulations are organized into specific interneuron and projection neuron classes depending on their specific features. Of particular interest in this chapter is how the expression of specific genes might correspond to whether GABAergic cells function as local interneurons or as projection cells with specific targets. We found that neurons expressing the 67 kilodalton isoform of glutamic acid decarboxylase (GAD67) comprise a large percentage of the GABAergic cells in the superficial layers of the SC and additionally that they function strictly as interneurons within this structure.

Expression of the calcium-binding protein, parvalbumin (PV), has been used to identify specific populations of neurons in several parts of the brain, including fast-spiking interneurons in the visual cortex for example (Helm et al., 2013; Runyan et al., 2010; Rupert & Shea, 2022). My own studies of parvalbumin-expressing SC cells indicate that they comprise subsets of both the GABAergic and nonGABAergic cells of the SC's visual layers, but interestingly the GABAergic projection cells that target the parabigeminal nucleus (PBG) never express parvalbumin while a significant proportion of excitatory SC-PBG

projection neurons do. What is it about the parvalbumin cell population of the SC that necessitates their segregation from the GABAergic SC-PBG projection cells? Do the PV+ SC-PBG neurons and their GABAergic counterparts form parallel pathways for visual signals to the PBG that might help the SC-PBG fulfill a specific visuomotor function? Answering these questions surrounding the relationship between the SC and PBG as it relates to the specific neuronal populations linking the two structures could provide a model circuit for understanding how visuomotor functions are integrated, processed, and ultimately coordinated. In the second data chapter, I utilized viral tract tracing as well optogenetics and electron microscopy to better characterize the synaptic relationship between SC-PBG projection cell populations and their partners residing in the PBG itself.

The PBG is small structure on the lateral wall of the midbrain that is thought to receive virtually all its input from the SC (Sherk, 1979b). PBG neurons are visually responsive like their tectal synaptic partners, and similarly are sensitive to visual motion(Sherk, 1978, 1979a). Interestingly, the PBG has some of the same projection targets as the SC, including the dLGN, pulvinar, and the SC. The PBG feedback projections to the SC are thought to be particularly important to homologous structures in avian species, the nucleus isthmi (NI) and optic tectum (OT), as they form a competitive inhibitory stimulus selection network that coordinates visuomotor responses across hemispheres of the brain (Asadollahi et al., 2010, 2011; Goddard et al., 2014; Mysore & Knudsen, 2013). The PBG is one of several cholinergic brainstem structures including the

pedunculopontine tegmentum (PPTg) and the laterodorsal tegmentum (LDTg) that send projections to the thalamus. However, as I showed in studies included in Sokahaze et al 2022, unlike the PPT and LDT, PBG cells express choline acetyltransferase (ChAT) but not the vesicular acetycholine transporter (VAChT), or brain nitric oxide synthase (BNOS, Figure 1.1). In the SC, inputs from the cholinergic neurons of the brainstem target different lamina. PBG projections innervate the superficial layers while PPT/LDT neurons target the deeper layers (Figure 1.2).

Many of the PBG's neurons that are positive for ChAT expression also express the glutamatergic marker vGlut2, suggesting that PBG neurons could be primarily glutamatergic and/or co-release glutamate (Deichler et al., 2020). Other cholinergic populations in the brainstem can transiently express vGlut2 during development but only the ChAT+ neurons of the PBG seem to express vGlut2 well into adulthood (Nasirova et al., 2020; Steinkellner et al., 2019). Cholinergic signaling from brainstem projections to the LGN excite thalamocortical relay neurons and inhibit local interneurons, boosting visual signals en route to the visual cortex in a contextual manner (Ahlsen et al., 1984; Dossi et al., 1991; Mccormick et al., 1987; McCormick & Pape, 1988; McCormick & Prince, 1986; Zhu et al., 1999; Zhu & Heggelund, 2001; Zhu & Uhlrich, 1997, 1998). Interestingly, in the mouse, the PBG sends a substantial cholinergic projection throughout the contralateral dLGN but sends to a more restricted projection to the dorsomedial shell of the ipsilateral dLGN where inputs from the SC converge (Sokhadze et al., 2022). Neurons located in these same regions of the LGN in

mice are often sensitive to stimulus direction as well as orientation, like many classes of neurons within the retina and the SC themselves (Piscopo et al., 2013; Zhao et al., 2013). Thus, cholinergic input from the PBG to the dLGN may boost or modulate signals encoding salient stimulus motion or visuomotor reflexes like eye movements in a context-dependent manner (Cui & Malpeli, 2003; Ma et al., 2013).

Given that PBG circuits might provide an alternative means for visuomotor signals through important nodes in the visual system's primary (geniculate) and secondary (tectal) pathways, plasticity in this small brainstem structure's axonal projections may provide a compensatory mechanism in circumstances in which there is a profound lesion or loss of function within the visual system. One well-documented example of some of the changes that occur when there is such a loss or deficit is observed when retinal axons fail to innervate these pathways. Retinal terminals, are known as RLPs at the ultrastructural level, as they are often observed as large profiles with round vesicles and unique, pale mitochondria (Bickford et al., 2010; Hammer et al., 2015). These profiles are very distinct so they are easily identified without any anatomical tracing or labeling. In both enucleation studies in which the eyes are removed, or genetic ablation studies where the optic tract never develops in the first place, significant anatomical changes occur to retinorecipient regions of the brain. In the dLGN, new axon terminals with features that are strikingly similar to that of the RLPs described above are observed at the ultrastructural level that have been dubbed "retinal replacement terminals" (Cullen & Kaiserman-Abramof, 1976; El-Danaf &

Huberman, 2015; Kaiserman-Abramof, 1983; Winkelmann et al., 1985). These "replacement" terminals are similar in size to retinal terminals and feature round, tightly packed vesicles but lack the characteristic pale mitochondria of RLPs. In the final data chapter, we take advantage of new viral vectors that induce the expression of horseradish peroxidase, which can be used to label profiles in electron micrographs, to compare axon terminals traced from the PBG, visual cortex, and/or retina in the dLGN of both wild-type and MATH5$^{-/-}$ mutants in which retinal ganglion cells fail to develop, to identify the source of these so-called "retinal replacement terminals". We establish that there is a significant overlap in the sizes of PBG and retinal terminals, and additionally, that cortical and tectal sources of input to the dLGN have neither the characteristics of retinal terminals nor those of PBG terminals, eliminating them as potential sources of these retinal replacement terminals. Thus, in the absence of retinal signaling, visuomotor nuclei in the brainstem and/or the secondary visual pathway could compensate for this lack of inputs by expanding their innervation of thalamocortical neurons. Put another way, many of the modulatory signaling pathways of the visual system could alternatively drive these visuomotor circuits in circumstances where there is a profound loss of function. This process could serve as a model for how sensorimotor systems can remain adaptive even through extreme deficits that might completely derail more rigid networks.

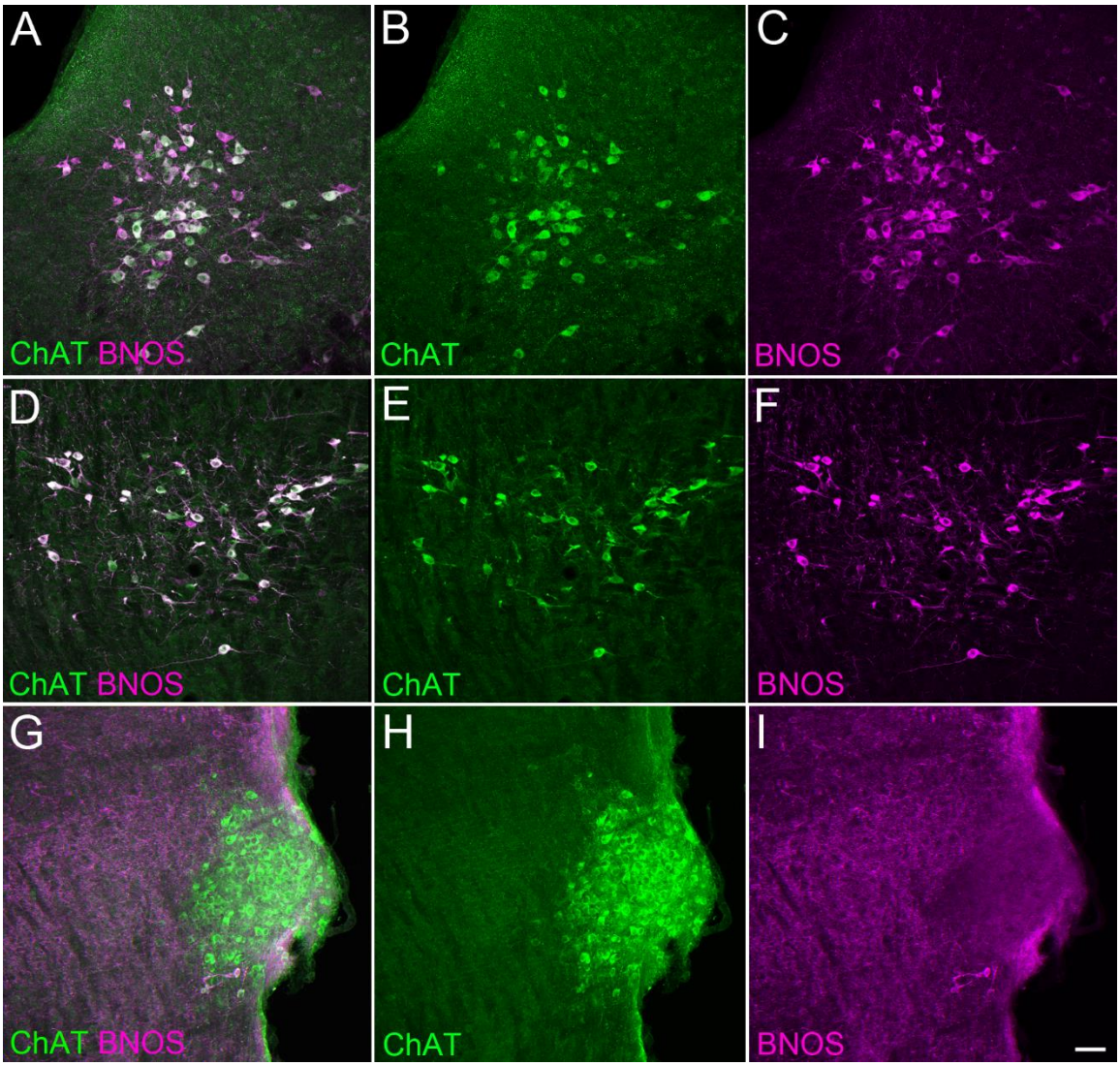

Figure 1.1. Pattern of ChAT and BNOS immunocytochemical labeling in PPTg, LDTg and PBG. Immunocytochemical labeling in coronal sections through PPTg (a–c), LDTg (d–f), and PBG (g–i) with antibodies against ChAT (green) and BNOS (magenta). Panels (a), (d), and (g) show both ChAT and BNOS channels. Panels (b), (e), and (h) depict the ChAT channel, and (c), (f), and (i) the BNOS channel. Cholinergic neurons (ChAT positive) in the PPTg and LDTg, but not PBG contain BNOS. Scale = 50 μm, from Sokhadze et al., 2022

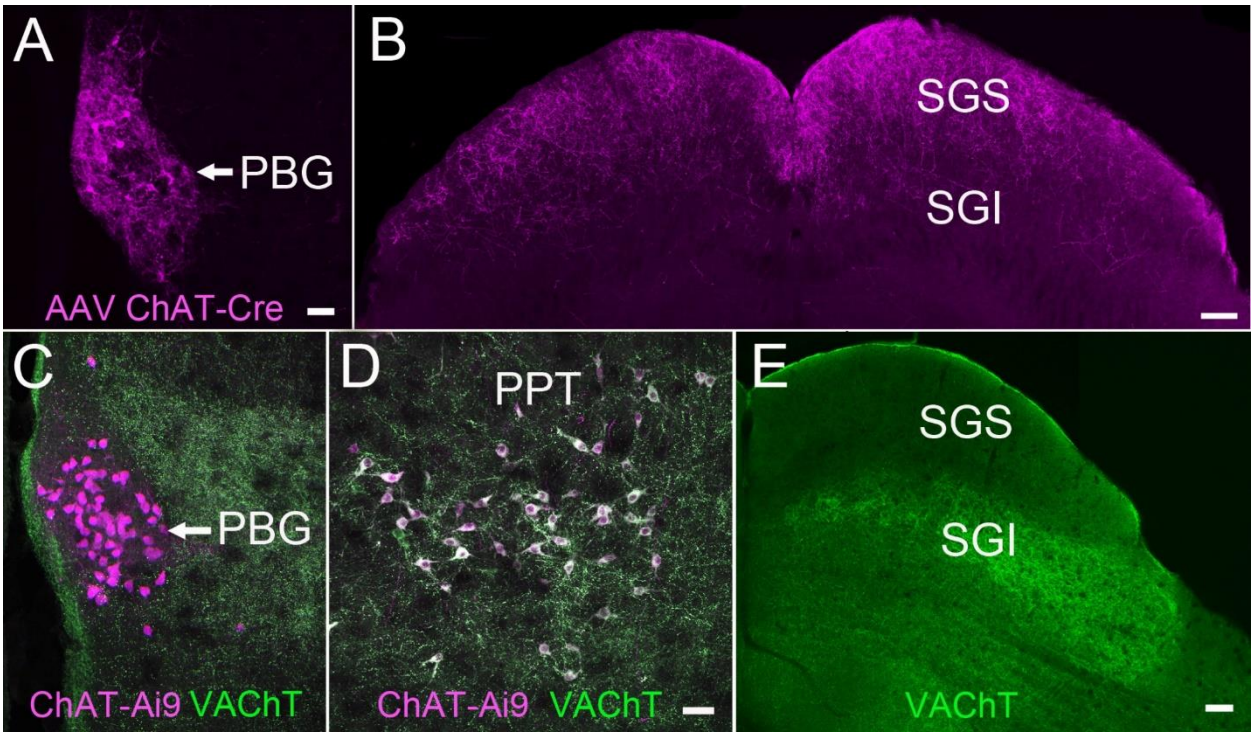

Figure 1.2. Cholinergic projections from brainstem nuclei to the SC. A) A cre-dependent viral tracer injection into the PBG of a ChAT-Cre mouse labels cholinergic neurons (magenta) throughout the nucleus that make bilateral axon projections to the SGS in (B). C) Cholinergic cells can be identified by their ChAT expression in a ChAT-Cre x Ai9 reporter mouse (magenta), but these cells do not express VAChT (green) like their counterparts in the PPT (D) that are co-labeled for ChAT (white). E) VAChT-positive fibers are seen throughout the SGI (green) but are absent from the SGS.

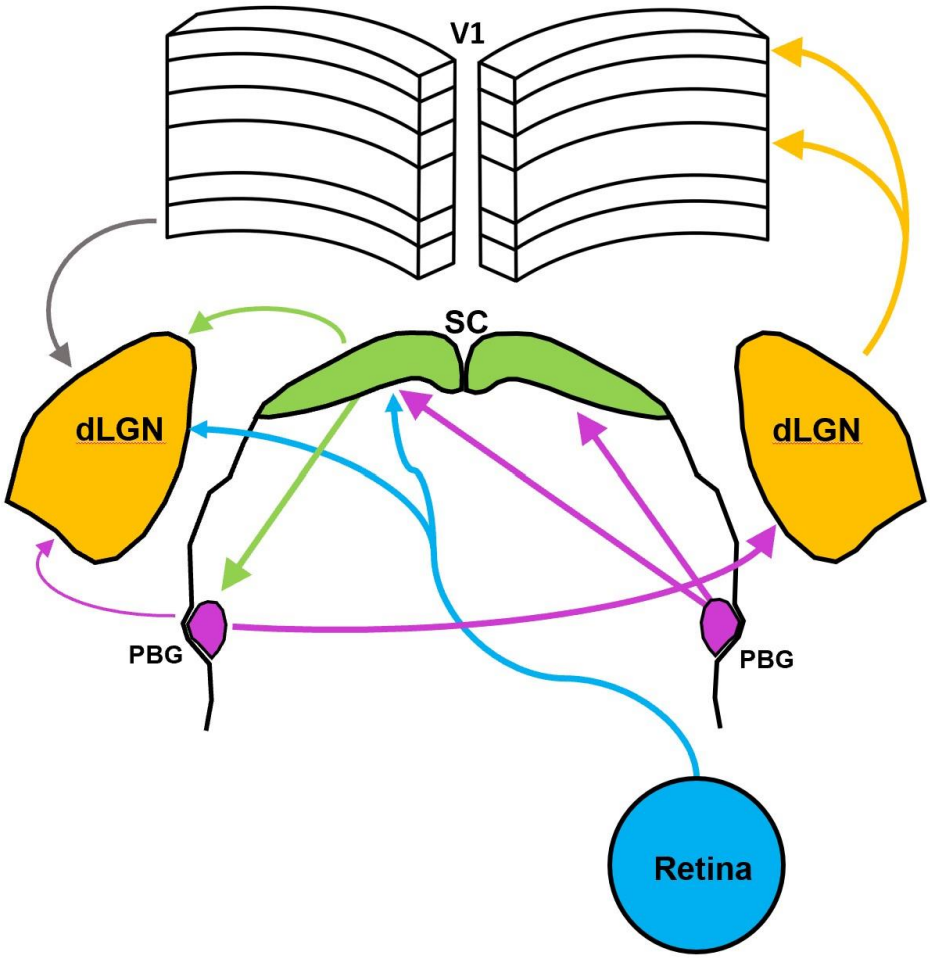

Figure 1.3. Circuits of Interest. This diagram summarizes the circuits of interest in this dissertation: The retina sends substantial axon projections (blue) through the optic tract to the SC and dLGN, with the bulk of these projections targeting the contralateral hemisphere. The dLGN (orange) receives ipsilateral inputs from the SC (green), V1 (grayscale), and PBG (magenta) as well as a larger projection from the contralateral PBG. The PBG receives input from the ipsilateral SC, but in turn provides feedback bilaterally to the SC. The dLGN sends axon projections to layers 1 and 4 of V1, but receives feedback input from layer 6.

CHAPTER II: GABAERGIC CELL TYPES IN THE SUPERFICIAL LAYERS OF THE MOUSE SUPERIOR COLLICULUS

Introduction

The superficial layers of the superior colliculus (SC) receive input from nearly every retinal ganglion cell (Ellis et al. 2016). Retinotectal axons enter the rostral SC via the stratum opticum (SO), and travel in the SO to innervate the stratum griseum superficiale (SGS) and stratum zonale (SZ) in a spatially precise, retinotopic, fashion (Xu et al. 2011). A laminar arrangement of retinotectal axons has also been noted: axons originating from specific ganglion cell types occupy different dorsal to ventral positions within the SGS (Cang et al. 2018; Triplett et al. 2014). The precision of retinotectal signaling is also highly dependent on intrinsic GABAergic circuits (Binns and Salt 1997; Kaneda and Isa 2013; Gale and Murphy 2016). The SGS contains one of the highest densities of GABAergic neurons in the brain (Mize 1992), and approximately one third of the postsynaptic targets of retinotectal terminals are GABAergic (Boka et al., 2006). A number of different GABAergic SC cell types have been described. The SC contains GABAergic projection cells that innervate the pretectum (PT), lateral geniculate nucleus (LGN) and parabigeminal nucleus (PBG; Born and Schmidt, 2007; Born and Schmidt, 2008; Gale and Murphy, 2014, 2018). In addition, a

number of different intrinsic GABAergic cell types have been described based on axon projections, orientation of dendritic arbors, grouping of synaptic vesicles within dendritic appendages or shafts, and/or the colocalization of a variety of immunocytochemical markers (Mize et al., 1982; Appell and Behan, 1990; Lane et al., 1996; Olivier et al., 2000; Behan et al., 2002; Boka et al., 2006; Gale and Murphy, 2014, 2018; Zingg et al., 2017; Villalobos et al., 2018). However, the structural and functional organization of GABAergic SC circuits is still largely unknown. The mouse provides an excellent model system to begin to unravel the complexities of SC GABAergic circuits and their relationship with synaptic terminals originating from the retina. These efforts are aided by a variety of transgenic lines that can be used to specifically label and manipulate GABAergic cell types. Most notably, a mouse line that expresses green fluorescent protein (GFP) in cells that contain the 67 kilodalton isoform of glutamic acid decarboxylase (GAD67-GFP), and a line that expresses Cre-recombinase in cells that contain GAD (GAD2-cre), have been used to isolate GABAergic cells of the SC (Gale and Murphy 2014; Gale and Murphy 2016; Masterson et al. 2019; Endo et al. 2003; Villalobos et al. 2018; Zingg et al. 2017). Such studies have revealed that GABAergic SC cells can exhibit a variety of morphologies, physiological properties, synaptic inputs and outputs, as well as the presence or absence of the calcium binding protein parvalbumin (PV). In the present study, we utilize virus and tracer injections in these 2 mouse lines, as well as immunocytochemical staining for GABA and PV, to characterize GABAergic SGS cells that project to the PT, LGN and PBG, as well as interneurons that do not

project outside the SC. In addition, we examine GABA and GAD67-containing elements of the mouse SGS using electron microscopy to further delineate the relationship between GABAergic circuits and retinotectal input.

Materials and Methods

Animals

All breeding and experimental procedures were approved by the University of Louisville Institutional Animal Care and Use Committee. Experiments were carried out using mice, of either sex, of C57BL/6J (Jax Stock No: 000664), a line in which neurons that contain glutamic acid decarboxylase (GAD) express Cre-recombinase (Jax Stock No: 010802; GAD2), or a line in which neurons that contain the 67KD isoform of GAD (GAD67) express green fluorescent protein (GFP; Jax Stock No: 007677, G42 line).

AAV injections in the SC

To label SC projections that originate from GABAergic cells, GAD2-cre mice were deeply anesthetized with a mixture of ketamine (100-150 mg/kg) and xylazine (10-15 mg/kg). The analgesic meloxicam (1-2 mg/kg) was also injected prior to surgery. The animals were then placed in a stereotaxic apparatus (Angle Two Stereotaxic, Leica, Wetzlar, Germany). An incision was made along the scalp, and a small hole was drilled in the skull overlying the SC. An adeno-associated virus (AAV) (Flex-rev-oChIEF-tdTomato (plasmid 30541, Addgene, packaged using AAV serotype 9) was injected unilaterally into the SC. Virus was delivered via a 34-gauge needle attached to a Nanofil syringe inserted in an

ultramicropump. A volume of 60 nl was injected at each of two sites at a rate of 15nl/minute. After removal of the needle, the scalp skin was sealed with tissue adhesive (n-butyl cyanoacrylate), lidocaine was applied to the wound, and the animals were placed on a heating pad until mobile. Postsurgery, animals were carefully monitored for proper wound healing, and oral meloxicam (1-2 mg/kg) was administered for 48 hours.

Cholera toxin subunit B (CTB) injections in SC projection targets

To label SC projection neurons via retrograde transport, GAD67-GFP adult mice were anesthetized as described above and placed in a stereotaxic apparatus. An incision was made along the scalp, and a small hole was drilled in the skull overlying the lateral geniculate nucleus (LGN), pretectum (PT), parabigeminal nucleus (PBG), or the ventral tegmental area (VTA). Using a Nanofil syringe and 34-gauge needle as described above for the AAV injections in SC, CTB-Alexafluor 555 was injected into each of the above locations. Injection volume varied by injection location as follows: 120 nl (LGN; 3 dorsal-ventral sites), 80 nl (PT), 20-50 nl (PBG and surrounding areas), 300 nl (VTA, 3 dorsal-ventral sites). After removal of the needle and sealing of the scalp with tissue adhesive, the same post-surgical protocol was followed as described for the AAV injections.

Herpes simplex virus (HSV) injections in SC projection targets

To label GABAergic SC projection neurons via retrograde transport, GAD2-cre adult mice were anesthetized as described above and placed in a

stereotaxic apparatus. An incision was made along the scalp, and a small hole was drilled in the skull overlying the LGN, PT, or PBG. Using the same equipment as described for CTB and AAV injections, heF1α-LS1LEYFP HT (MIT viral vector core) was injected into each of the locations listed above. Injection volume varied by injection location as follows: 120 nl (3 dorsal-ventral sites; LGN), 50 nl (PT), 50 nl (PBG).

Histology

Two days following injection of CTB, or 10-14 days following the injection of viruses, mice were deeply anesthetized with Avertin (0.5mg/gm) and transcardially perfused with a fixative solution of 4% paraformaldehyde, or 2% paraformaldehyde and 2% glutaraldehyde in 0.1M phosphate buffer (PB). Additional C57BL/6J or GAD67-GFP mice that were not injected were also perfused for immunocytochemistry. In each case, the brain was removed from the skull and 70 μm thick coronal sections were cut using a vibratome (Leica Microsystems, Buffalo Grove, IL). Sections that contained fluorescent labels were mounted on slides and imaged using a confocal microscope (Olympus FV1200BX61), or additionally stained using antibodies as described below. Selected sections were incubated overnight in a 6-12μg/ml concentration of a mouse monoclonal antibody against parvalbumin (Sigma, catalogue #P3088, RRID:AB_477329, immunogen was frog muscle parvalbumin), a 0.5 μg/ml concentration of a mouse monoclonal antibody against NeuN (Chemicon, catalogue #MAB377, RRID:AB_2298767, immunogen was purified cell nuclei from mouse brain.), and/or a 0.5 μg/ml concentration of a rabbit polyclonal

antibody against GABA (Sigma-Aldrich, St. Louis, MO, catalogue #A2052, RRID:AB_477652, immunogen was GABA conjugated to bovine serum albumin using glutaraldehyde; the GABA antibody shows positive binding with GABA and GABAkeyhole limpet hemocyanin, but not bovine serum albumin, in dot blot assays; manufacturer's product information). In mouse tissue, the GABA antibody stains most neurons in the thalamic reticular nucleus and a subset of neurons in the dorsal thalamus and cortex. This labeling pattern is consistent with other GABAergic markers used in a variety of species (Houser et al. 1980; Fitzpatrick, Penny, and Schmechel 1984; Montero and Singer 1984; Montero and Zempel 1985). In addition to a subset of neurons in the SC, the parvalbumin antibody stained a dense population of neurons in the thalamic reticular nucleus as previously described (Clemente-Perez et al. 2017; Villalobos et al. 2018). The NeuN antibody stains all neurons (identified by nuclei that have less condensed chromatin) and not glial cells (identified by nuclei that contain condensed chromatin; Wei et al., 2011). The following day, the sections were incubated in a 1:100 dilution of goat-anti-mouse and/or goat-anti-rabbit antibody(s) directly conjugated to fluorescent compounds (Alexafluor 546 Cat. No. A11030/ A11010 [RRID: AB_144695/AB_2534077], or Alexafluor 633 Cat. No. A21050 [RRID: AB_141431], Invitrogen, Carlsbad, CA). The sections were then mounted on slides and imaged using a confocal microscope.

Quantification of GABAergic and parvalbumin cell populations in the SC

Selected tissue sections from GAD67-GFP mice were imaged using a confocal microscope (Olympus FV1200BX61) with a 40x objective. Stacks of 1

μm optical images of the SGS were obtained in regions that contained a dense distribution of CTB-labeled cells. Cells labeled with CTB and/or antibodies were counted using Neurolucida 360 software (version 2018.2.1; Microbrightfield, Williston, VT). Labeled cells were only counted in regions of antibody penetration. Only one image stack was obtained per section to avoid overlap between sampling regions and to prevent bleaching of fluorescent labels.

Analysis of HSV-labeled projection cells

The distribution of HSV-labeled cells relative to the surface of the SC was measured from confocal image stacks. Prism (RRID:SCR_002798) was used for statistical analysis of these depth measurements (Kruskal-Wallis test). Confocal images of HSV-labeled cells that project to the PBG were additionally categorized based on their morphological characteristics. Three categories were used, adapted and slightly modified from a study by Villalobos et al. (2018): narrow-field vertical, horizontal, and stellate. The vertical or horizontal orientation of the dendritic arbors was defined relative to the dorsal surface of the SC in coronal sections. Vertically-oriented dendrites were located within 30 degrees of a line perpendicular to the dorsal surface of the SC. Horizontally-oriented dendrites were located within 30 degrees of a line parallel to the dorsal surface of the SC. The primary dendrites of narrow-field vertical cells were oriented in the vertical direction and the width or their dendritic arbor was less than 250 μm (measured parallel to the SC surface). The primary dendrites of horizontal cells were oriented in the horizontal direction (as defined above). Stellate cells included any neuron with a dendritic arbor that exhibited no clear orientation, or

neurons with arbors that were roughly symmetrical in all directions. Only cells labeled in SGS or SO were analyzed for these morphological characteristics. Additionally, only cells that were labeled beyond their secondary dendrites were included in the analysis. For presentation of confocal stacks, images were imported into Adobe Photoshop software (San Jose, CA), the brightness and contrast were adjusted, and tissue imperfections were removed using the clone stamp tool.

Electron Microscopy

Selected sections from GAD67-GFP mice were incubated overnight in a 0.1 µg/ml concentration of a rabbit polyclonal anti-GFP antibody (Millipore, Billerica, MA, catalogue #AB3080, RRID:AB_91337, created with highly purified native GFP from Aequorea victoria as an immunogen). Sections were then incubated in a 1:100 dilution of a biotinylated goat-anti-rabbit antibody (Vector Laboratories, Burlingame, CA, catalogue #BA-100, RRID:AB_23136061, 1 hour) , followed by avidin and biotinylated horseradish peroxidase (ABC solution, Vector Laboratories, 1 hour) and reacted with nickel-enhanced diaminobenzidine (DAB). All GFP antibody binding was confined to cells and terminals that contained GFP, as determined by their fluorescence under blue epifluorescent illumination; no staining was detected in sections that did not contain GFP. SC sections that contained DAB-labeled GFP, and additional SC sections obtained from C57BL/6J mice, were postfixed in 2% osmium tetroxide, dehydrated in an ethyl alcohol series, and flat embedded in Durcupan resin between two sheets of Aclar plastic (Ladd Research, Williston, VT). Durcupan–embedded sections were

first examined with a light microscope to select areas for electron microscopic analysis. Selected areas were mounted on blocks, ultrathin sections (70-80 nm, silver-gray interference color) were cut using a diamond knife, and sections were collected on Formvar-coated nickel slot grids. Selected sections were stained for the presence of GABA. A postembedding immunocytochemical protocol described previously (Bickford et al. 2010; N. Zhou et al. 2018; Masterson et al. 2019) was employed. Briefly, we used a 0.25 µg/ml concentration of a rabbit polyclonal antibody against GABA (Sigma-Aldrich, St. Louis, MO, catalogue #A2052, RRID:AB_477652). The GABA antibody was tagged with a goat-anti-rabbit antibody conjugated to 15-nm gold particles (BBI Solutions USA, Madison, WI, catalogue# GAR12/0.25, RRID:AB_1769132). The sections were air dried and stained with a 10% solution of uranyl acetate in methanol for 30 minutes before examination with an electron microscope.

Ultrastructural Analysis

For analysis of retinotectal synaptic connections, ultrathin sections obtained from C57BL/6J mice were stained for GABA and examined using an electron microscope. Retinotectal terminals were identified by their unique “pale” mitochondria with widened cristae; RLP profiles, (Boka et al., 2006; Bickford et al., 2010, 2015; Masterson et al., 2019), and those involved in a synapse were imaged. The areas of the pre- and postsynaptic profiles were measured using Image J, RRID: nif-000-30467, or Maxim DL © 5 software) and the gold particles were counted to calculate the gold density overlying each profile. The presence or absence of synaptic vesicles in postsynaptic profiles was also noted. As

previously described (Masterson et al. 2019), profiles were identified as GABAergic if the gold particle density overlying them was greater than the maximum density overlying RLP profiles (n = 124; average 9.27 ± 8.05 gold particles/μm2). This analysis revealed that in the C57BL/6J tissue, GABAergic profiles could be identified by a density of > 30 gold particles/μm2. For analysis of GFP-labeled synaptic connections, ultrathin sections obtained from GAD67-GFP mice were stained to reveal GFP and GABA and examined using an electron microscope. GFP was identified by the DAB reaction product (Zhou et al. 2018; Masterson et al. 2019), and profiles involved in a synapse were imaged (n = 94). The areas of the preand postsynaptic profiles were measured using Image J, RRID: nif-000-30467) and the gold particles were counted to calculate the gold density overlying each profile. For each synaptic partner, the presence or absence of DAB reaction product, synaptic vesicles, and dark or pale mitochondria was noted. As described above, profiles were identified as GABAergic if the gold particle density overlying them was greater than the maximum density overlying surrounding RLP profiles (n = 31; average 6.8 ± 4.2 gold particles/μm2). This analysis revealed that in the GAD67-GFP tissue, GABAergic profiles could be identified by a density of > 17 gold particles/μm2. For presentation of ultrastructural features, electron microscopic images were imported into Adobe Photoshop software (San Jose, CA), and the brightness and contrast were adjusted.

Results

The SGS contains at least four categories of GABAergic neurons

To aid in our study of the GABAergic neurons of the SGS, we used the GAD67-GFP mouse line which labels a dense population of neurons in the SGS (Figure 2.1a). First, to determine what proportion of SGS cells contain GFP and/or GABA, we stained sections from transgenic mice with antibodies against both GABA (Figure 2.1b-d) and NeuN (Figure 2.1e-g, to stain all SGS neurons). In confocal image stacks within the zone of antibody penetration (9 image stacks, tissue from 3 animals), we quantified cells that contained NeuN, NeuN/ GABA, or NeuN/GABA/GFP (n = 1982 NeuN-stained cells, 616 GABA-stained cells, and 417 GFP-labeled cells). This analysis revealed that 31.08 ± 3.71% of SGS neurons are GABAergic, and 67.70 ± 6.54% of these GABAergic cells contain GFP in the GAD67-GFP line. To determine whether cells that contain GFP and/or GABA in the GAD67 line also contain PV, we stained sections from the transgenic mice with antibodies against PV and GABA and quantified labeled cells in confocal image stacks within the zone of GABA antibody penetration (52 image stacks, tissue from 5 animals, n = 4089 GABAergic cells, 2175 GFPlabeled cells, 1560 PV-labeled cells). This more extensive tissue analysis revealed that 53.19 ± 10.62% of the GABAergic cells contained GFP. This analysis also revealed that approximately one quarter of the cells labeled with GFP in the GAD67-GFP line could also be labeled with an antibody against PV (n = 497, 22.85 ± 11.29%; Figure 2.1h-j, white arrows). Similar proportions of GABAergic cells contained PV (n= 1043, 25.51±8.35%). This was also the case

for the GABAergic cells that did not contain GFP (n = 1914); of these, approximately one quarter contained PV (n = 546, 28.53 ± 4.86%). The proportion of antibody-labeled PV cells that also contained GFP (n = 497; 31.86 ± 12.51%) was similar to that reported in a previous study of PV cells labeled in transgenic lines (Villalobos et al 2018; PV cells that contain GFP = 43 ± 4%). However, the proportion of antibody-labeled PV cells that were also stained with the GABA antibody (n = 1043, 66.86 ± 14.20%) was higher than that found for PV cells labeled in a transgenic line (PV cells that contain GABA = 36 ± 3%; Villalobos et al., 2018). Taken together, our immunocytochemical experiments indicate that the GAD67-GFP line labels approximately 60% of the GABAergic neurons in the SGS. Of these, approximately one quarter contain PV, indicating that GAD67-GFP cells are themselves not a homogenous group. Furthermore, our results indicate that 40% of GABAergic cells in the SGS do not contain GFP and of these, approximately one quarter contain PV, indicating that GABA, GAD67-GFP and PV labeling can be used to divide the GABAergic neurons of the SGS into four groups: 1) GABA+GFP (~45%), 2) GABA+GFP+PV (~15%), 3) GABA+PV (~10%), and 4) GABA only (~30%). In the following sections, we describe experiments which suggest that groups 1-3 are interneurons and group 4 includes projection neurons.

Extrinsic SC projection targets labeled in GAD2-Cre mice

Cre-dependent AAV injections placed in the SC of GAD2-Cre mice (Figure 2.2a) labeled axon projections to a variety of extrinsic targets. The primary extrinsic targets of GAD2 cells are the parabigeminal nucleus (PBG; Figure

2.2b), the pretectum (PT; Figure 2.2c) and the ventral lateral geniculate nucleus (vLGN; Figure 2.2d). Sparse projections were also observed in the opposite SC, but since previous studies have identified these as originating from neurons ventral to the SGS (Bickford and Hall, 1989; Appell and Behan 1990; Olivier et al. 2000), we did not examine these connections further.

GABAergic SGS cells that project to the PBG

HSV injections in the PBG of GAD2-Cre mice (Figure 2.3a) labeled a population of cells primarily located in the SGS (Figure 2.3b; somata located 319.6 ± 184.4 μm from the dorsal surface of the SC, n = 181; Figure 2.6). To characterize their morphology, we used a procedure modified from Villalobous et al. (2018), described in detail in the methods section. Cells that exhibited extensive dendritic labeling (n=65) were characterized in each section (n = 5) as narrow field vertical (NFV; 32.3 ± 11.5%), stellate (43.1 ± 13.5%) and horizontal (24.6±9%). These 3 cell types cells were differentially distributed within the SGS (Figure 2.6), with NFV closest to the SC surface (207 ± 89.9 μm), stellate cells slightly deeper (256.6 ± 118.7 μm) and horizontal cells farthest from the SC surface (350.9±164.1μm). However, these depth differences were not found to be statistically significant (Kruskal Wallis test). As expected, no wide field vertical cells (matching characteristics described in Masterson et al., 2019) were labeled by these injections as these cells are glutamatergic cells that innervate the pulvinar nucleus (Gale and Murphy 2014; Gale and Murphy 2016; Gale and Murphy 2018; Zhou et al. 2017). To determine whether any GABAergic PBG-projecting cells contain PV, we stained HSVinjected tissue with a PV antibody

(Figure 2.3c); we examined 181 HSV-labeled cells within the zone of antibody penetration and found no cells that were labeled with both the virus and the PV antibody. Next, to determine whether any SGS cells with ipsilateral descending projections are labeled with GFP in the GAD67-GFP mouse line, we injected CTB into PBG and surrounding areas (Figure 2.3d,e). In these cases we examined 490 CTB-labeled cells (Figure 2.3f) and found that none of these contained both CTB and GFP. We also stained this tissue with the PV antibody which labeled a subset (16.5 ± 6.8%) of SGS cells with ipsilateral descending projections (Figure 2.3g). Thus, the SGS GABA and PV cells that project to the PBG and surrounding areas form separate populations, and neither are labeled in the GAD67-GFP line.

GABAergic SC cells that project to the PT or LGN

To determine whether any SGS cells labeled in the GAD67-GFP mouse line project to the PT or LGN, we injected CTB into the PT (Figure 2.4a) or LGN (Figure 2.4b) in GAD67-GFP mice; we examined 859 CTB-labeled cells in the SGS (739 in PT-injected cases and 120 in LGN-injected cases) and found just 4 cells (0.48%) that contained both CTB and GFP. Thus, the vast majority of SGS cells that project to the PT or LGN are not labeled in the GAD67- GFP line. We also stained this tissue with the PV antibody. The PV antibody labeled a subset of SC-PT cells (27.2 ± 15.2%; Figure 2.4c) and SC-LGN cells (11.7 ± 5.2%) labeled via CTB injections.

HSV injections in the PT (Figure 2.5a) or vLGN (Figure 2.5d) of GAD2-Cre mice labeled cells that were primarily distributed in SC layers ventral to the SGS

(SC-PT somata located 508.5 ± 212.3 μm from the dorsal surface of the SC, n = 343, Figure 2.5b,c, Figure 2.6; SC-vLGN somata located 531.5 ± 263.7 μm from the dorsal surface of the SC, n = 811; Figure 2.3e,f; Figure 2.6). The distribution of cells that project to the PT or vLGN were significantly different from those that project to the PBG ($p<0.0001$), but there was no significant difference between the distribution of cells that project to the PT versus vLGN (Kruskal Wallis). To determine whether any GABAergic PT- or vLGN-projecting cells contain PV, we stained HSV-injected tissue with a PV antibody; we examined 1154 HSV-labeled cells within the zone of antibody penetration and found two cells (0.17%) that contained both virus and PV. Thus, GABAergic and PV-containing SC cells that project to the PT or LGN form separate populations.

Proportions of GABAergic projection neurons and interneurons in the SGS

A recent study identified SC projections to the ventral tegmental area (VTA) following Cre-dependent virus injections in vesicular GABA transporter (vGAT)-Cre mice (Zhang et al. 2019), although we were unable to detect projections to this region using the GAD2-Cre mouse line. To determine whether any SGS cells labeled in the GAD67-GFP mouse line project to the VTA, we placed large injections of CTB into the VTA (Figure 2.7a) in GAD67- GFP mice. SC cells labeled following these injections were located in the ipsilateral SC in layers deep to the SGS (Figure 2.7b). Similarly, all crossed descending projections from the SC arise from cells deep to the SGS (Bickford and Hall 1989). Thus, our retrograde CTB tracing studies indicate SGS cells labeled in the GAD67-GFP line do not contribute to the ascending or descending projections of

the SC (although we cannot rule out that they may project to targets that we did not inject with CTB, such as the periaqueductal gray). Furthermore, our retrograde HSV tracing combined with PV immunocytochemistry indicate that GABAergic projection neurons in the SGS do not contain PV. Thus, of the 4 categories of cells that we identified above, we can identify 3 groups as potential interneurons (GABA +GFP ~45%, GABA+GFP+PV ~15%, and GABA+PV ~10%), and the fourth group as potential projection neurons (GABA only ~30%).

GAD67-GFP SGS cells include intrinsic interneurons with presynaptic dendrites

Our results described above suggest that SGS neurons labeled in the GAD67-GFP line are interneurons. Thus, we were interested in determining whether these cells are a source of GABAergic presynaptic dendrites within the SGS. In the rat SC, we previously found that 27% of profiles postsynaptic to retinotectal terminals contained GABA, and 71% of these postsynaptic GABAergic profiles contained vesicles (Boka et al., 2006). We obtained similar results in C57BL/6J mice. We examined retinotectal terminals in C57BL/6J tissue stained to reveal GABA with gold particles. As illustrated in Figure 2.8, retinotectal terminals (pseudo colored green) can be identified by their unique "pale" mitochondria with widened cristae (asterisks); these profiles are referred to as RLP profiles (large profiles with round vesicles and pale mitochondria). RLP profiles are embedded within complex synaptic arrangements of GABAergic profiles that contain vesicles (Figure 2.8a-d, pseudo colored red) and nonGABAergic dendrites that do not contain vesicles (Figure 2.8a-d, pseudo

colored blue). RLP profiles make synaptic contacts with both GABAergic (Figure 2.8a-d, red arrows) and nonGABAergic dendrites (Figure 2.8a-c, blue arrows). We examined the synaptic contacts of 124 RLP profiles and found that 39 (31%) of the postsynaptic profiles could be classified as GABAergic based on a gold particle density that exceeded the maximum gold particle density overlying RLP profiles (average gold particle density overlying RLP profiles 9.3 ± 8.0 gold particles/μm2 ; average gold particle density overlying GABAergic profiles 72.5 ± 25.2 gold particles/μm2). Of the GABAergic profiles that received retinotectal input, 34 (87%) contained synaptic vesicles (Figure 2.8a-c, shown at high magnification in 8d), and these GABAergic profiles could occasionally be seen to contact nonGABAergic dendrites (Figure 2.8d, blue arrow). Thus, in the rodent SC, approximately one third of retinotectal synapses target GABAergic neurons, and the vast majority of these postsynaptic neurons form intrinsic connections via presynaptic dendrites. We next examined tissue obtained from GAD67-GFP mice. The GFP was identified via antibody binding revealed with a DAB reaction product (Figure 2.8e-f) and GABA content was assessed with an antibody tagged to gold particles as described above. We examined 94 GFP-labeled profiles involved in synaptic connections. As previously reported (Masterson et al. 2019), the gold particle density overlying these GFP-labeled profiles was significantly higher than that overlying RLP profiles (GFP 57.7 ± 25.1 gold particles/μm2 ; RLP 6.8 ± 4.2 gold particles/μm2 ; paired t test, $p < 0.0001$). Of the 94 synaptic connections formed by the GFP-labeled profiles, 31 were with RLP profiles (Figure 2.8e-f, red arrows). Although the vesicle content of GFP-labeled profiles

was occasionally obscured by the DAB reaction product, all profiles postsynaptic to RLP profiles exhibited the ultrastructure of presynaptic dendrites identified in the C57BL/6J mice. Thus, GAD67-GFP interneurons in the SGS are at least one source of GABAergic presynaptic dendrites in the SGS. The remaining synaptic partners of the GFP-labeled profiles were nonGABAergic dendrites (n = 54), nonGABAergic profiles with vesicles (n = 3), GABAergic dendrites (n = 4) and GABAergic profiles with vesicles (n = 2). These remaining synaptic connections may also be formed by interneurons of the SGS, although it is possible that some may be contributed by GFP-labeled axon terminals that originate from neurons outside the SC.

Discussion

Our results support the following conclusions: 1) Approximately 30% of SGS neurons in the mouse are GABAergic. 2) GABAergic projection neurons comprise up to 30% of the GABAergic neurons in the SGS, and none of these cells contain PV. 3) GABAergic neurons that project to the PBG are primarily located in the SGS and exhibit NFV, stellate, and horizontal morphology. 4) GABAergic neurons that project to the PT and vLGN are primarily located in the deeper layers of the SC. 5) The GAD67-GFP mouse line primarily labels intrinsic interneurons in the SGS, which make up approximately 60% of the GABAergic SGS neurons. 6) Approximately 45% of GABAergic SGS cells are GAD67- GFP interneurons that do not contain PV. 7) Approximately 15% of GABAergic SGS neurons are GAD67-GFP interneurons that contain PV. 8) Approximately 10% of GABAergic SGS cells are interneurons that contain PV but are not labeled with

GFP in the GAD67-GFP line. 9) Approximately 30% of retinotectal synaptic targets are the presynaptic dendrites of GABAergic interneurons and 10) GAD67-GFP interneurons are a source of GABAergic presynaptic dendrites in the SGS (summarized in Figure 2.9).

Projections from the SGS to the PBG

Previous studies in a variety of species have shown that projections to the PBG arise almost exclusively from the superficial layers of the SC (Diamond, Fitzpatrick, and Conley 1992; Bennett-Clarke et al. 1989) and recent studies in the mouse indicate that these projections arise from both GABAergic neurons (Gale and Murphy 2014) and glutamatergic neurons that contain PV (Shang et al. 2015, 2018). Our results corroborate these findings; we found that PBG projections arise from GABAergic SGS cells and none of these cells stained with a PV antibody. We also found that 16.5 ± 6.8% of SGS cells with ipsilateral descending projections contained PV. Whether the remaining cells are GABAergic neurons that project to the PBG, or whether ipsilateral descending projections arise from additional subtypes of SGS cells, remains to be determined. Gale and Murphy (2014) showed that glutamatergic projections to the PBG arise from cells labeled in the Grp-KH288-Cre line, but it is not known whether these cells contain PV. In other rodents, projections from the SGS to the PBG have also been shown to express substance P (Bennett-Clarke et al. 1989), but it is unknown whether these also contain PV or GABA. Nevertheless, since we found that other GABAergic projections from the SC arise primarily from deeper layers, it is likely that the majority of GABAergic projection cells in the

SGS are those that innervate the PBG. Using the retrograde transport of CTB and subsequent intracellular filling, Gale and Murphy (2014) found that SGS-PBG cells exhibit NFV and stellate morphology. Additionally, virus injections in the PBG of GAD2-cre mice labeled horizontal cells in the SGS. Similarly, we found that SGS-PBG cells exhibited NFV, stellate and horizontal dendritic fields. Moreover, since our virus tracing was carried out in GAD2-cre mice, we found that GABAergic SGSPBG cells exhibit this variety of morphologies. Finally, we also found that these different morphological types were located at slightly different depths within the SGS. NFV cells were located closest to the SC surface; since these cells extend dendrites vertically they can reach the dorsal most regions of the SGS. In contrast, horizontal cells were generally located farther from the dorsal surface of the SC and extend dendrites parallel to the SC surface. Thus, these cells could potentially be innervated by different types of retinal ganglion cells that target different dorsal-ventral locations within the SGS. Transynaptic labeling studies (Zingg et al., 2017) indicate that inputs from both the retina and V1 innervate SC cells that project to the PBG. However, transynaptic labeling in GAD2- Cre mice indicates that V1 innervates GABAergic interneurons that do not project outside the SC. Therefore, GABAergic SGS-PBG cells may receive direct input from the retina, but not V1, and nonGABAergic SGS-PBG cells receive direct input from V1, and potentially the retina. Interestingly, optogenetic activation of PV-containing cells in the SGS, or PV projections to the PBG elicit escape responses (Shang et al., 2015, 2018), but activation of PBG terminals originating from SC cells that receive V1 input does

not (Zingg et al., 2017). Therefore, key questions for future studies will be to determine whether all nonGABAergic projections to the PBG contain PV, what inputs target GABAergic and nonGABAergic SGS cells that project to the PBG, and how activation of GABAergic versus nonGABAergic SGS-PBG cells affects behavior.

Projections from the SC to the LGN and PT

Projections from the mouse SC to dLGN have been described as both glutamatergic (Bickford et al. 2015; Gale and Murphy 2018) and GABAergic (Gale and Murphy 2014). SC-dLGN cells are located in the SGS and are topographically organized (Bickford et al. 2015). Following CTB injections in the dLGN of GAD2-Ai9 mice, less than 5% of the SCdLGN cells could be identified as GABAergic. Moreover, virus injections in the SC of C57BL/6J mice labeled a discrete band of terminals in the lateral shell of the dLGN which, when optogenetically activated, elicited only glutamatergic responses in dLGN cells (Bickford et al. 2015). Finally, large cre-dependent virus injections (AAV serotype 9, chicken β actin promoter) in the SC of GAD2-cre mice label only very sparse projections to the dLGN after survival times of 10-16 days (Bickford et al., 2015; and Figure 2.2d of the current study). However, in a previous study, after survival times of 4-6 weeks, virus injections (AAV serotype 2.1 synapsin promoter) in the SC of GAD2-Cre mice labeled a dense distribution of terminals in the dLGN which was not restricted to the shell (Gale and Murphy 2014). Furthermore, when activated optogenetically, these terminals could elicit GABAergic responses in dLGN neurons (Gale and Murphy 2014). Although inconsistences in the results

of the studies described above remain to be resolved, a possible explanation is the finding that AAVs can be transynaptically transported during long survival times, particularly those with synapsin promoters (Zingg et al. 2017). In the current study, we find that GABAergic SC cells project to the PT, and previous studies indicate that GABAergic cells in the PT project to the dLGN (Cucchiaro et al., 1991; Wang et al. 2002; Masterson et al., 2016). Thus, after long survival times, virus injections in the SC could label PT-LGN cells via transynaptic transport, resulting in virus-labeled GABAergic axons in the dLGN. Alternatively, since GABAergic cells in the PT project to the SC (Baldauf et al. 2003), GABAergic PT cells could have been labeled via retrograde transport; in fact, the viruses used in this Gale and Murphy (2014) study were reported to label neurons via retrograde transport. Such alternative viral transport routes would explain the differences in previous studies and account for the current findings that GABAergic projections from the SC innervate the vLGN, PT and PBG, but not the dLGN. Furthermore, glutamatergic SC projections to the dLGN arise from the SGS (Bickford et al., 2015), while GABAergic projections to the vLGN and PT arise primarily from cells located ventral to the SGS.

GABAergic interneurons of the SGS

Based on the uptake of [3H]GABA and immunocytochemistry, Mize (1982,1988) identified 2 main types of GABAergic neurons with intrinsic connections in the cat SGS: horizontal cells and granule cells. GABAergic horizontal cells were defined as cells that have long smooth dendrites oriented parallel to the SC surface, while GABAergic granule cells were defined as cells

with stellate or obliquely-oriented dendrites. These two cells types were found to exhibit different types of synaptic connections. The dendrites of horizontal cells received input from V1 and contained small accumulations of synaptic vesicles along the length of their dendritic shafts, clustered at locations where periodic synaptic contacts were made with nonGABAergic dendrites. In contrast, GABAergic granule cells were identified as the source of presynaptic dendritic appendages that receive input from retinotectal terminals and contact nonGABAergic dendrites within complex “synaptic islands”. In the mouse, there is also evidence for these two general categories of GABAergic cell types. In GAD2-cre mice, V1 injections of a virus that is transported transynaptically primarily labeled horizontal cells that do not project outside the SC (Zingg et al. 2017), whereas few V1 synaptic contacts are found on GABAergic profiles within synaptic islands (Masterson et al., 2019). Moreover, optogenetic activation of terminals that originate from V1 rarely activate GAD67-GFP neurons (Masterson et al., 2019), which in the current study we have shown are a source of presynaptic dendrites that receive input from retinotectal terminals in complex “synaptic islands”. However, available data from the mouse also suggests that two broad morphological categories of GABAergic interneurons that are differentially innervated by cortical or retinal inputs is insufficient to fully describe the complexity of GABAergic circuits of the SGS. First, GAD67-GFP neurons labeled via the intracellular injection of biocytin exhibit a variety of morphologies (Endo et al. 2005; Villalobos et al. 2018; Masterson et al. 2019). In addition, GABAergic SGS cells may be subdivided based on immunocytochemistry,

genetic composition, and/or membrane properties. For example, recordings from GAD67-GFP cells in the mouse SGS revealed 3 distinct types of firing characteristics in response to current injection (Endo et al., 2003), whereas firing characteristics are more uniform in the subset of GAD67-GFP neurons that contain PV (Villalobos et al. 2018). In addition, Rorb-Cre mice identify a subtype of GABAergic interneuron with horizontal characteristics (Gale and Murphy, 2018). Finally, we identified a subtype of interneuron that contains PV and GABA, but is not labeled with GFP in the GAD67-GFP line. Although the features of all GAD67- GFP cells may not be uniform (Villalobos et al. 2018; Endo et al. 2003), our results suggest that they exhibit the unifying feature of being interneurons that do not project outside the SC (although we cannot rule out that they may project to targets that we did not inject with CTB, such as the periaqueductal gray). Our results also indicate that GAD67-GFP cells are a source of the presynaptic dendritic appendages that form complex synaptic arrangements with retinotectal terminals. Thus, this mouse line provides a useful model to investigate how GABAergic dendritic terminals may affect retinotectal visual signals. A recent in vivo calcium imaging study carried out in the GAD67-GFP line (Kasai and Isa, 2016) has shown that both GFP-positive and GFP-negative SGS cells in the dorsal SGS exhibit receptive fields with small excitatory centers flanked by inhibitory surrounds. These results suggested that GAD67-GFP interneurons contribute to center surround organization via long range lateral connections within the SGS. In contrast, horizontal cells in the mouse SGS have been shown to respond to large visual stimuli and inhibitory circuits

formed by these neurons are suggested to underlie the tuning of widefield vertical cells to ensure detection of the movement of small objects (Gale and Murphy 2016). Studies in the optic tectum of the zebrafish also indicate that subsets of GABAergic interneurons respond to large visual stimuli to contribute to the detection of small moving visual stimuli (Del Bene et al. 2010). Finally, studies of the lamprey optic tectum suggest that local feedforward inhibition imposes a visual signal integration time window that restricts excitation buildup, while an interconnected GABAergic network suppresses competitive visual signals to ensure the selectivity of gaze commands (Kardamakis, Saitoh, and Grillner 2015; Del Bene et al. 2010). Thus, a variety of evidence indicates the existence of both local and global inhibition within the SGS. Key questions for future studies will be to determine whether horizonal and granule cell circuits shape visual signals in the SC in different ways. As a first step, it will be important to determine whether V1 and retinal inputs target different subsets of interneurons, or different segments of the dendritic arbors of individual interneurons. It will also be important to determine whether individual interneurons are targeted by specific subtypes of ganglion cells or integrate several channels of visual information. Finally, since SGS glutamatergic cells also form synaptic connections within the SC (Villalobos et al. 2018; Gale and Murphy 2014; Gale and Murphy 2018), it will be important to determine how the intrinsic connections of both GABAergic and glutamatergic cell types interact to sculpt retinotectal signals.

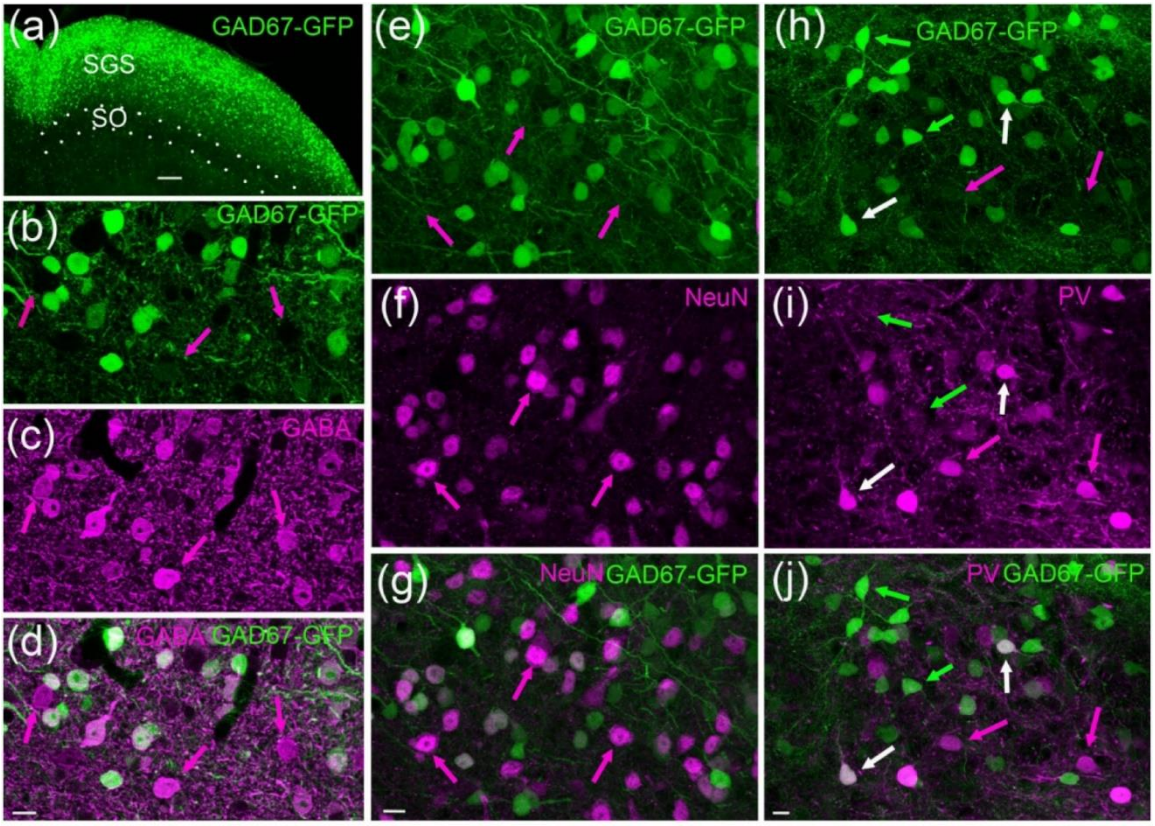

Figure 2.1. The GAD67-GFP mouse line labels subsets of GABAergic and PV cells in the SGS. a) The GAD67-GFP mouse line labels a dense population of neurons in the SGS. b-d) SGS of a GAD67-GFP mouse stained with an antibody against GABA (b, GFP, c, GABA, d, GFP and GABA). Magenta arrows indicate GABAergic neurons not labeled with GFP. e-g) SGS of a GAD67-GFP mouse stained with an antibody against NeuN (e, GFP, f, NeuN, g, GFP and NeuN). Magenta arrows indicate neurons not labeled with GFP. h-j) SGS of a GAD67-GFP mouse stained with an antibody against PV (h, GFP, i, PV, j, GFP and PV). Magenta arrows indicate PV neurons not labeled with GFP, green arrows indicate GFP neurons not labeled with PV, and white arrows indicate neurons

labeled with both GFP and PV. Scale bar in a = 100 μm. Scale bars in d, g and j = 10 μm.

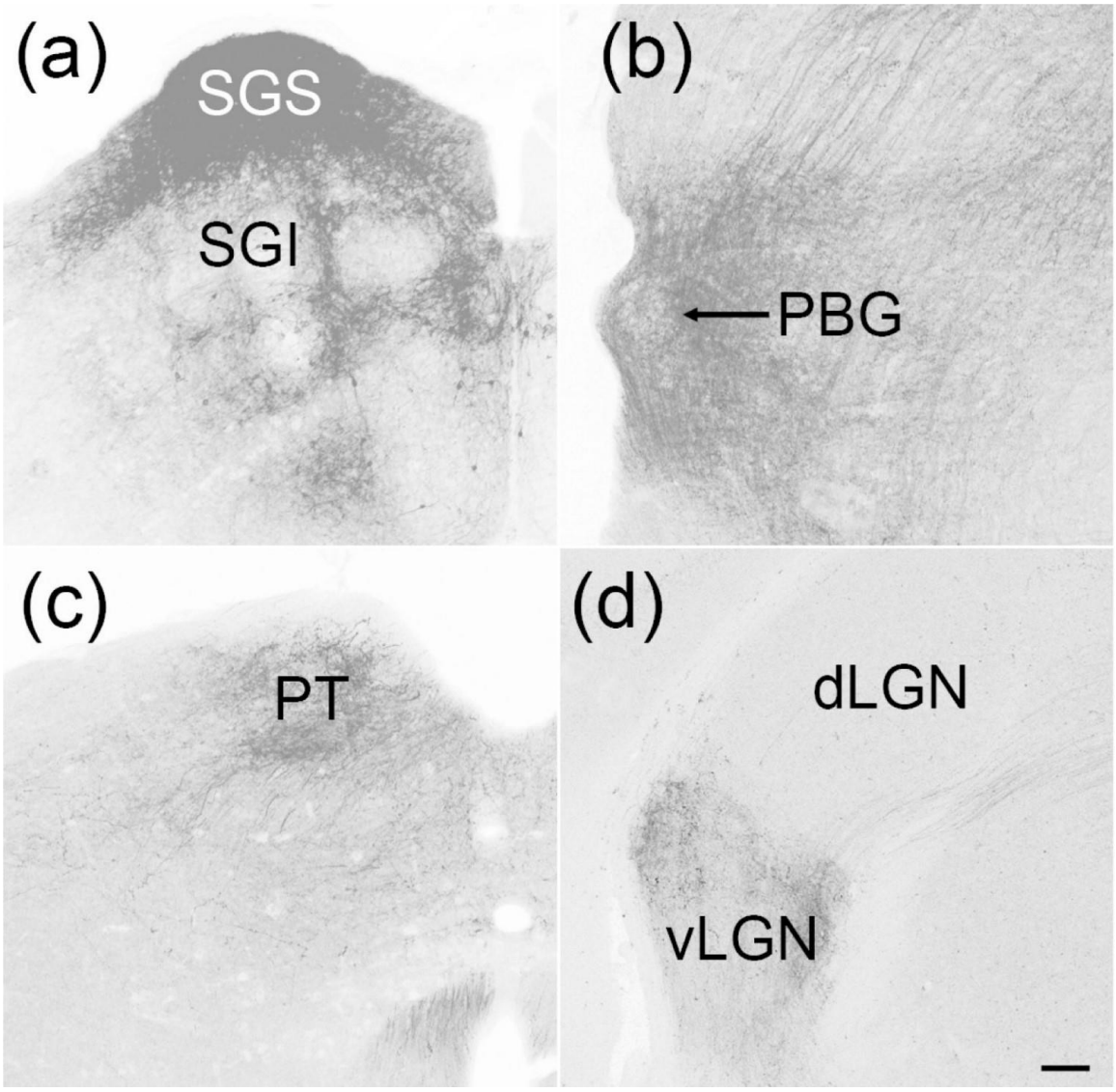

Figure 2.2. GABAergic extrinsic projection targets of the SC Cre-dependent adeno associated virus (AAV) injections placed in the SC of GAD2-Cre mice (a) labeled axon projections to the parabigeminal nucleus (PBG, b), the pretectum (PT, c) and the ventral lateral geniculate nucleus (vLGN, d). Scale bar = 100 μm

and applies to all panels. SGS, stratum griseum superficiale, SGI, stratum griseum intermediale.

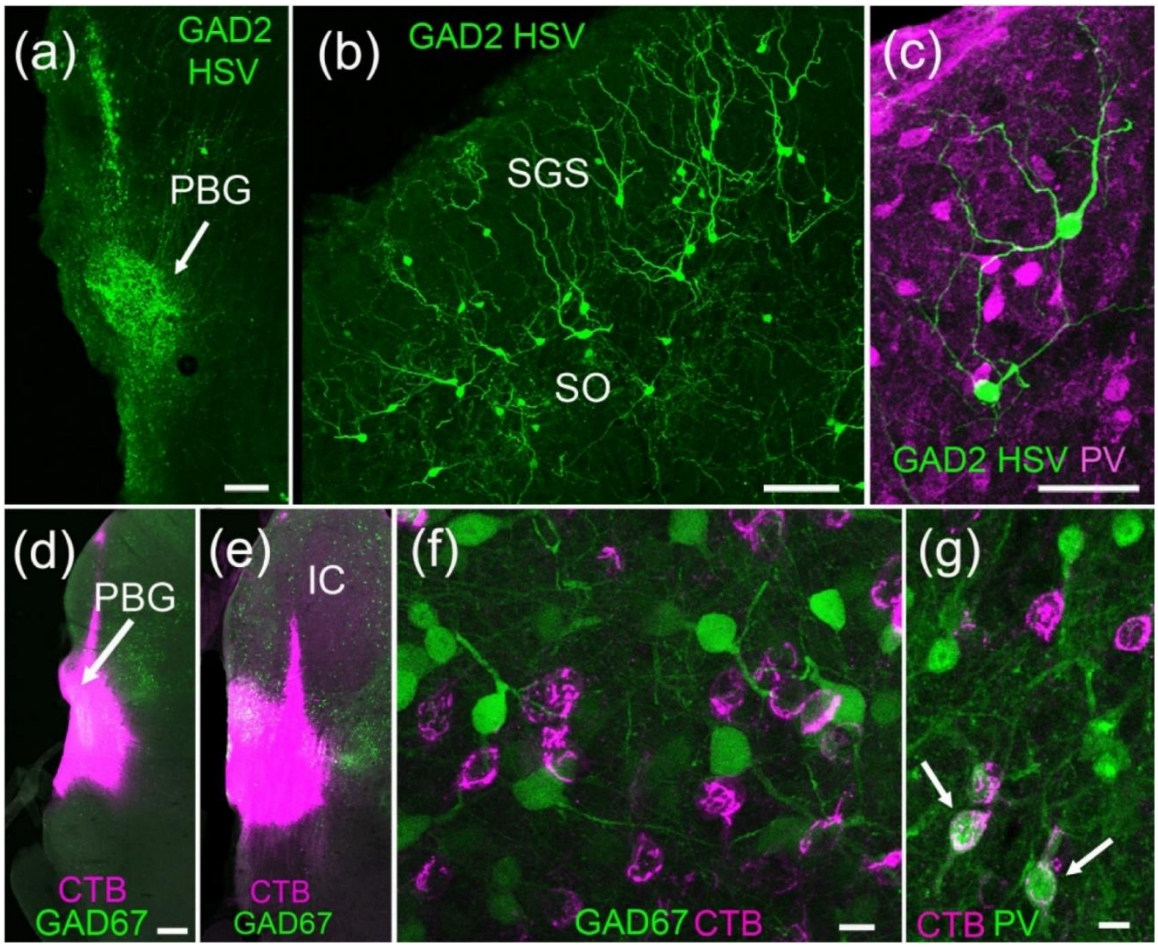

Figure 2.3. GABAergic SGS cells that project to the PBG. SC cells labeled by the retrograde transport of Cre-dependent herpes simplex virus (HSV) injections in the PBG (a) of GAD2-Cre mice were primarily distributed in SGS (b). c) None of these virus-labeled SC-PBG cells (green) were stained with a PV antibody (purple). Cholera toxin subunit B (CTB, purple) was injected into the PBG (d) and surrounding areas (e) of GAD67-GFP mice. f) No CTB (purple) was found in GAD67-GFP cells (green), but a subset of CTB-labeled cells were stained with a PV antibody (g, white arrows; 16.5 ± 6.8% of SC-PBG cells). Scale in a = 100

μm. Scale in b = 100 μm , c = 40 μm. Scale in d = 100 μm and also applies to e. Scales in f and g = 10 μm.

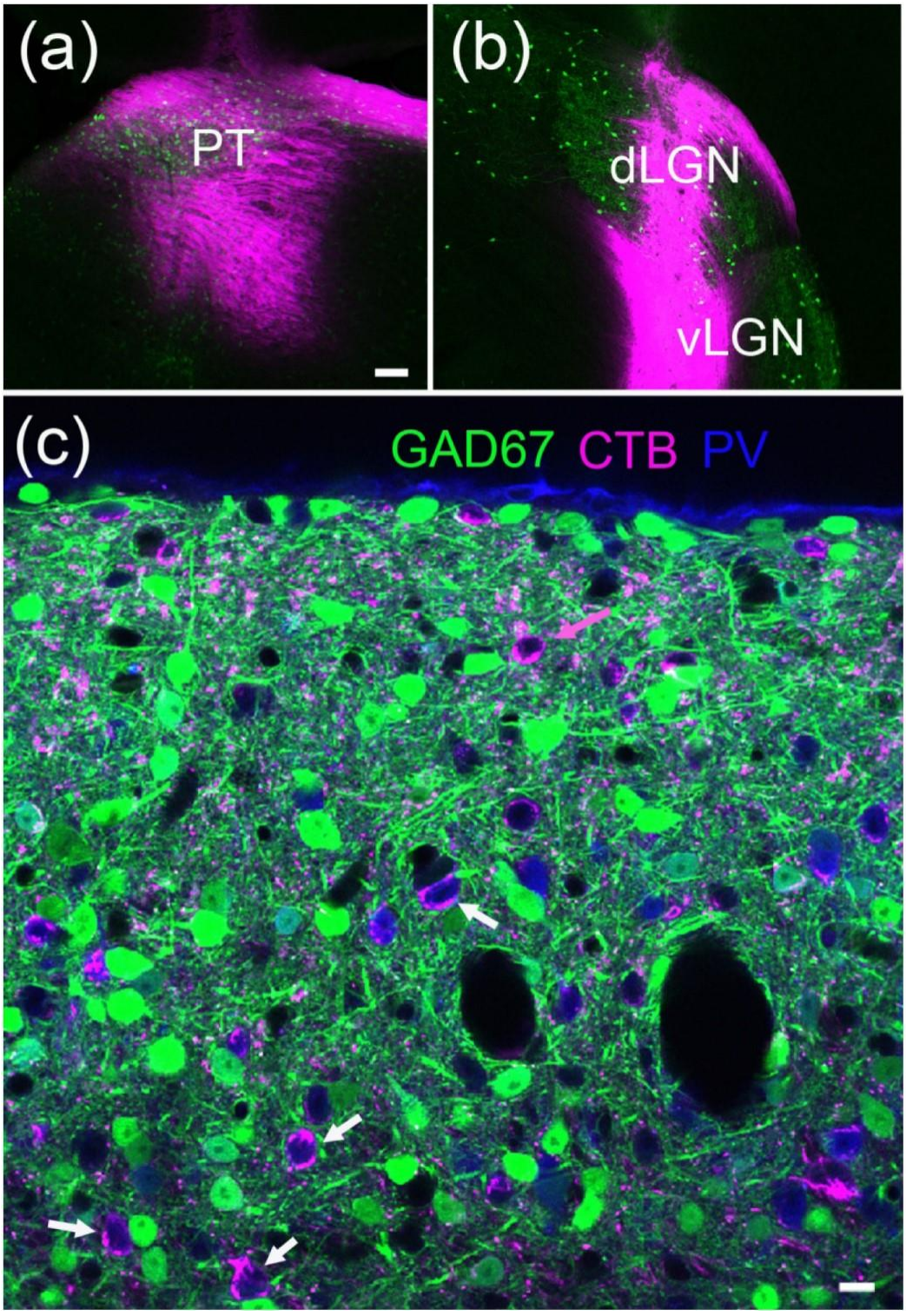

Figure 2.4. (last page): GAD67-GFP cells do not project to the PT or vLGN. Cholera toxin subunit B (CTB, purple) was injected into the PT (a) or LGN (b) in GAD67-GFP mice and the tissue was stained with a PV antibody (blue). c) Virtually no CTB (purple) was found in GAD67-GFP cells (green), but a subset of CTB-labeled cells contained PV (white arrows; 27.2 ± 15.2% of SCPT cells, and 11.7 ± 5.2% of SC-LGN cells). A cell that contains CTB but not PV is indicated with a magenta arrow. Scale in a = 100 μm and applies to b. Scale in c = 10 μm.

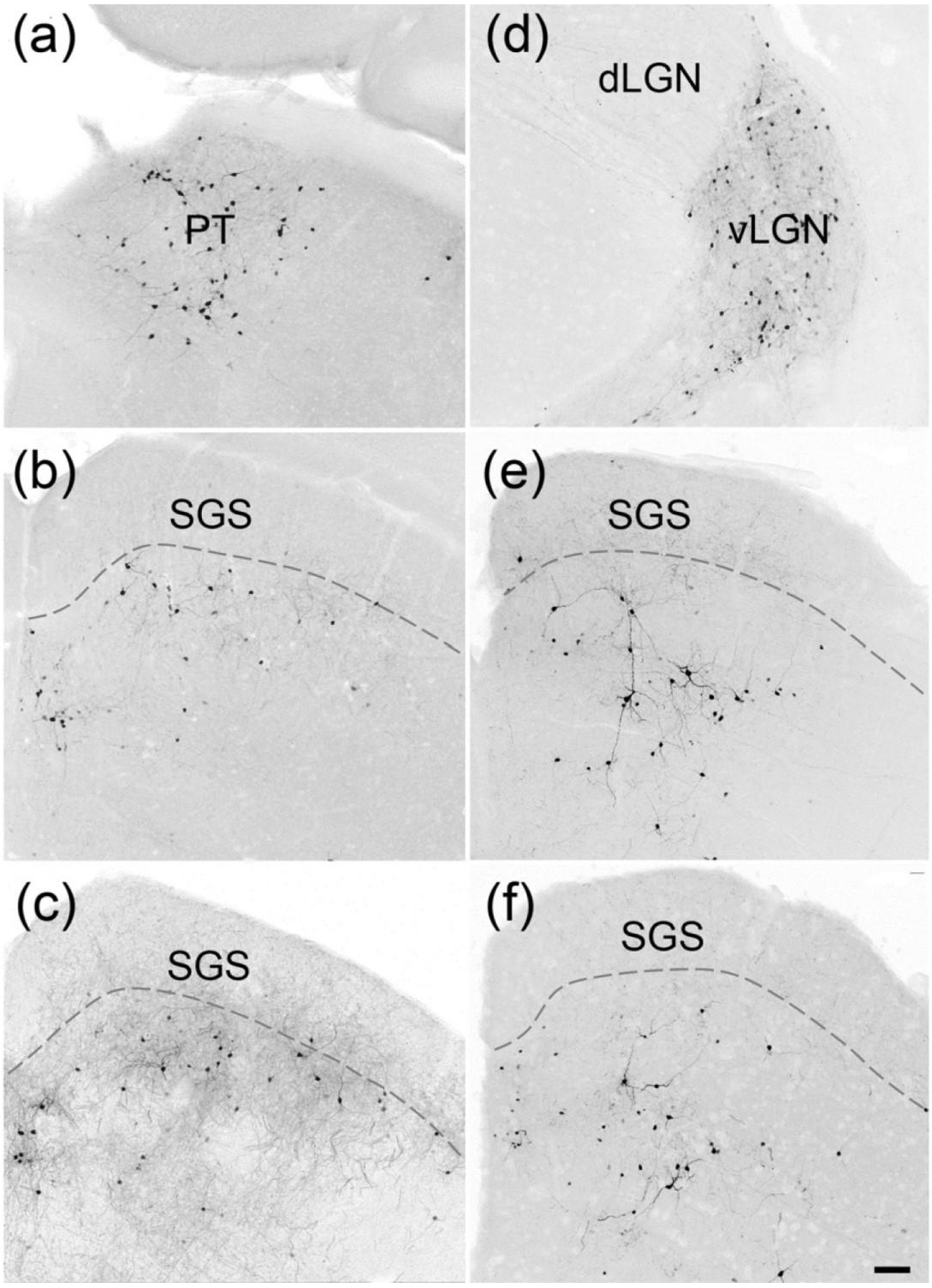

Figure 2.5. Distribution of GABAergic cells that project to the PT or vLGN. SC cells labeled by the retrograde transport of Cre-dependent HSV injections in the

PT (a) or vLGN (d) of GAD2- Cre mice were primarily distributed in SC layers deep to the SGS. b,c) SC-PT cells. e,f) SC-vLGN cells. Scale bar = 100 μm and applies to all panels.

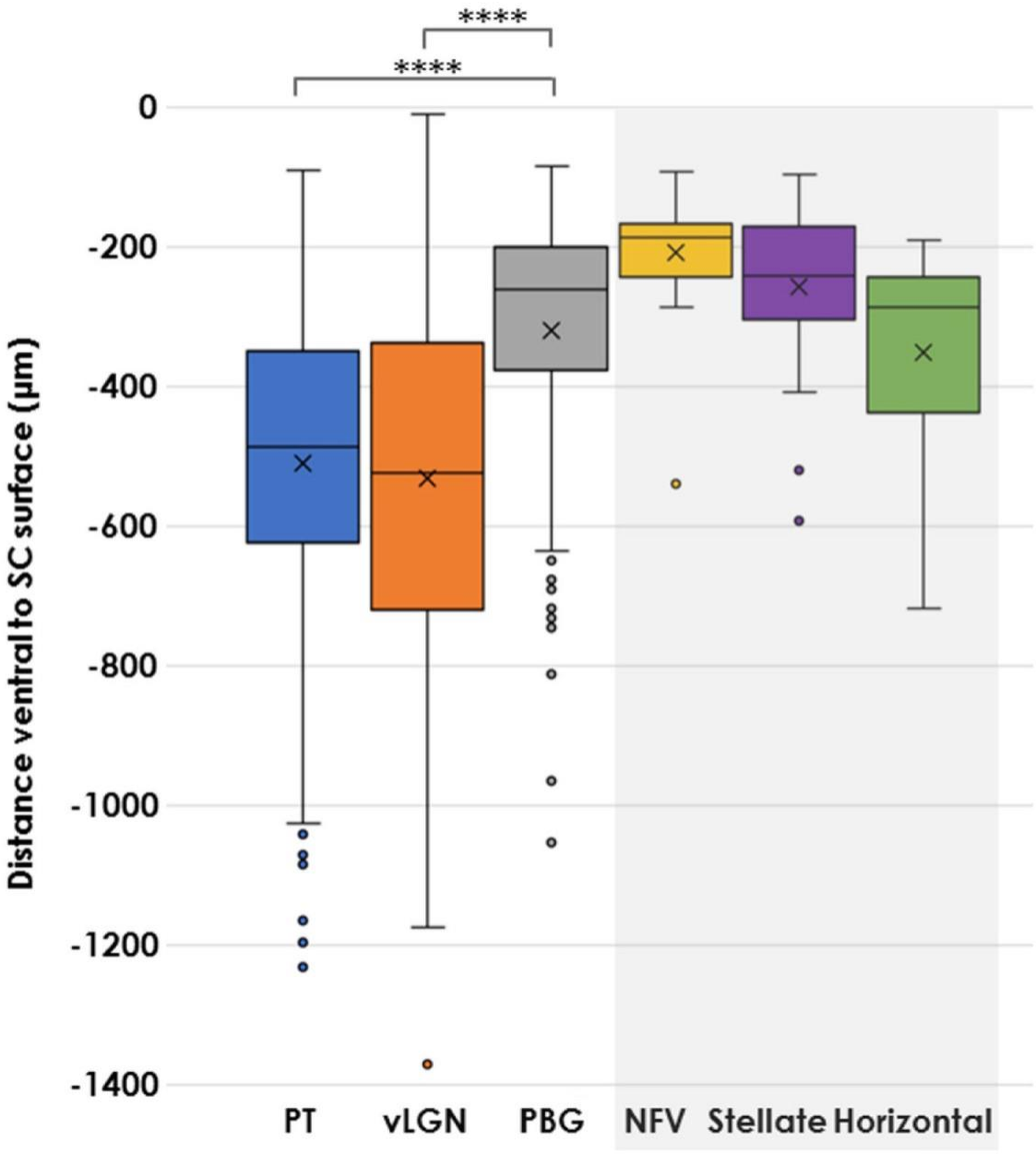

Figure 2.6. Distributions of GABAergic SC projection neurons. SC cells labeled by the retrograde transport of Cre-dependent HSV injections in the PBG, vLGN

or PT of GAD2-Cre mice were distributed at different depths relative to the dorsal surface of the SC. The box and whisker plot illustrates the mean depth of labeled cells (X), first and third quartiles (boxes), data ≤ 1.5x the interquartile range (lines), and outliers (circles). The distribution of cells that project to the PT or vLGN were significantly different from those that project to the PBG ($p<0.0001$****), but the distribution of NFV, stellate and horizontal cells that project to the PBG were not significantly different from one another. There was also no significant difference between the distributions of cells that project to the PT versus vLGN.

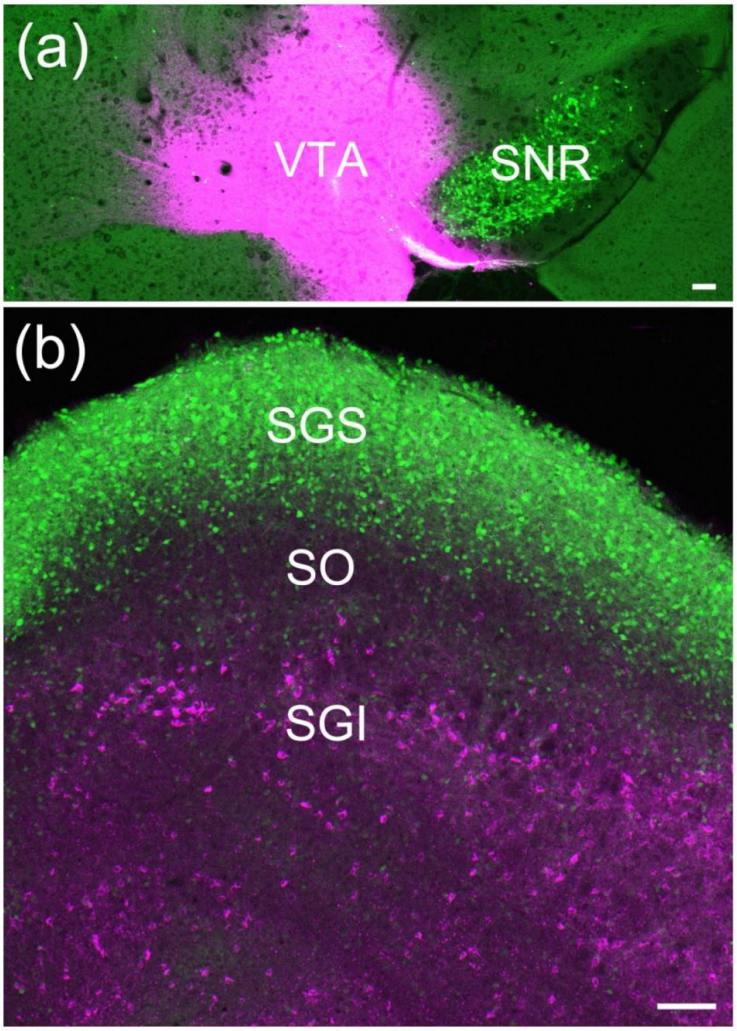

Figure 2.7. (Last page): Distribution of SC cells that project to the ventral tegmental area (VTA). Large CTB injections in the VTA of GAD67-GFP mice (a, magenta) labeled SC cells ventral to the SGS (b, magenta). Scale in a = 200 μm. Scale in b = 100 μm. SGI, stratum griseum intermediale, SNR, substantia nigra pars reticulata, SO, stratum opticum.

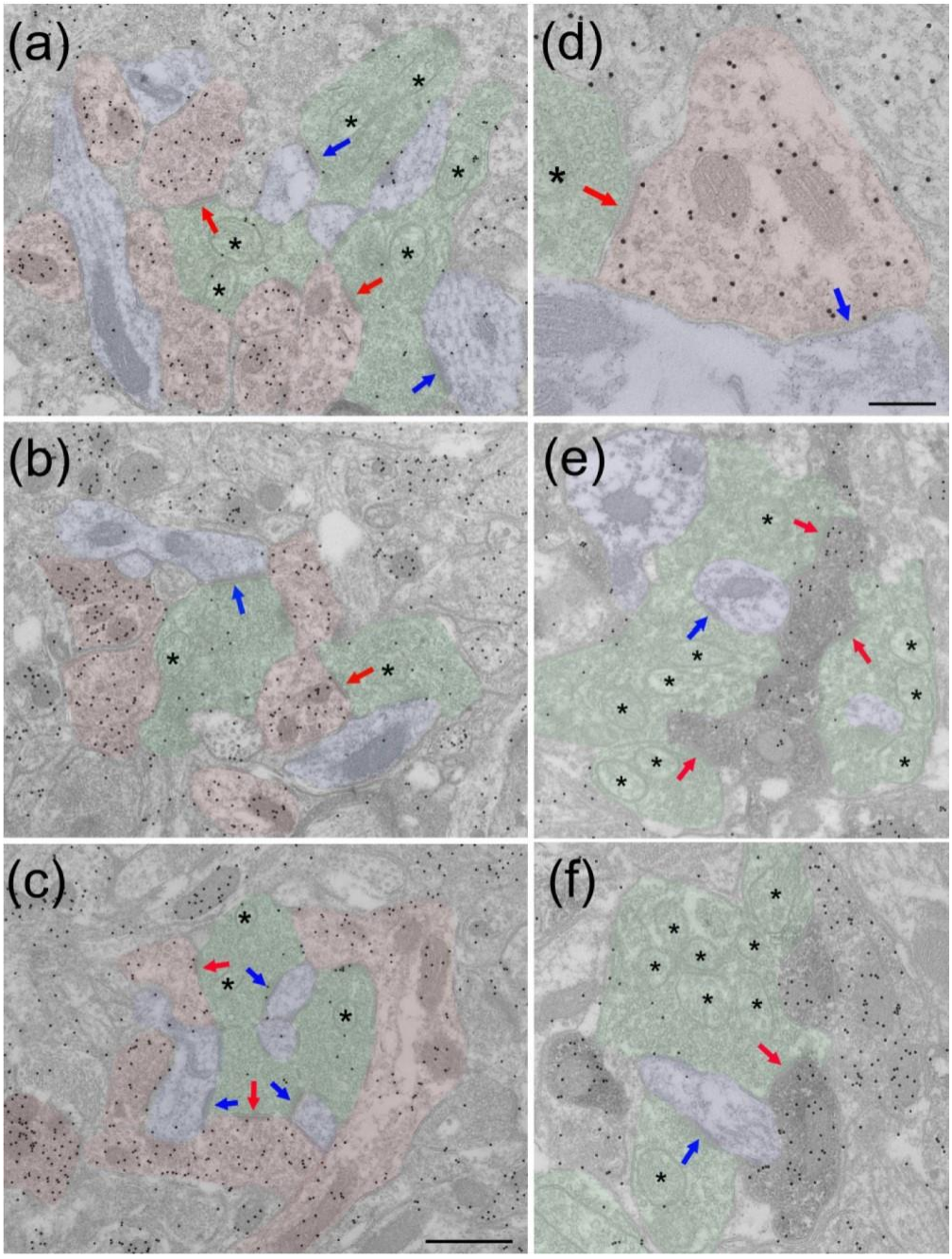

Figure 2.8. Retinotectal synaptic connections. Retinotectal terminals (green) can be identified by their unique “pale” mitochondria with widened cristae (asterisks). a-c) Retinotectal terminals are embedded within complex synaptic arrangements of GABAergic profiles that contain vesicles (red) and nonGABAergic dendrites that do not contain vesicles (blue). Retinotectal terminals make synaptic contacts with both GABAergic (red arrows) and nonGABAergic dendrites (blue arrows). d) GABAergic profiles can occasionally be seen to be postsynaptic to retinotectal terminals (green, red arrow) and presynaptic to nonGABAergic dendrites (blue, blue arrow). e-f) In tissue from GAD67-GFP mice, profiles labeled with a GFP antibody (dark reaction product) stain for GABA (high density of gold particles) and are postsynaptic to retinotectal terminals (green, red arrows). Retinotectal terminals that contact GFP-labeled profiles also make synapses on adjacent nonGABAergic dendrites (blue, blue arrows). Scale in c = 600nm and also applies to a,b,e and f. Scale in d = 200 nm.

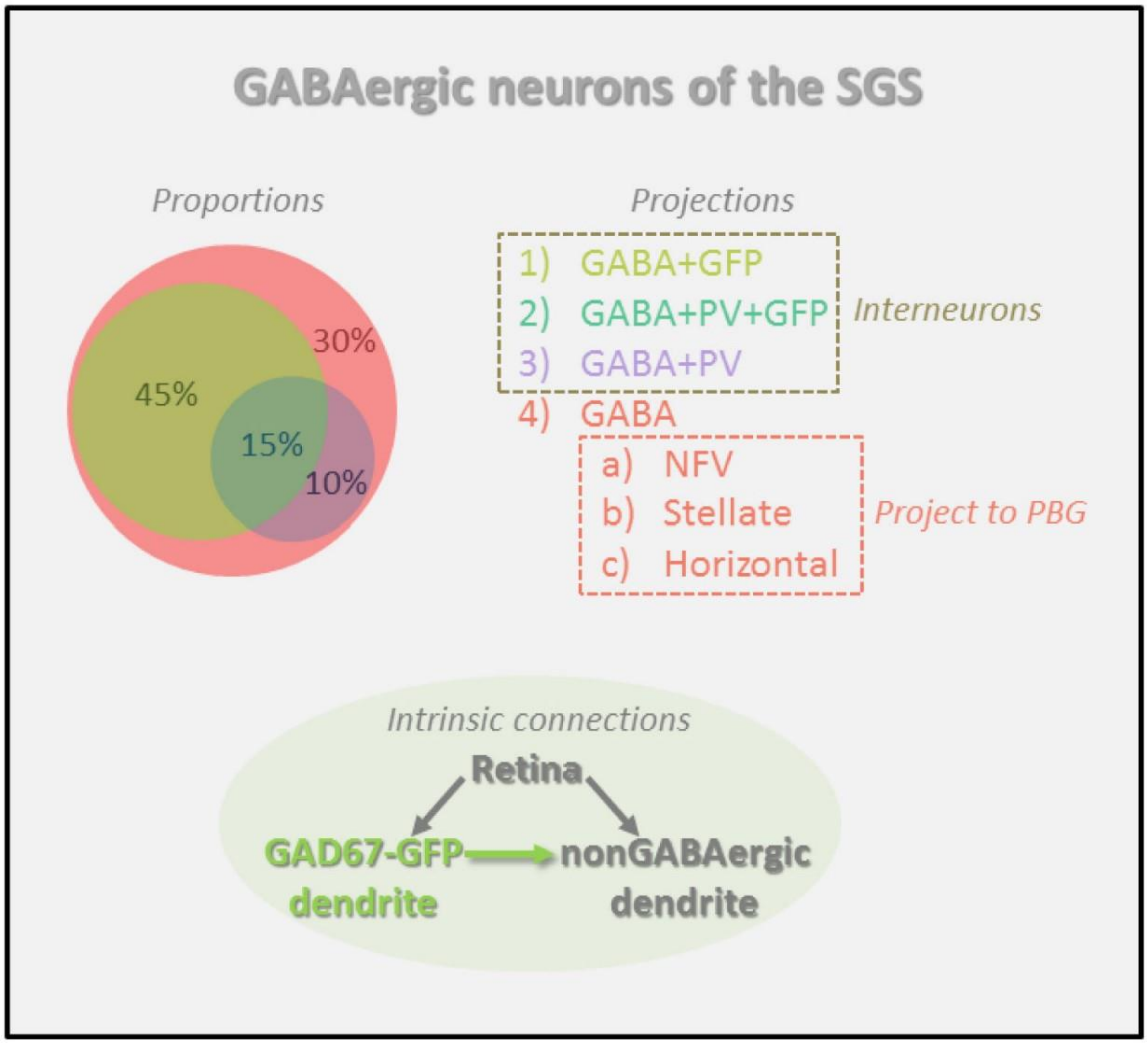

Figure 2.9. Summary of GABAergic cell types in the mouse SGS. The Venn diagram illustrates the approximate proportions of GABAergic SGS neurons listed to the right. GABAergic neurons that contain GFP in the GAD67-GFP line and/or are labeled with a PV antibody are identified as interneurons. The remaining cells are potential projection neurons that include NFV, stellate, and horizontal cells that project to the PBG. The GAD67-GFP mouse line labels intrinsic interneurons in the SGS which are a source of GABAergic presynaptic dendrites that receive retinal input and contact nonGABAergic dendrites.

CHAPTER III: SYNAPTIC PROPERTIES OF MOUSE TECTO-PARABIGEMINAL PATHWAYS

Introduction

Growing evidence has implicated the superior colliculus (SC) as a critical hub for the generation of appropriate actions in response to visual stimuli (Masullo et al., 2019; Shang et al., 2015; Wei et al., 2015; Zingg et al., 2017). The SC is well suited for this role, given that its superficial layers receive abundant input from the retina, while premotor neurons reside in its deeper layers (Basso et al., 2021; Ellis et al., 2016; Masullo et al., 2019; Sahibzada et al., 1986). Retinal input to the SC is organized in a retinotopic fashion, creating a topographic representation of visual space across its superficial layers (Chandrasekaran et al., 2005; Sparks & Mays, 1980), while the deeper layers contain motor or priority maps (Robinson, 1972; Schiller & Stryker, 1972; Sparks, 1978). This organization allows for specialized populations of neurons within the SC to form discreet functional modules to direct motor responses to visual stimuli in a targeted fashion (Masullo et al., 2019). In addition, the visual layers of the SC target many extrinsic structures which can also trigger visually-evoked movements. These targets include the parabigeminal nucleus (PBG), a small group of neurons on the lateral wall of the midbrain (Graybiel, 1978). The PBG,

sometimes referred to as the “satellite of the superior colliculus”, receives input from the superficial visual layers of the SC and projects to multiple visuomotor structures including the dorsal lateral geniculate nucleus, pulvinar, central amygdala and superficial layers of the SC (Graybiel, 1978; Shang et al., 2015; Sherk, 1979b; Sokhadze et al., 2022; Usunoff et al., 2007; Whyland et al., 2020). Recent studies indicate that activation of superior colliculus inputs to the PBG contributes to the production of visually-evoked defensive behaviors (Shang et al., 2015, 2018; Zingg et al., 2017). Moreover, perturbing the zebrafish nucleus isthmi (NI), considered to be the PBG homologue, disrupts behavioral action selection (Fernandes et al., 2021).

Across species, recordings from PBG neurons indicate that they exhibit robust visual responses. In the cat, PBG neurons were found to respond to input from either eye, and exhibit velocity tuning and direction selectivity (Sherk, 1978, 1979a). In the mouse, PBG neurons also exhibit direction-selectivity and additionally are responsive to looming (rapidly expanding) and sweeping (small, fast moving) visual stimuli (Reinhard et al., 2019). Likewise, neurons in the pigeon NI exhibit direction selectivity (Wang et al., 2022). Beyond simply encoding visual stimulus movement and direction, the PBG also appears to encode the saliency of visual stimuli. In cats, PBG cells respond to visual stimuli that predict the anticipated utility of saccade targets, supporting a potential role for the PBG in movement choice (Ma et al., 2013). Additionally, presentation of visual stimuli in one or both hemifields can either excite or inhibit neurons in the PBG, likely contributing to the binocular interactions necessary for proper

visuomotor coordination across hemispheres of the brain (Ma et al., 2013). Finally, in zebrafish, the NI plays an essential role in weighing the saliency of competing visual stimuli, creating a contextually based mechanism for generating appropriate motor responses (Fernandes et al., 2021).

The response properties of neurons residing in the PBG appear to be inherited in large part from their SC input. First, in both cats and rodents, the PBG exhibits a rough retinotopic organization that mimics that found in the SC(Deichler et al., 2020; Sherk, 1978, 1979b). Second, the receptive field properties of SC and PBG neurons are similar in many respects(Sherk, 1979a). However, several pathways from the SC to the PBG have been identified which may be integrated in the nucleus to create unique response properties. One pathway originates from SC neurons that express parvalbumin (which may include narrow field vertical cells labeled in the Grp-KH288-cre line) and another pathway is composed of neurons that contain GABA but not parvalbumin (Gale & Murphy, 2014, 2018; Hoy et al., 2019; Shang et al., 2015, 2018; Villalobos et al., 2018; Whyland et al., 2020). These two pathways provide opposing influences on the activity of PBG neurons; NFV SC neurons labeled in the Grp-KH288-cre line excite the PBG, while GABAergic SC neurons inhibit the PBG(Gale & Murphy, 2014, 2018). Moreover, these pathways may provide the PBG with a variety of visual signals. NFV neurons labeled in the Grp-KH288 line exhibit small receptive fields, prefer small fast-moving stimuli, and are often direction-selective(Hoy et al., 2019). GABAergic SC neurons that project to the PBG can exhibit stellate, NFV or horizontal morphologies (Whyland et al., 2020); horizontal GABAergic SC

neurons exhibit large receptive fields and are rarely direction-selective (Gale & Murphy, 2014, 2018), while the broader population of GABAergic neurons residing in the SGS, especially those in the most superficial SGS, generally exhibit direction-selectivity which is suppressed by surrounding motion in the opposite direction (Barchini et al., 2018).

How these SC signals are potentially integrated by PBG neurons is unknown. In the current study, we characterized the ultrastructure and synaptic properties of GABAergic and glutamatergic/parvalbumin SC inputs to the mouse PBG as well as the dendritic morphology of postsynaptic PBG neurons. We also identified nontectal GABAergic input to the PBG, potentially arising from neurons in and surrounding the PBG. These studies provide a critical first step toward uncovering how the PBG contributes to the initiation of visually-evoked behavior.

Materials and Methods

Animals

All breeding and experimental procedures were approved by the University of Louisville Institutional Animal Care and Use Committee. Experiments were carried out using mice, of either sex, in C57BL/6J mice (Jax Stock No: 000664), a line in which neurons that contain the 67KD isoform of glutamic acid decarboxylase (GAD) express green fluorescent protein (GAD67-GFP; Jax Stock No: 007677, G42 line), a line in which neurons that contain GAD express cre-recombinase (GAD2-cre; Jax Stock No: 010802; GAD2), and a line

in which neurons that contain parvalbumin (PV) express cre-recombinase (PV-cre; Jax Stock No: #008069).

***Biotinylated dextran amine (BDA) and adeno-associated (AAV) virus injections*.**

To label and/or optogenetically activate SC-PBG projections, BDA or AAVs were injected bilaterally into the SC of C57BL/6J, GAD2-Cre, or PV-Cre mice. The AAVs used for fluorescent labeling and activation of SC-PBG projections were: AAV1-CAG-Flex-EGFP-WPRE.bGH, AAV9-Flex-Rev-O-ChieftdTomato, or AAV1-Acagw-O-Chieftdtom (which carries a vector for the Channelrhodopsin variant Chimera EF with I170 mutation [ChIEF] fused to the red fluorescent protein, tdTomato [for production details, see Jurgens et al., 2012]). In other experiments, to label SC-PBG projections for electron microscopy, BDA was injected unilaterally in the SC, or pENN.AAV1.hSyn.Cre.WPRE.hGH was injected in the eyes or the primary visual cortex (V1) to express cre-recombinase in SC neurons that receive input from the retina or V1, and the SC was subsequently injected bilaterally with AAV1-CAG-Flex-EGFP-WPRE.bGH. For AAV delivery in V1 or the SC, P21-P35 mice were deeply anesthetized with a mixture of ketamine (100–150 mg/kg) and xylazine (10–15 mg/kg). The analgesic meloxicam (1–2 mg/kg) was also injected prior to surgery. The animals were then placed in a stereotaxic apparatus (Angle Two Stereotaxic, Leica, Wetzlar, Germany). An incision was made along the scalp, and a small hole was drilled in the skull overlying the SC or V1. Virus was infused into the brain via a 34-gauge needle attached to a Nanofil syringe inserted in an

ultramicropump. A volume of 60 nl (SC) or 100 nl (V1) was injected at each site (SC: 3.75 mm caudal to Bregma, 0.6 mm lateral to midline, 1.3 mm ventral to Bregma; V1: 3.4 mm caudal to Bregma, 2.4 mm lateral to midline, 1.15 mm ventral to Bregma), at a rate of 20 nl/min. After removal of the needle, the scalp skin was sealed with tissue adhesive (n-butyl cyanoacrylate), lidocaine was applied to the wound, and the animals were placed on a heating pad until mobile. After surgery, animals were carefully monitored for proper wound healing, and injectable meloxicam (1–2 mg/kg) was administered for 48 h.

For BDA injections, P30-P40 mice were prepared for cranial surgery as described above and a glass pipette (20 – 40 µm tip diameter) containing a 5% solution of BDA (Invitrogen) in saline was lowered into the SC (from bregma: 3.8 mm posterior, 0.6 mm lateral, and 1.2 mm ventral), and BDA was iontophoretically ejected using 3 µA continuous positive current for 20 min. Post operative care was carried out in the same manner as described for virus injections.

To express cre-recombinase in SC-PBG projection neurons that receive input from the retina, C57Blk6 pups (p15-18) received bilateral intravitreal injections of pAAV1.hSyn.Cre.WPRE.hGH. Each pup was anesthetized with isoflurane via a small nose cone, the sclera was pierced with a sharp-tipped glass pipette, and excess vitreous was drained. Another pipette filled with the AAV solution was inserted into the hole made by the first pipette. The pipette containing the AAV was attached to a picospritzer and a volume of approximately 1 µl of solution was injected into the eye. The nose cone used to administer

isoflurane was then removed and, once alert, the pup was returned to the cage containing the dam and littermates.

Histology for examination of the PBG and SC-PBG projections

Ten to fourteen days following the injection of viruses or one week after BDA injections, mice were deeply anesthetized with Avertin (0.5mg/gm) or ketamine (100-150 mg/kg) and transcardially perfused with a fixative solution of 4% paraformaldehyde, or 2% paraformaldehyde and 2% glutaraldehyde in 0.1M phosphate buffer (PB). Additional GAD67-GFP mice that were not injected were also perfused for immunocytochemistry. In each case, the brain was removed from the skull and 70 μm thick coronal sections were cut using a vibratome (Leica Microsystems, Buffalo Grove, IL). For BDA experiments, sections were incubated in avidin and biotinylated horseradish peroxidase (ABC solution, Vector Laboratories) overnight, reacted with nickel-enhanced diaminobenzidine (DAB) and processed for electron microscopy (described below). For the transsynaptic viral tracing experiments, selected sections were incubated overnight in a 0.1 μg/ml concentration of a rabbit polyclonal anti-GFP antibody (Millipore, Billerica, MA, catalogue #AB3080, RRID: AB_91337, created with highly purified native GFP from Aequorea victoria as an immunogen). Sections were then incubated in a 1:100 dilution of a biotinylated goat-anti-rabbit antibody (Vector Laboratories, Burlingame, CA, catalogue #BA-100, RRID: AB_23136061, 1 hour), followed by ABC solution, 1 hour), reacted with nickel-enhanced DAB and processed for electron microscopy (described below). All GFP antibody binding was confined to cells and terminals that contained GFP, as determined

by their fluorescence under blue epifluorescent illumination; no staining was detected in sections that did not contain GFP. To identify axon terminals in the PBG positive for the vesicular GABA transporter (VGAT), selected tissue sections from GAD67 mice were incubated overnight in a 1:500 dilution of polyclonal anti-VGAT antibody (Synaptic Systems, Göttingen, Germany, catalogue #131 103, RRID: AB_887870, created using synthetic peptide corresponding to residues near the amino terminus of rat VGAT). Sections were then incubated in a 1:100 dilution of goat-anti-rabbit antibody directly conjugated to a fluorescent compound (Alexafluor 546, Cat. No. A11010, RRID: AB_2534077, Invitrogen, Carlsbad, CA), washed in PB and mounted on slides to view using a confocal microscope.

Slice preparation and optogenetic stimulation

Eight to twelve days following SC virus injections, mice were deeply anesthetized with isoflurane. Mice used for slice preparation ranged in age from P29 to P45 (average age p32). Mice were decapitated and the brain was removed from the head, chilled in cold slicing solution (in mM: 2.5 KCl, 26 $NaHCO_3$, 2.5 KCl, 1.25 NaH_2PO_4, 10 $MgCl_2$, 2 $CaCl_2$, 234 sucrose, and 11 glucose) for 2 min, and quickly transferred into a Petri dish with room temperature slicing solution to block the brain for subsequent sectioning. Coronal slices (300 μm) were cut in cold slicing solution using a vibratome (Leica VT1000 S). Then slices were transferred into a room temperature incubation solution of oxygenated (95%O_2/5%CO_2) artificial cerebrospinal fluid containing the following (in mM: 126 NaCl, 26 $NaHCO_3$, 2.5 KCl, 1.25 NaH_2PO_4, 2 $MgCl_2$, 2 $CaCl_2$, and

10 glucose) for 30 min to 6 hours. Individual slices were transferred into a recording chamber, which was maintained at 32°C by an inline heater and continuously perfused with room temperature oxygenated ACSF (2.5 ml/min, 95%O2/5%CO2). Slices were stabilized by a slice anchor or harp (Warner Instruments, 64– 0252). Neurons were visualized on an upright microscope (Olympus, BX51WI) equipped with both differential interference contrast optics and filter sets to detect fluorescence in the sections using a 4× or 60× water-immersion objective (Olympus) and a CCD camera. Recording electrodes were pulled from borosilicate glass capillaries (World Precision Instruments) by using a Model P-97 puller (Sutter Instruments). To record inhibitory post-synaptic currents (IPSCs) as well as excitatory post-synaptic currents (EPSCs) in PBG neurons, voltage-clamp recordings were conducted using a cesium-based internal solution containing (in mM): 117 Cs-gluconate, 11 CsCl, 1 MgCl2, 1 CaCl2, 0.1 EGTA, 10 HEPES, 2 Na2-ATP, 0.4 Na2-GTP , with pH adjusted to 7.3 with CsOH and osmolarity 290 –295 mOsm. For current-clamp recordings, electrodes were filled with an intracellular solution containing the following (in mM): 117 K-gluconate, 13.0 KCl, 1 MgCl2, 0.07 CaCl2, 0.1 EGTA, 10 HEPES, 2 Na2-ATP, and 0.4 Na2-GTP, with pH adjusted to 7.3 with KOH and osmolarity 290 –295 mOsm. Biocytin (0.5%) was added to intracellular solutions to allow morphological reconstruction of the recorded neurons.

Whole-cell recordings were obtained from all regions of the PBG in both GAD2-Cre and PV-Cre mice, regardless of the AAV used (cre-dependent or non-cre-dependent). Recordings were obtained with an AxoClamp 2B amplifier

(Molecular Devices), and a Digidata 1440A was used to acquire electrophysiological signals. The stimulation trigger was controlled by Clampex 10.3 software (Molecular Devices). The signals were sampled at 20 kHz, and data were analyzed offline using pClamp 10.0 software (Molecular Devices). For current-clamp recordings, voltage signals were obtained from cells with resting potentials of -50 to -65mV. For voltage-clamp recordings, currents were recorded at 0mV or -60mV.

For photoactivation of SC-PBG terminals, light from a blue light-emitting diode (Prizmatix UHP 460) was reflected into a 60× water-immersion objective. This produced a spot of blue light onto the submerged slice with a diameter of ~0.3 mm. Pulse duration and frequency were under computer control. For repetitive stimulation, pulse duration was 1 ms. Synaptic responses were recorded using light intensities of 10 –112 mW/mm 2 (the intensity was measured using a light meter placed under the dry objective), and light pulse frequencies of 1, 2, 5, 10, and 20 Hz. To block GABAergic transmission pharmacologically, GABA receptors ($GABA_A$) were blocked via bath application of the antagonist 2-(3-carboxypropyl)-3-amino-6-(4-methoxyphenyl)-pyridazinium bromide (SR95531, 20 µM; Tocris Bioscience, catalog #1262).To block NMDA and AMPA signaling pharmacologically, APV (10 µM; Sigma, catalog #A-5282) and/or CNQX (8 µM; Tocris Bioscience, catalog #0190)/DNQX (80 µM; Sigma, catalog #D0540-50MG) were bath applicated to block NMDA and AMPA receptors, respectively.

Electron microscopy

PBG sections that contained DAB-labeled BDA or GFP were postfixed in 2% osmium tetroxide, dehydrated in an ethyl alcohol series, and flat embedded in Durcupan resin between two sheets of Aclar plastic (Ladd Research, Williston, VT). Durcupan–embedded sections were first examined with a light microscope to select areas for electron microscopic analysis. Selected areas were mounted on blocks, ultrathin sections (70-80 nm, silver-gray interference color) were cut using a diamond knife, and sections were collected on Formvar-coated nickel slot grids. Selected sections were stained for the presence of GABA. A postembedding immunocytochemical protocol described previously (Bickford et al. 2010; N. Zhou et al. 2018; Masterson et al. 2019) was employed. Briefly, we used a 0.25 µg/ml concentration of a rabbit polyclonal antibody against GABA (Sigma-Aldrich, St. Louis, MO, catalogue #A2052, RRID:AB_477652). The GABA antibody was tagged with a goat-anti-rabbit antibody conjugated to 15-nm gold particles (BBI Solutions USA, Madison, WI, catalogue# GAR12/0.25, RRID:AB 1769132). The sections were air dried and stained with a 10% solution of uranyl acetate in methanol for 30 minutes before examination with an electron microscope.

Processing of cells filled during physiological recording

Following recording, slices were placed in a fixative solution of 4% paraformaldehyde in PB for at least 24 h. The sections were then rinsed in PB and incubated overnight in a 1:1000 dilution of streptavidin- conjugated to AlexaFluor-633 (Invitrogen) in PB containing 1% Triton X-100. The following day,

the slices were washed in PB, preincubated in 10% normal goat serum in PB, and then incubated overnight in a 1:500 dilution of a rabbit anti-DSred antibody (Clontech, catalog #632496) in PB with 1% normal goat serum. The following day, the sections were rinsed in PB and incubated for 1 h in a 1:100 dilution of a goat-anti-rabbit antibody conjugated to AlexaFluor-546 (Invitrogen). The sections were then rinsed in PB and mounted on slides to be imaged with a confocal microscope (Olympus FV1200BX61).

Morphological analysis of PBG neurons

To classify neurons recorded *in vitro* by their morphological characteristics, confocal-imaged, biocytin-filled cells were first traced in PowerPoint by hand using the marker tool. Images of the resultant 2-D traces were then uploaded in ImageJ (Fiji) where they were first binarized and then analyzed via the “Sholl Ring” analysis tool. The “start radius” for these analyses was set to 15 pixels, with a “step size” (Sholl ring size) of 10 pixels. The center and end radius of the Sholl rings for each cell were defined by a region of interest (ROI, straight line) drawn from the approximate center of the soma to the most distal point in the dendritic arbor before performing the analysis. The Sholl ring diagrams produced by these ImageJ analyses were then used to quantify the number of dendritic “crossings” in each of 8 radially organized sections around the center (defined by the ROI described above) of each cell. Cells in which less than 20% of these crossings could be found in 4 contiguous radial sections in any orientation were considered “Asymmetric”. Cells where any 4 contiguous sections always represented 20% or more of the total crossings regardless of

orientation were considered “Stellate”. Cells in which more than 50% of total crossings could be found in 2 symmetrical (on opposite sides) sections were classified as “Narrow-Field”. These Narrow-Field cells could be further classified as symmetric or asymmetric based on the criteria described above for the Asymmetric and Stellate (symmetric) cell types. Radar plots illustrating the orientation and density of cell arbors based on the number of Sholl ring crossings in each 1/8 radial section were made using Microsoft Excel. Radial sections were defined via a lined overlay that split each cell’s anatomy into 8 sections of equal radial size, centered on each cell’s soma (also the origin of each ROI used to define the parameters of the Sholl rings).

Electron microscopy image processing and analysis

To quantify the number of glutamatergic or GABAergic terminals in the PBG’s “core” versus its “shell” based on the tissue’s ultrastructure, 7x7 (~2000 μm^2) montages of ultrathin sections, with each image taken at a magnification of 10,000x (~7.8 x 5.8 µm), were collected on the electron microscope. These montages were then “stitched” together using image processing software, 3mod. The montages were then pieced together by hand using Microsoft PowerPoint to create a “Montage Collage” for each ultrathin section of interest. To define the “core” and “shell” of the PBG for each collage, an ellipse was drawn around the approximate edge of the outermost cell soma of the core, with a second ellipse drawn around the first with a radius exactly 4 microns larger. This second, larger ellipse defined the bounds of the PBG core for each ultrathin section of interest. The area outside this ellipse containing SC-PBG terminals was defined as the

“shell”. Terminals identified in each collage were marked for quantification using the “sculpt” tool in 3mod, which tracks the number of contours (points in this case) used to create an area of interest. After marking each collage in this way to identify all glutamatergic and GABAergic (labeled with antibodies conjugated to gold particles) terminals, the total number of each was quantified after the PBG core and shell had been spatially defined as described above.

Results

Topography of SC-PBG projections

The injection of two different viruses in different regions of the same SC revealed a coarse topography of SC-PBG projections. For example, injections that induced cells in the medial SC to express TdTomato and cells in the lateral SC to express GFP (Figure 3.1A) labeled projections to the ipsilateral PBG that were largely non-overlapping. Injections in the medial SC labeled axons and terminals in the more rostral regions of the PBG (Figure 3.1B), whereas injections in the lateral SC labeled axons and terminals in more caudal regions of the PBG (Figure 3.1C). Likewise, injections in the rostral and caudal regions of the same SC labeled non-overlapping projections to the ipsilateral PBG. Injections in the caudal SC (Figure 3.1D) primarily labeled projections to the caudal PBG (Figure 3.1F) while injections in the rostral SC labeled projections that primarily targeted the more rostral regions of the PBG (Figure 3.1E). Thus, the SC projections to the mouse PBG roughly preserve the retinotopic organization of the superficial layers of the SC; the rostral PBG likely receives

input from the upper/nasal visual field (represented in the rostral and medial regions of the SC) while the caudal PBG likely receives input from lower/peripheral visual field (represented by the caudal and lateral regions of the SC).

SC projections define "core" and "shell" regions of the PBG

The SC virus injections revealed another organizational feature of the PBG which we define as the "core" (center of the PBG) and "shell" (periphery of the PBG). In fluorescent images, projections from the SC appear to be more densely distributed in the shell of the PBG (particularly apparent in the rostral PBG; Figure 3.1 panels B and E). As described below, our ultrastructural studies revealed that the core contains densely packed somata, while the shell contains more myelinated axons. Thus, the density of SC projections in the shell detected via fluorescence likely represent the abundance of myelinated axons traveling from the SC to innervate the PBG.

GABAergic and parvalbumin-expressing SC-PBG projections

The SC neurons that project to the PBG include at least two distinct populations: neurons that express parvalbumin (Shang et al., 2015, 2018) and GABAergic neurons that do not express parvalbumin (Whyland et al., 2020). These two PBG-projecting populations represent only a fraction of all the GABAergic and/or parvalbumin-expressing neurons within the SC (Villalobos et al., 2018; Whyland et al., 2020). Moreover, these two PBG-projecting populations may be further subdivided, and/or additional populations of SC neurons may

project to the PBG (Gale & Murphy, 2014, 2018; Hoy et al., 2019). However, we focused on these two broad categories for an initial evaluation of SC-PBG circuits. homologues

Viruses were injected in the SC of PV-cre (Figure 3.1G) or GAD2-cre (Figure 3.1J) to induce the expression of GFP in a cre-dependent manner. As previously described (Shang et al., 2015), parvalbumin-expressing neurons densely innervate both the rostral (Figure 3.1H) and caudal PBG (Figure 3.1I). GABAergic SC neurons also innervate the rostral (Figure 3.1K) and caudal PBG (Figure 3.1L). However, GABAergic projections from the SC to the PBG were not as dense as those arising from parvalbumin-expressing neurons in the SC. GABAergic projections from the SC were also densely distributed in regions of the tegmentum surrounding the PBG, whereas projections from parvalbumin SC neurons to the tegmentum surrounding the PBG were sparse.

Ultrastructure and GABA content of SC-PBG terminals

To examine the ultrastructure and distribution of GABAergic and non-GABAergic tectal terminals in the PBG, we injected the SC of C57Blk6 mice with BDA to label SC-PBG terminals and additionally stained sections containing labeled terminals with an antibody against GABA tagged with gold particles. SC-PBG terminals were identified by the DAB reaction product contained within them (Figure 3.2A,B) and were separated into GABAergic (Figure 3.2A) and non-GABAergic (Figure 3.2B) categories based on a qualitative assessment of the density of overlying gold particles. We examined a total of 103 SC-PBG terminals that were engaged in synapses. Of these, only 7 (~7%) were GABAergic,

corroborating the differences in the density of SC projections labeled in PV-cre and GAD-cre mice (Figure 3.1G-L). The PBG dendrites postsynaptic to both GABAergic and nonGABAergic SC terminals were found to be nonGABAergic (i.e. contained a low density of gold particles (Figure 3.2A,B).

To determine whether GABAergic and non-GABAergic SC-PBG populations are differentially innervated by retinal ganglion cells or V1, we placed injections of a virus that is transported transynaptically to expresses cre-recombinase in postsynaptic cells in the eyes or V1 of C57Blk6 mice; we followed these injections with cre-dependent virus injections in the SC to label SC-PBG projection populations with GFP in an input-defined manner. We then used an antibody against GFP to label the terminals in the PBG with a DAB reaction product and prepared the tissue for electron microscopy. As for the BDA-labeled terminals described above, we additionally stained these terminals with an antibody against GABA tagged with gold particles so that we could examine the distribution of GABAergic and nonGABAergic synaptic terminals in the PBG. These experiments did not reveal significant differences in the proportions of GABAergic and nonGABAergic SC-PBG projections arising from neurons that receive input from the retina or V1. For both labeled populations (postsynaptic to retina vs V1 inputs) a modest proportion of labeled terminals in PBG contained GABA. For SC-PBG projections arising from neurons that receive retinal input 9.27% (28 of 302 synaptic terminals) contained GABA. For SC-PBG projections arising from neurons that receive V1 input, 4.8% (11 of 229 synaptic terminals) contained GABA. These proportions were not significantly different

from those revealed in our BDA-injection experiments (7%; p = 0.22004, p = 0.77087, respectively; two proportion z-test). The sizes of GABAergic (0.586µm^2±0.403, n = 39) and nonGABAergic (0.600µm^2±0.456, n = 492) SC-PBG synaptic terminals were also not found to be significantly different (Mann-Whitney, p = 0.7957).

GABAergic and non-GABAergic synaptic terminal density in the PBG "core" and "shell"

We next examined the overall distribution of GABAergic and nonGABAergic terminals in the PBG, comparing "core" and "shell" regions. As illustrated in Figure 3.2F-G), the core contains densely packed neuron somata, while the shell contains a dense distribution of myelinated axons. A total of 1,405 terminal profiles (that contained presynaptic vesicles) were identified in 2 montages of sections that contained the core and shell. The sections were stained with the GABA antibody so that the proportions of GABAergic and nonGABAergic terminals could be quantified. In each montage, a large portion of the terminals contained GABA (montage 1: 44% of terminals in the core and 42% in the shell were GABAergic; montage 2: 49.8% of terminals in the core and 40.9% in the shell were GABAergic). The proportions of GABAergic terminals in the core versus shell were not found to be significantly different (p = 0.98324, two proportion z-test) but both were significantly higher than the proportion of SC-PBG terminals that contained GABA (p < 0.001 [3.71739 x 10^{-60}], two proportion z test). The density of terminal profiles was also similar in the core and shell of the PBG (montage 1: core contained 266 terminals identified within 1693 µm^2 or

0.157 terminals/μm^2, shell contained 336 terminals identified within approximately 2840 μm^2 or 0.118 terminals/μm^2; montage 2: core contained 297 terminals within 2597 μm^2 or 0.114 terminals/μm^2, shell contained 506 terminals within approximately 4063μm^2 or 0.125 terminals/μm^2).The terminal densities were not found be significantly different in the core versus the shell ($p = 0.924712$, two proportion z test).

Nontectal GABAergic terminals in the PBG are labeled in the GAD67-GFP line

Since we found that less than 10% of the labeled SC terminals in the PBG contain GABA, while our montage analysis revealed that over 40% of the terminals in the PBG contain GABA, the PBG must be innervated by other sources of GABAergic neurons. In fact, when we examined confocal images of the PBG in GAD67-GFP mice we observed an abundance of GFP-labeled neurons in the brainstem adjacent to the PBG (Figure 3.3A) and occasional GFP-labeled neurons within the PBG (Figure 3.3E,F). Additionally, in GAD67-GFP mice the PBG contains a dense population of GFP-labeled fibers that can also be labeled with antibodies against vesicular GABA transporter (vGAT; Figure 3.3B), a protein that is contained within synaptic terminals (Chaudhry et al., 1998). In a previous study, we found that GAD67-GFP neurons in the SC do not project to the PBG (Whyland et al. 2020). Therefore, the PBG terminals that contain GFP in the GAD67-GFP line identify an additional, non-tectal source of GABAergic input to the PBG. These may arise from the GFP-labeled neurons in the tegmentum surrounding the PBG and/or the sparse GFP-labeled neurons in the PBG.

PBG Optogenetic activation of GAD2 and PV SC-PBG terminals; GABAergic and glutamatergic postsynaptic responses

To examine the postsynaptic effects of activation of GAD2 and PV SC-PBG terminals, a virus that induces the expression of the light-sensitive cation channel, channelrhodopsin (ChR) in the presence of cre-recombinase was injected into the SC of GAD2-cre and PV-cre mice. Two weeks later, slices of the PBG of injected mice were prepared for *in-vitro* recordings. Whole-cell patch clamp recordings of PBG neurons were obtained and SC-PBG axons and terminals that expressed ChR2 were activated via 1 ms pulses of blue LED light (1, 2, 5, 10, 20 Hz). Examples of the recordings are illustrated in Figure 3.4 and the results are summarized in Tables 1 and 2. In slices from injected GAD2-cre mice, photoactivation of SC terminals consistently elicited inhibitory postsynaptic currents (IPSCs) greater than 200 pA in PBG neurons held at 0mV during voltage clamp recordings (Figure 3.4A). Adding the GABAergic receptor antagonist SR95531 to the circulating ACSF solution extinguished these IPSCs (second trace in panel 3A), confirming that the presynaptic release of GABA was responsible for the observed IPSCs. Wash out of the antagonist from the ACSF solution restored the evoked IPSCs (bottom trace in panel 3A). In contrast, in slices from injected PV-cre mice, photoactivation of SC terminals during current clamp recordings from PBG neurons (resting membrane potentials typically ~ -60mV) consistently elicited excitatory postsynaptic potentials (EPSPs) with amplitudes of 10mV or more (evoked EPSPs triggered action potentials in 5 of the recorded neurons). Adding the NMDA receptor antagonist APV and the

AMPA receptor antagonist CNQX abolished the EPSPs (second trace, panel 3B). Wash out of these glutamatergic receptor antagonists restored the evoked EPSPs (bottom trace, panel 3B). In summary, these experiments confirmed that GAD2 SC neurons release GABA in the PBG, PV SC neurons release glutamate in the PBG, and these two inputs elicit opposing effects on their postsynaptic targets.

GABAergic and glutamatergic inputs convergence on single PBG neurons

Next, we tested whether these GABAergic and glutamatergic SC inputs synapse on separate PBG populations or whether they converge to innervate single PBG neurons. For these experiments, we injected a virus in the SC to express ChR2 in a non-cre-dependent manner. Then in slices from injected mice we photoactivated SC terminals while recording from PBG neurons voltage clamped at 0 mV or -60mV. These experiments revealed that the majority of responsive PBG neurons (18/26, 69.2% of responsive cells) responded with both IPSCs and EPSCs. Example traces are illustrated in Figure 3.4 and the results summarized in Table 2. In the example trace shown in Figure 3.4C, 1 ms blue light pulses evoked IPSCs of ~50 pA while the cell was held at 0 mV. When the same cell was held at -60 mV blue light pulses evoked EPSCs of ~100 pA (Figure 3.4D). Another example of these mixed responses recorded from the same PBG neuron is shown in panels 3E and 3F. It should be noted that the amplitudes of evoked EPSCs were often larger than their IPSC counterparts, and additionally that most cells that did not have mixed responses only responded with EPSCs (6/8, 75%). As summarized in Table 2, the average ratio of EPSC to

IPSC maximum amplitudes recorded in single PBG neurons was 1.74 ± 1.29. This observation is congruent with virus labeling and electron microscopic results which suggest that GABAergic terminals make up a minority of the input from the SC to the PBG. Finally, as summarized in Table 2, both EPSC and IPSC amplitudes increased in amplitude during the course of 10Hz photostimulation (a paired pulse ratio was quantified by dividing the average amplitude of the 2nd through 10th EPSC/IPSC by the amplitude of the first EPSC/IPSC in the train). For EPSCs, the mean paired pulse ratio @ 10 Hz was 1.206. For IPSCs, the mean paired pulse ratio @ 10 Hz was 1.011. These ratios were not found to be significantly different (Mann-Whitney, p = 0.3178).

Table 1: GABAergic and glutamatergic responses to SC input and PBG morphology

Responsive cells N = 40	Max Amplitude @ 10 Hz	Membrane Resistance	Filled Cells (n)	Stellate	Asymmetric	Narrow Field
Cre-dependent AAV in SC of PV-Cre, current clamp recordings, n = 13	15.11 mV (±6.6)	302 MΩ (±139)	(8/13)	(2/8)	(4/8)	(2/8)
Non-cre-dependent AAV in SC, current clamp recordings, n = 20	11.77 mV (±7.06)	663 MΩ (±199)	(11/20)	(5/11)	(4/11)	(2/11)
All current clamp recordings n = 33	13.09 mV (±6.97)	521 MΩ (±250)	(19/33)	(7/19)	(8/19)	(4/19)
Cre-dependent AAV in SC of GAD2-cre, voltage clamp recordings, n=7	*274.5 pA (±209).*	--------	(0/7)	(0/7)	(0/7)	(0/7)
Non-responsive filled cells current clamp n=26	------	542±180 MΩ	26	20/26	4/26	2/26
Non-responsive filled cells voltage clamp n=6	------	-------	6	3/6	1/6	2/6

Table 2: GABAergic and glutamatergic SC input convergence and PBG morphology

Non-cre-dependent AAV in SC, voltage clamp recordings	Max Amplitude EPSC (-60mV, 10 Hz)	Max Amplitude IPSC (0mV, 10 Hz)	EPSC/IPSC Ratio (max amplitudes @ 10 Hz)	Mean Paired Pulse Ratio @ -60 mV (10Hz)	Mean Paired Pulse Ratio @ 0 mV (10Hz)
All responsive n = 26	251.2 pA (±235.8)	174.1 pA (±113.2)	1.74 (±1.29)	1.206 (±0.481)	1.011 (±0.191)
Stellate n = 8	218.8 pA (±138.7)	142.3 pA (±45.6)	1.71 (±1.12)	1.193 (±0.413)	1.017 (±0.167)
Asymmetric n = 5	298.8 pA (±213.5)	180.3 pA (±54.2)	1.97 (±1.45)	1.262 (±0.313)	0.964 (±0.07)
Narrow-Field n = 3	457.2 pA (±338.3)	166.7 pA (±51.4)	2.91 (±1.08)	1.567 (±0.847)	0.897 (±0.143)
Unfilled n = 7	180.1 pA (±190.3)	200 pA (±178.5)	0.99 (±0.87)	1.0 (±0.233)	1.088 (±0.246)
Other Statistics:	**Fired Only Action Potentials at -60 mV n = 3**	**Voltage Clamp Excitatory Reponses only n = 4**	**Voltage Clamp Inhibitory Reponses only n = 2**	**Voltage Clamp Excitatory Response at 0 and -60 mV n = 2**	**Excitatory and Inhibitory Responses n = 18**

PBG cell morphology

We next wanted to determine whether any of the morphological features of the PBG cells filled with biocytin during in our *in-vitro* slice experiments correlated with recorded physiological characteristics. As illustrated in Figure 3.5, the biocytin-filled PBG neurons exhibited a variety of sizes and morphologies. As described in the methods section, Sholl ring analysis of dendritic arbors was used to categorize biocytin-filled PBG neurons as stellate, asymmetric, narrow-field symmetric, or narrow-field asymmetric. Examples of each cell type are shown in Figure 3.6. We were able to successfully fill 70 PBG neurons in our slice experiments. Whether these cells were responsive to optical stimulation or not, the majority of biocytin-filled cells were categorized as stellate (37 of 70 or 52.9%), with asymmetric cells forming the next largest group (21 of 70 or 30%). Narrow-field cells formed the smallest group (12/70, 17.1%), with the majority of these categorized as narrow field symmetric (8 of 12 or 66.6% symmetric, 4 of 12 or 33.3% asymmetric). However, with exception of soma size which had a

modest inverse correlation to membrane resistance (measured in current clamp experiments, n = 23; correlation coefficient: -0.467; p = 0.0248), none of the other physiological characteristics that we measured exhibited a strong correlation with the morphologies analyzed (max amplitude of responses, EPSC/IPSC ratio, and paired-pulse ratios; Kruskal Wallis, p>0.9999 for most comparisons).

Discussion

Our anatomical and physiological dissections of SC-PBG circuits in the mouse yielded the following conclusions: 1) SC-PBG projections exhibit a rough topography which may preserve the retinotopy of the SC. 2) The PBG can be divided into “core” regions that contain densely packed somata, and “shell” regions that contain more myelinated axons, but both regions contain similar densities of synaptic terminals. 3) GABAergic and nonGABAergic SC neurons that project to the PBG receive input from the retina and V1. 4) Less than 10% of SC projections to the PBG contain GABA. 5) Approximately 40% of the overall input to the PBG is GABAergic. 6) Terminals labeled in GAD67-GFP mice indicate the PBG receives GABAergic input from nontectal sources. 7) GABAergic SC-PBG projections do not contain parvalbumin and inhibit PBG neurons. 8) SC-PBG projections that express parvalbumin release glutamate to excite PBG neurons. 9) Most PBG neurons receive convergent excitatory and inhibitory input from the SC. 10) PBG neurons exhibit a variety of dendritic morphologies but these did not correlate with the physiological properties measured in the current study. These conclusions are discussed in further detail below.

Topography and core/shell organization of the SC-PBG projections

Our virus injections indicate that the rostral/medial SC targets the rostral PBG while the caudal/lateral SC targets the caudal PBG. Thus, the rostral PBG of the mouse likely receives input from the upper/nasal (binocular) visual field while the caudal PBG likely receives input from lower/peripheral visual field. Retrograde tracing experiments in the common Degu, a diurnal rodent, show a similar pattern. In this species, parasagittal sections revealed that the PBG can be clearly divided into anterior and posterior subdivisions, each with distinct reciprocal connectivity with the SC; cells located in the rostral/medial SC tended to project to the rostral PBG, while cells located in the caudal/lateral SC projected to the caudal PBG (Deichler et al., 2020). Moreover, it was found that the rostral PBG projects to the rostral/medial regions of the contralateral SC, suggesting that the rostral subdivision of the PBG may be specialized for the detection of predators in the binocular visual field (Deichler et al., 2020; Tokuoka et al., 2020). In the cat, physiological recordings and retrograde tracing from the SC also indicate that the PBG is retinotopically organized and that the rostral PBG may be a specialized zone representing the binocular visual field (Sherk, 1979b; Sherk 1978)..

Our virus labeling experiments also highlighted an intriguing pattern of innervation in the PBG in which the edges of the nucleus (“shell”) consistently appear more densely innervated by SC inputs. Our ultrastructural analysis indicates that this pattern may simply reflect the high density of myelinated axons in the periphery of the nucleus. Although the center (“core”) of the nucleus

contains more somata, we found that the density of synaptic terminals in each region was similar. Therefore, SC axons may enter the PBG from the “shell” but it does not appear to be more extensively innervated relative to the “core”.

GABAergic and glutamatergic SC projections converge on single PBG neurons

Our *in vitro* physiology experiments confirmed the presence of two SC-PBG projection populations with opposing effects on the PBG: GABAergic neurons that don’t contain parvalbumin inhibit PBG neurons, and glutamatergic neurons that do contain parvalbumin excite PBG neurons. While our electron microscopy studies indicate that less than 10% of the SC input to the PBG is GABAergic we found that the majority of PBG neuron receive both GABAergic and glutamatergic input from the SC. Thus, the GABAergic and glutamatergic SC-PBG pathways are not segregated in the PBG but converge to influence the receptive field properties of most PBG neurons.

Transynaptic retrograde tracing studies have revealed that SC-PBG neurons cells receive input from retinal ganglion cells, V1, as well as other sources (Reinhard et al., 2019). Anterograde transsynaptic tracing studies suggested that V1 does not innervate GABAergic projection cells in the SC (Zingg et al., 2017). Thus, we reasoned that the use of transsynaptic viral tracing techniques to label SC neurons that receive input from V1 would not label any GABAergic synaptic terminals in the PBG. Instead, we found no differences in the proportion of GABAergic and nonGABAergic SC-PBG terminals following BDA injections in SC, or in experiments where we transynaptically labeled SC

neurons that receive input from the retina or V1. Therefore, whether GABAergic and nonGABAergic SC-PBG neurons receive distinct presynaptic inputs remains an open question.

Morphology of PBG neurons

The mouse PBG is approximately ~250-300 microns in its anterior-posterior extent and ~100-150 microns in its mediolateral extent. Yet, within this small, tightly packed space we found that biocytin-filled PBG cells exhibited a wide variety of morphologies. Since SC-PBG projections are organized in a topographic manner, the orientation of PBG dendrites is likely an important component of the construction of their receptive field properties. Therefore, using criteria similar to those used to categorize SC neurons (Gale & Murphy, 2014; Whyland et al., 2020), we divided the PBG neurons into four groups: stellate, asymmetrical, and narrow field (asymmetric vs symmetric). In a previous study conducted in rats in which PBG neurons were also filled via biocytin, most filled neurons' dendrites were oriented toward the lateral wall of the midbrain, with fewer cells having more of a dorsal-ventral orientation ("cylindrical shape") (Goddard et al., 2007). Our biocytin-filled neurons showed a greater diversity of shapes and orientations, comparable to previous descriptions of rat PBG neurons based on Golgi staining techniques (Tokunaga & Otani, 1978). In this Golgi study, PBG neurons were also placed into four categories, which were similar to those we used: pyramidal (stellate), fusiform (stellate or narrow-field symmetrical), hemispheric (asymmetrical), and cylindrical (narrow-field, either type).

While we did not detect structure-function correlations in our study, parameters that we measured were limited. PBG morphology may be related to projection target, a feature we did not investigate in the current study. The PBG projects to the ipsilateral pulvinar, and bilaterally to the dorsal lateral geniculate nucleus (dLGN), central amygdala, and SC (Diamond et al., 1992; Shang et al., 2015, 2018; Sokhadze et al., 2022; Usunoff et al., 2007; Whyland et al., 2020). Retrograde tracing studies have revealed that PBG neurons can branch to innervate several different contralateral targets, while ipsilateral projections arise from separate populations of PBG neurons (Sefton & Martin, 1984; Usunoff et al., 2006, 2007). Moreover, several studies have noted that PBG neurons that project to the contralateral SC are larger than those that project to the ipsilateral SC, and additionally that the PBG forms anterior/posterior subdivisions corresponding to these contralateral or ipsilateral projections, respectively (Baizer et al., 1991; Deichler et al., 2020; Jen et al., 1984; Jiang et al., 1996; Künzle & Schnyder, 1984; Watanabe & Kawana, 1979) . Most PBG neurons express choline acetyl transferase (but not the vesicular acetylcholine transporter, VAChT; Sokhadze et al., 2022), and the type 2 vesicular glutamate transporter (vGlut2). However additional protein expression patterns may be limited to subsets of PBG neurons (Y. Q. Wang et al., 1988). Subsets of PBG neurons are also labeled in a variety of transgenic mouse lines including NTSR1-GN209-Cre and ChAT-Cre mice (Gale & Murphy, 2014; Sokhadze et al., 2022). Therefore, future studies may reveal that projection targets and or protein

expression patterns are related to features that we quantified in our characterization of PBG morphology.

GABAergic projections to the PBG from nontectal sources

Our electron microscopic analysis revealed that approximately 40% of the synaptic terminals in the PBG contain GABA, but that less than 10% of SC-PBG projections contain GABA. This discrepancy suggests that the PBG receives an additional nontectal source of GABAegic input. In fact, we found that in GAD67-GFP mice, the PBG contains may GFP/vGAT-labeled puncta. Since we previously determined that SG-PBG neurons do not contain GFP in the GAD67-GFP line (Whyland et al., 2020), we conclude that these GFP-labeled puncta in the PBG do not originate from the SC. It is unlikely that these projections originate from distant sources since previous retrograde tracing studies have concluded that the SC is the sole source of input to the PBG (Sherk 1979b). These studies would have necessarily excluded neurons labeled in and around the injection sites from analysis. Therefore, these nontectal GABAergic inputs likely originate from neurons in and around the PBG that contain GFP in the GAD67-GFP line.

The avian nucleus isthmi contains a subdivision of GABAergic neurons, the nucleus isthmi magnocellularis (Imc) which projects to the optic tectum as well as the cholinergic neurons of the nucleus isthmi parvocellularis (Ipc; Asadollahi et al., 2011; Goddard et al., 2014; Mysore & Knudsen, 2013; Schryver & Mysore, 2019). The Imc has been proposed to provide global inhibition of the tectum and the Ipc as part of a proposed “stimulus selection network” that boosts

the transmission of salient stimuli while suppressing nonrelevant stimuli (Asadollahi et al., 2010; Asadollahi & Knudsen, 2016; Schryver & Mysore, 2019). (Marín et al., 2007). Retrograde tracing studies in mammals have identified GABAergic neurons in the peri-parabigeminal area that project to the SC (Apell and Behan). If these GABAergic peri-parabigeminal neurons also project to the PBG, their function might be similar to that suggested for the avian Imc.

It is also possible that the PBG contains intrinsic GABAergic interneurons. In the GAD67-GFP line we identified a small number of GFP-labeled neurons within the PBG, and previous Golgi studies have suggested that PBG neurons might be divided into intrinsic neurons and projection neurons (Tokunaga & Otani, 1978). We did not identify any dendrodendritic connections in our electron microscopic images, and we did not identify any axon-like projections within the PBG originating from the neurons we filled with biocytin. However, thin axons are often difficult to fill with biocytin, axons projections may have exited our 300 μm thick slices, and if interneurons are sparse, they may not have been included in our sample. The GAD67-GFP, GAD2-cre and/or other mouse lines may be useful for future investigations of this previously unrecognized complexity of PBG circuits.

Functional implications

As outlined in the Introduction, PBG neurons respond to looming and sweeping visual stimuli, exhibit direction-selective responses, and may further encode the saliency of signals to contribute to the initiation of appropriate behavioral responses (Reinhard et al., 2019 and others from intro). In fact,

optogenetic and chemogenetic manipulations of tectal inputs to the mouse PBG have been found to alter behavioral responses. Optogenetic activation of PBG inputs that originate from parvalbumin neurons initiate escape responses (Shang et al., 2015, 2018), while chemogenetic inactivation of NFV SC neurons that project to the PBG (in the Grp-KH288-cre line) impairs accurate orienting and pursuit in a prey capture paradigm which is dependent on binocular vision (Allen et al., 2022; Berson, 2021; Hoy et al., 2019; Johnson et al., 2021).Thus, there is substantial evidence that PBG circuits in the mouse play important roles in visually-guided behavior.

Our study revealed previously unappreciated complexities in the circuits of the PBG that likely impact the initiation and choice of behavioral responses. We found that most PBG neurons receive convergent excitatory and inhibitory inputs from the SC and that additional GABAergic inputs may arise from neurons in and around the PBG. Moreover, we found that the dendritic arbors of PBG vary widely in their orientations and extent. While it is still unclear how these circuits details impact PBG responses and subsequent animal behavior, they serve to direct future anatomical studies and may help to inform and interpret current and future functional studies.

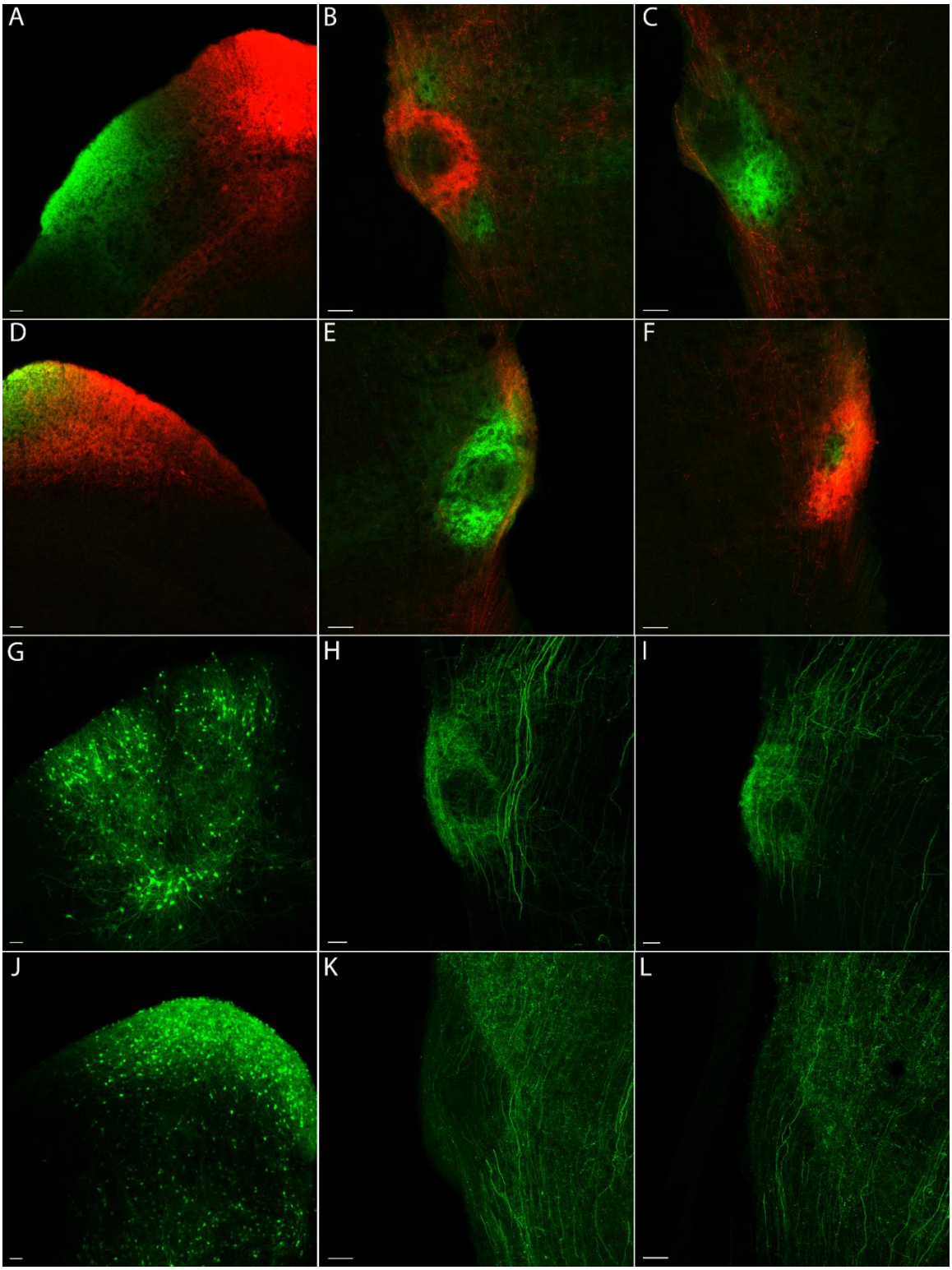

Figure 3.1. Viral tracer injections into the superior colliculus demonstrate SC-PBG projection patterns. A) A coronal section of the SC shows how an injection

of an AAV that expresses the fluorophore tdTomato in all neuronal cell-types into the medial SC labels axon projections primarily to the rostral PBG in (B), while an AAV injection that expresses GFP into the lateral SC (A) labels projections primarily to the caudal PBG (C). D) A coronal section of the caudal SC demonstrates how an AAV targeted to the caudal SC that expresses tdTomato primarily labels axon projections to the caudal PBG (F), while an AAV injected into the rostral SC that expresses GFP mostly labels axon projections to the rostral PBG (E). G) A cre-dependent AAV injected into the SC of a transgenic mouse that expresses cre-recombinase in parvalbumin-positive neurons, labels a dense population of PV+ cells and their projections to the rostral and caudal PBG with GFP (H and I, respectively). J) Similarly, a cre-dependent AAV injection into the SC of a GAD2-Cre transgenic mouse labels a dense population of GABAergic neurons in the SC as well as their projections to both rostral and caudal PBG (K and L, respectively). Scale bars = 50 µm in all panels.

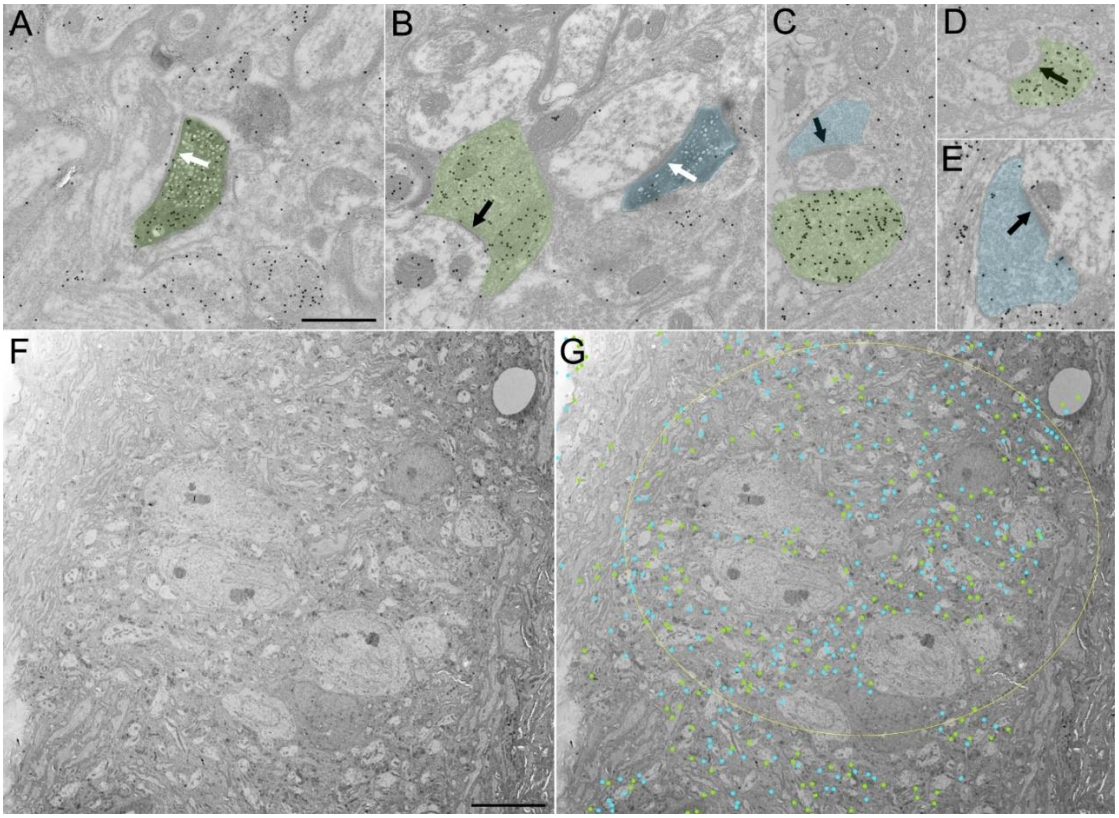

Figure 3.2. Electron micrographs show an abundance of both GABAergic and non-GABAergic terminals throughout the PBG's "core" and "shell" regions. A) A BDA-labeled GABAergic axon terminal (green) originating from the SC, as identified by a high relative density of gold particles and synaptic vesicles, makes a synapse (white arrow) with a nonGABAergic cell in the PBG. B) A GABAergic (green) terminal and BDA-labeled, non-GABAergic (blue) terminal make synapses (black and white arrows, respectively) near each other within the PBG. Two unlabeled terminals within one of the EM montages, one GABAergic (green) and the other nonGABAegic (blue), are separated by a small dendritic process where the non-GABAergic terminal makes a synapse (black arrow). D-E) Example GABAergic (green, D) and nonGABAergic (blue, E) axon terminals making synapses (black arrows) within one of the EM montages of PBG. F) Low

magnification image of the PBG's core in an ultrathin section that was analyzed for GABAergic and non-GABAergic axon terminal density. G) Same image as in (F) but with labeling showing the approximate location of axon terminals (green dots denote GABAergic terminals, blue dots denote non-GABergic terminals, yellow ellipse denotes the PBG "core") identified by analysis of a montage collage covering the same region of the PBG ultrathin section. Scale bars in (A-E) = 600 nm, (F, G) = 8 µm.

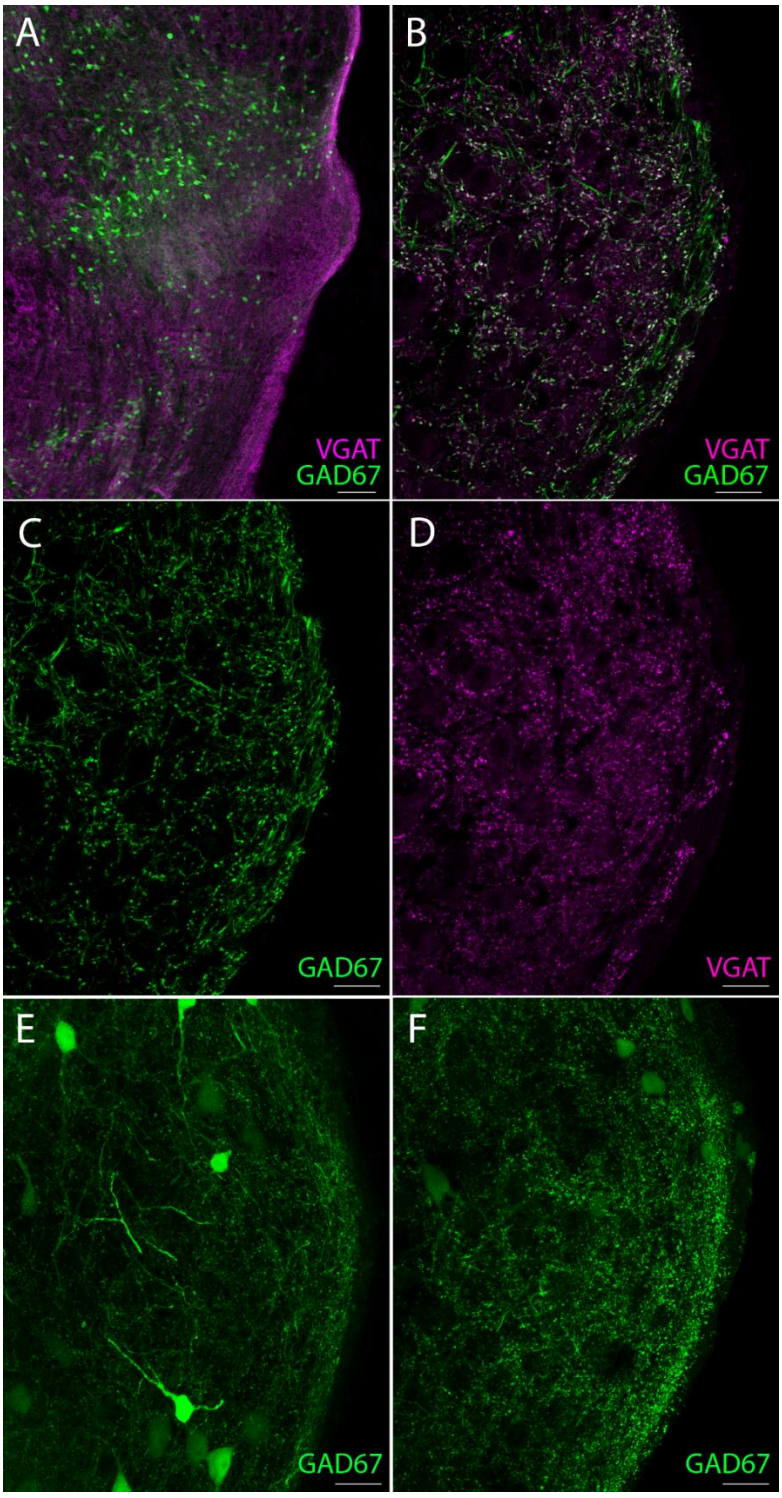

Figure 3.3. GAD67 neurons in brainstem areas adjacent to the PBG provide another source of GABAergic terminals in the PBG. A) Low magnification

confocal image of numerous GAD67 neurons (green), fluorescently labeled with GFP in the GAD67-GFP reporter mouse, occupying areas of the brainstem just medial to the PBG (lateral protrusion) which is clearly labeled with an antibody stain for vesicular GABA transporter (VGAT, magenta). B) High magnification confocal image of GAD67 (green) and VGAT+ (magenta) fibers intermingled in the PBG, with many fibers clearly co-labeled (white). C) Same image as in (B) but with only GAD67 fibers shown. D) same image as in (B) but with only antibody labeled VGAT+ fibers shown. E-F) Two other confocal image examples of the PBG where GAD67 fibers are seen throughout the nucleus as well as a few GAD67+ somas. Scale bar in (A) = 100 µm, (B-F) = 20 µm.

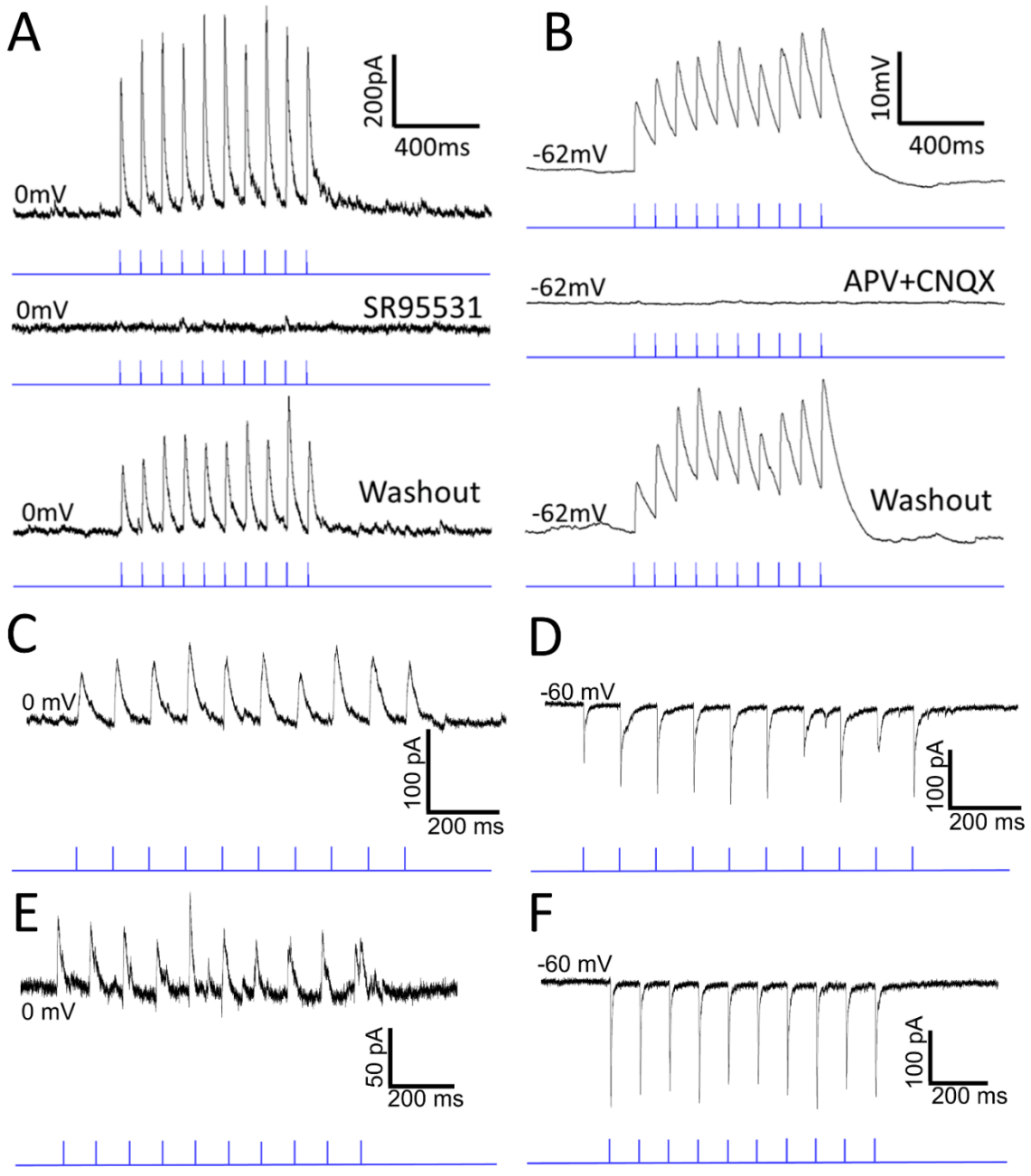

Figure 3.4. Whole-cell patch clamp recordings in the PBG confirm both excitatory (PV+) and inhibitory (GABA) inputs from the SC. Panel (A) shows a current trace from an *in vitro* whole-cell patch clamp experiment in which a cre-dependent AAV that expresses the light-sensitive cation channel, Channelrhodopsin, was injected into the SC of a GAD2-Cre transgenic mouse in which GABAergic neurons

express cre-recombinase. Optical stimulation of axon terminals in the tissue slice with 1 ms pulses of blue light reliably produces IPSCs (top trace) in the patched neuron that can be extinguished (middle trace of A) via the administration of the selective GABA-A antagonist SR95531 into the circulating ACSF, confirming the presence of GABAergic inputs to the PBG. After washing out this antagonist, the same cell resumes IPSC responses to optical stimulation (bottom trace of A). Panel (B) shows a voltage trace from a similar experiment in which a cre-dependent AAV was injected into a transgenic mouse in which cre-recombinase is expressed instead in parvalbumin-positive cells. Optical stimulation of axon terminals in the tissue slice reliably evoked EPSPs that could be silenced with the administration of the NMDA and AMPA blockers, APV and CNQX, confirming that PV+ SC-PBG projections are glutamatergic. Washing out these antagonists recovered the excitatory responses seen in the first trace of B (bottom trace of B). C) An example current trace demonstrates how in patch clamp experiments in which a non cre-dependent AAV was injected into the SC instead (thus infecting all neuronal cell-types), both IPSCs (C) and EPSCs (D) can be reliably evoked depending on what voltage the patched cell is held at (0 or -60 mV, C and D respectively). E-F) Voltage traces from another example recorded neuron in which both IPSCs and EPSCs could be reliably evoked via optical stimulation of axon terminals in the tissue slice by varying the voltage the patched cell was held at, thus confirming that PBG cells can receive convergent inputs from both excitatory (PV) and inhibitory (GABA) sources residing in the SC.

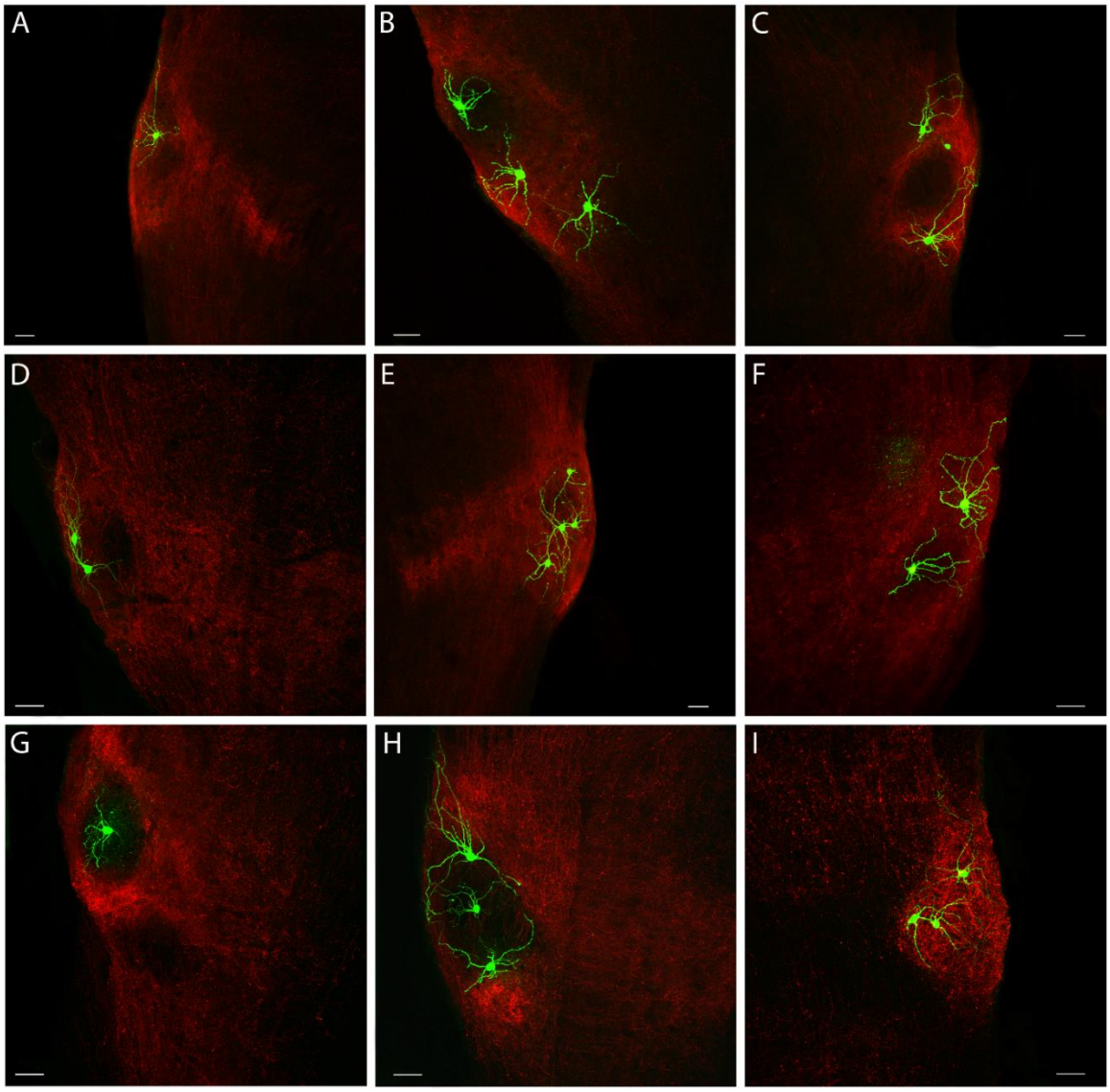

Figure 3.5. Biocytin-filled cells from slice physiology experiments in the PBG exhibit a variety of neuronal morphologies. A-I) The addition of biocytin to the internal recording solution in our whole-cell *in vitro* physiology experiments enabled the visualization of patched cells in green (GFP). These cells exhibited a wide array of morphologies in the example coronal sections shown despite belonging to the relatively small PBG. The AAVs injected into SC to express Channelrhodopsin in SC-PBG neurons of interest also express the red

fluorophore tdTomato, allowing for the visualization of the infected SC-PBG axons and their terminals in PBG (all panels). Scale bars = 50 µm for all panels.

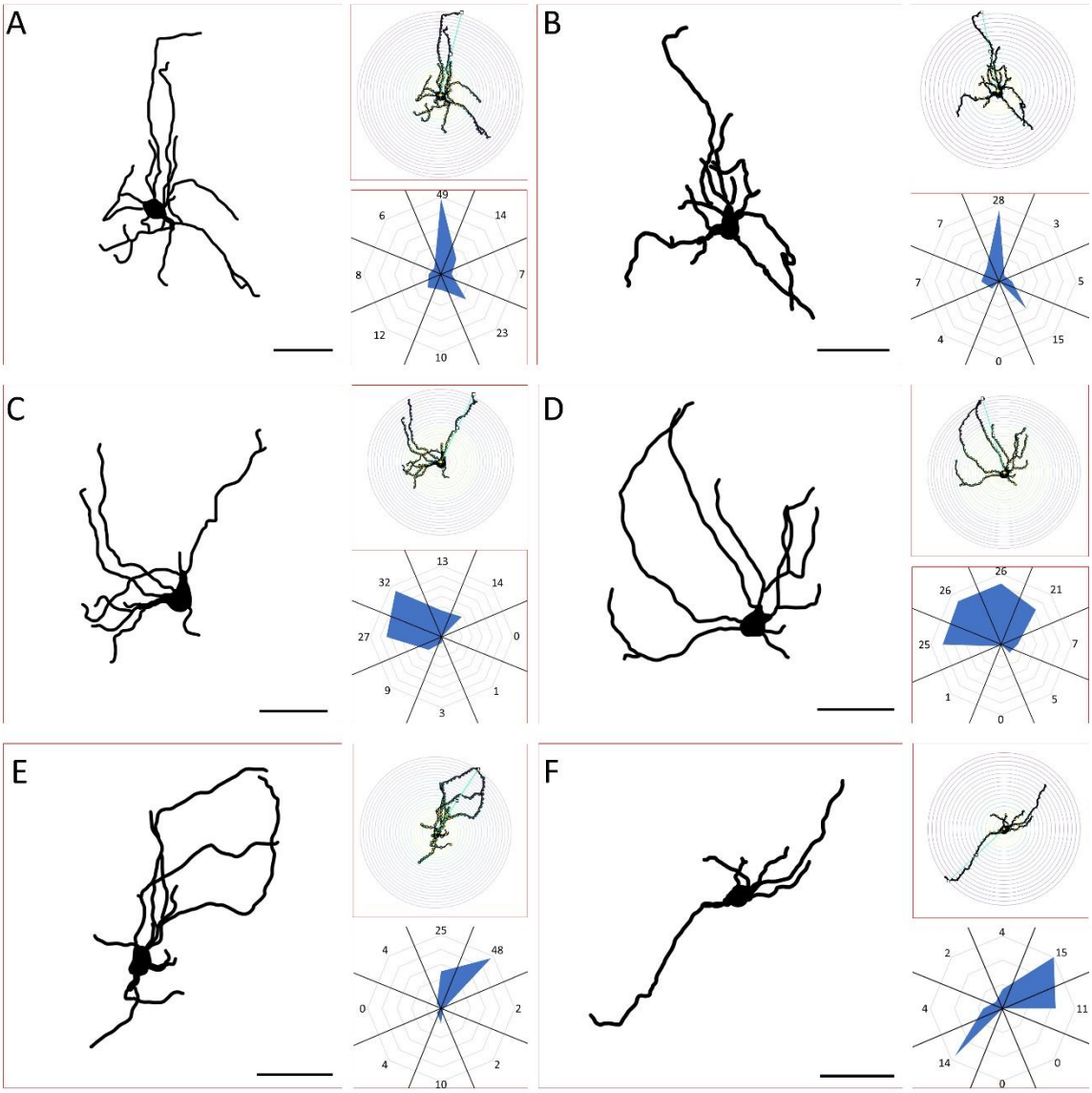

Figure 3.6. Classification of PBG morphological cell types**.** A-B) Example traces from biocytin-filled PBG neurons classified as stellate can be seen in the large panels, accompanied to the right by their respective Scholl ring diagrams (top, small panels) and radar orientation plots (bottom, small panels), demonstrating how their morphological characteristics were quantified for each. Neurons where

4 contiguous radial sections always comprised 20% or more of the total Scholl ring crossings were considered stellate. C-D) Example traces of PBG neurons classified as asymmetric. Asymmetric cells had 4 contiguous radial sections comprising less than 20% of the total Scholl ring crossings. E-F) Example traces of PBG neurons classified as narrow field, with one example of an asymmetric narrow field cell (E) and one example of a symmetric narrow field cell (F). Narrow field cells had two radial sections on opposite sides comprising more than 50% of the total Scholl ring crossings.

CHAPTER IV: THE PARABIGEMINAL NUCLEUS IS A SOURCE OF "RETINAL REPLACEMENT TERMINALS" IN MICE THAT LACK RETINOFUGAL INPUT

Introduction

Vision loss early in life, or as a consequence of adult-onset disease or trauma has a major impact on the form and function of retino-recepient targets in the brain (Ptito et al., 2021). For example in the dorsal lateral geniculate nucleus (dLGN, the thalamic relay of retinal signals en route to the visual cortex), the absence or elimination of retinal input leads to a number of degenerative effects including an overall shrinkage of the dLGN, a loss of dLGN neurons, a reduction in soma size as well as a decrease in the dendritic complexity of remaining neurons (Abbott et al., 2015; Bhandari et al., 2022; El-Danaf et al., 2015; Gupta et al., 2009). While these studies have focused largely on the structural integrity and cellular composition of the dLGN, recent evidence suggests that the vision loss also alters the connectivity between the dLGN and central structures that do not receive retinal input (Brooks et al., 2013; Frangeul et al., 2016; Giasafaki et al., 2022; Grant et al., 2016; Seabrook et al., 2013; Sokhadze et al., 2018). Indeed, a deeper understanding of these axon target interactions, especially at

the ultrastructural level, is a critical first step in developing effective treatments for the restoration of vision following disease or trauma (Goldberg et al., 2016).

Retinal ganglion cells normally innervate the dLGN with large terminals that contain round vesicles and pale mitochondria (RLP profiles; Bickford et al., 2010; Hammer et al., 2015). Synaptic profiles exhibiting this ultrastructure are missing in congenitally anophthalmic mice (Cullen & Kaiserman-Abramof, 1976; Kaiserman-Abramof, 1983), microphthalamic mice (Winkelmann et al., 1985), enucleated mice (Cullen & Kaiserman-Abramof, 1976; Kaiserman-Abramof, 1983), or mice in which retinal ganglion cells fail to develop and lack retinofugal projections (El-Danaf et al., 2015). In the absence of RLP profiles, these previous ultrastructural studies have noted the presence of large terminals in the dLGN that appear to assume the location and synaptic targets of the missing retinal terminals. In particular, except for the fact that these terminals contain dark mitochondria, these “retinal replacement terminals” exhibit most of the ultrastructural features of retinogeniculate terminals, that is, large size, round synaptic vesicles, synaptic contacts on the dendrites of thalamocortical relay cells (including dendritic protrusions), and the dendrites of interneurons (including dendritic terminals or F2 profiles; Bickford et al., 2010; Hammer et al., 2015; Morgan & Lichtman, 2020). However, the source of these terminals remains unclear.

In the absence of retinal input, two sources of replacement terminals have been suggested. First, it has been reported that axons of layer V cortical neurons aberrantly innervate the dLGN following enucleation (Grant et al., 2016) and

could potentially assume the morphology of retinal terminals. It has also been reported that projections from the midbrain parabigeminal nucleus (PBG) to the dLGN increase following enucleation and may assume the morphology of retinal terminals (Stevenson & Lund, 1982). An expansion of projections from the PBG to the dLGN has also been observed in a mutant mouse line that lacks math5, a transcription factor needed for the differentiation of retinal ganglion cells from progenitors. As a result, retinal ganglion cells fail to develop in math5$^{-/-}$ mice, an optic nerve does not develop, and these mice lack retinofugal projections (Charalambakis et al., 2019; El-Danaf et al., 2015; Seabrook et al., 2013; Sokhadze et al., 2018; Wang et al., 2001). In this line, PBG projections expand to fill both the ipsilateral and contralateral dLGN (Sokhadze et al., 2018). To test whether the cortex and/or the PBG are the source or retinogeniculate replacement terminals in math5–/– mice, we compared the ultrastructure of geniculate terminals that originate from the cortex or PBG labeled in this line with geniculate terminals that originate from the retina, cortex or PBG labeled in wild-type (WT) mice with intact retinal projections.

Methods

All breeding and experimental procedures were approved by the University of Louisville Institutional Animal Care and Use Committee. Experiments were carried out using mice, of either sex, of C57BL/6J (IMSR Cat# JAX_000664, RRID: IMSR_JAX:000664), a line in which most layer five, and a subset of layer six, cortical neurons express Cre-recombinase (Tg (Rbp4-cre) KL105Gsat; RRID: MMRRC_036400- UCD), a line that fails to develop an optic

nerve or retinofugal projections due to a >95% loss of retinal ganglion cells during early development (math5−/−; El-Danaf et al., 2015; Seabrook et al., 2013; Wang et al., 2001; RRID: MMRRC_042298-UCD), and math5−/− mice crossed with Rbp4-cre mice.

Tracer and virus injections

To label projections from the cortex, parabigeminal nucleus (PBG), or superior colliculus (SC), adult mice (median age postnatal day 47) were deeply anesthetized with a mixture of ketamine (100–150 mg/kg) and xylazine (10–15 mg/kg). The analgesic meloxicam (5 mg/kg) was also injected prior to surgery. The animals were then placed in a stereotaxic apparatus (Angle Two Stereotaxic, Leica, Wetzlar, Germany). An incision was made along the scalp, and a small hole was drilled in the skull overlying the primary visual cortex (V1; 3.4 mm caudal to Bregma, 2.4 mm lateral to midline, 1.15 mm ventral to Bregma), the PBG (4.3 mm caudal to Bregma, 1.85 mm lateral to midline, 3.2 mm ventral to Bregma), or the SC (3.75 mm caudal to Bregma, 0.6 mm lateral to midline, 1.3 mm ventral to Bregma) . Adeno-associated viruses (AAVs; AAV1-DIO-Matrix-dAPEX2, gift from David Ginty; Addgene plasmid #117177; RRID: Addgene_117177), AAV1-Matrix-dAPREX2 (Addgene plasmid# 117176; RRID: Addgene_117176), AAV9-Ef1a-DIO-dAPEX2 (Addgene plasmid #117174; RRID: Addgene_117174), AAV8.2-DIO-mCherry-WPRE (RRID: Addgene_50459-AAV8), pAAV1- CAG-GFP (RRID: Addgene_37825-AAV1), or the tracer biotinylated dextran amine (BDA, Invitrogen) were injected unilaterally in V1, PBG, or the SC. For BDA injections, a glass pipette (10 µm tip diameter)

containing a 5% solution of BDA in saline was lowered into V1, and BDA was iontophoretically ejected using 3 μA continuous positive current for 20 min. The viruses were delivered via a 34-gauge needle attached to a Nanofil syringe inserted in an ultramicropump. The needle was lowered into V1, PBG or the SC and volumes of 70–120 nl were injected at a rate of 30 nl/min. After removal of the pipette or needle, the scalp skin was sealed with tissue adhesive (n-butyl cyanoacrylate), and the animals were placed on a heating pad until mobile. Post-surgery, animals were carefully monitored for proper wound healing, and meloxicam (5 mg/kg) was administered for 48 h. To label projections from the retina, C57Blk6 pups (p15-18) received unilateral intravitreal injections of AAV1-Matrix-dAPREX2. Each pup was anesthetized with isoflurane via a small nose cone, the sclera was pierced with a sharp-tipped glass pipette, and excess vitreous was drained. Another pipette filled with the AAV solution was inserted into the hole made by the first pipette. The pipette containing the AAV was attached to a picospritzer and a volume of approximately 1 μl of solution was injected into the eye. The nose cone used to administer isoflurane was then removed and, once alert, the pup was returned to the cage containing the dam and littermates.

Electron microscopy (V1, PBG, and retinogeniculate terminal ultrastructure)

One week following BDA injections, 2 weeks following V1 or PBG virus injections, and 2–3 weeks after intravitreal injections, mice were transcardially perfused with 2% paraformaldehyde and 2% glutaraldehyde in 0.1 M phosphate

buffer at pH 7.4 (PB). The brains were removed from the skull and placed in the fixative solution overnight at 4◦C. The next day, the brains were cut using a vibratome into coronal sections at a thickness of 70 µm. Sections from virus-injected animals were reacted with nickel-enhanced diaminobenzidine (DAB) immediately after sections were cut to prevent loss of enzyme activity. Sections from BDA-injected animals were placed overnight in a solution of avidin and biotinylated horseradish peroxidase (ABC solution, Vector Laboratories). The following day, after rinsing in PB, the sections were reacted with nickel-enhanced DAB.

Sections that contained DAB-labeled axons and terminals were postfixed in 2% osmium tetroxide, dehydrated in an ethyl alcohol series, and flat embedded in Durcupan resin between two sheets of Aclar plastic (Ladd Research, Williston, VT). Durcupan–embedded sections were first examined with a light microscope to select areas for electron microscopic analysis. Selected areas were mounted on blocks, ultrathin sections (60–80 nm, silver-gray interference color) were cut using a diamond knife, and sections were collected on Formvar-coated nickel slot grids. Selected sections were stained for the presence of GABA. A postembedding immunocytochemical protocol described previously (Bickford et al., 2010; Masterson et al., 2019; Zhou et al., 2018) was employed. Briefly, we used a 0.25 µg/ml concentration of a rabbit polyclonal antibody against GABA (Sigma-Aldrich, St. Louis, MO, catalogue #A2052, RRID:AB_477652, immunogen was GABA conjugated to bovine serum albumin using glutaraldehyde; the GABA antibody shows positive binding with GABA and

GABA-keyhole limpet hemocyanin, but not bovine serum albumin, in dot blot assays; manufacturer's product information). In mouse tissue, the GABA antibody stains most neurons in the thalamic reticular nucleus and a subset of neurons in the dorsal thalamus and cortex. This labeling pattern is consistent with other GABAergic markers used in a variety of species (Fitzpatrick et al., 1984; Houser et al., 1980; Montera & Zempel, 1985; Montero & Singer, 1984). The GABA antibody was tagged with a goat anti-rabbit antibody conjugated to 15-nm gold particles (BBI Solutions USA, Madison, WI, catalogue# GAR12/0.25, RRID:AB_1769132). The sections were air dried and stained with a 10% solution of uranyl acetate in methanol for 30 min before examination with an electron microscope.

Images of DAB-labeled terminals involved in synapses were collected and the areas of the presynaptic profiles were measured using ImageJ software (RRID: SCR_002285). Other ultrastructural features, such as the presence or absence of dendritic inclusions within terminals, were noted. For presentation of ultrastructural features, electron microscopic images were imported into Adobe Photoshop software (San Jose, CA), and the brightness and contrast were adjusted.

Confocal microscopy (tectogeniculate and cholinergic terminal distributions)

Two weeks following SC virus injections, mice were transcardially perfused with 4% paraformaldehyde in PB. The brains were removed from the skull and placed in the fixative solution overnight at 4◦C. The next day, the brains

were cut using a vibratome into coronal sections at a thickness of 70 µm, mounted on slides, and imaged using a confocal microscope.

Cholinergic brainstem projections to the dLGN were labeled via immunohistochemistry using brain sections from mice prepared as described above. Selected sections were washed with 0.3% Triton X-100 and 10% normal donkey serum (NDS) in phosphate-buffered saline (PBS; 0.01 M phosphate buffer with 0.9% NaCl) for 1 h and incubated overnight (12 h) in a 1:100 dilution of a rabbit polyclonal antibody against vesicular acetylcholine transporter (vAChT; Synaptic Systems Cat# 139103, RRID: 887864) in 1% NDS in PBS. The immunogen for this antibody was a recombinant protein corresponding to AA 475 to 530 from rat VAChT. The neurons and boutons labeled with this antibody correspond to those labeled previously using choline acetyl transferase antibodies (Deichler et al., 2020; Sokhadze et al., 2022; Steinkellner et al., 2019). Following incubation in the VAChT antibody, the next day sections were incubated in a 1:100 dilution of a donkey anti-rabbit antibody directly conjugated to a fluorescent compound, Alexa Fluor 647(Cat#A32849, RRID: AB_2762840) for 1 h. After three rinses with PB for 10 min each, the sections were mounted on slides and imaged using a confocal microscope. Confocal images of SC projections and VAChT labeling were imported into Adobe Photoshop and inverted. The brightness and contrast were adjusted, and bubbles or other imperfections were removed to optimize presentation.

Material collected in previous studies

Measurements of BDA-labeled corticogeniculate terminals labeled in C57BL/6J mice, and images of the distribution of tectogeniculate terminals and VAChT terminals in C57BL/6J mice were previously collected and published (Bickford et al., 2015; Sokhadze et al., 2022).

Statistical analysis

GraphPad Prism (RRID: SCR_002798) was used for statistical analysis. For all results involving comparisons of more than two groups, Kruskal–Wallis tests were used to determine whether terminal sizes were significantly different. All graphs featured in the figures of the results section were produced with GraphPad Prism.

Results

Electron microscopy was used to obtain images of virus- or tracer-labeled terminals in the dLGN that were involved in synaptic connections. Retinogeniculate terminals (in wild-type mice with intact retinal ganglion cells) were identified as profiles in which all mitochondria were labeled with a dark reaction product (Figure 4.1a and b). For all other projections, the tracer or virus injections resulted in a dark reaction product that filled the cytoplasm of axons and synaptic terminals with a dark reaction product which surrounded synaptic vesicles (Figures 4.2, 4.5, and 4.7).

Retinogeniculate terminals in WT mice

As previously described (Bickford et al., 2010), mouse retinogeniculate terminals were large profiles that synapse on the nonGABAergic dendrites of

relay cells (Figure 4.1a and b, green) and the GABAergic dendritic terminals of interneurons (F2 profiles; Figure 4.1b, red). Postsynaptic dendrites often protruded into the retinogeniculate terminals (Figure 4.1a and b). For measurements of retinogeniculate profiles, any dendritic protrusions enclosed within the terminal profile were included in the area measurements. We found no significant difference in the sizes of virus-labeled retinogeniculate terminals ipsilateral (n = 113 synaptic terminals; 2.956 ± 1.868 µm2) or contralateral (n = 105 synaptic terminals; 2.798 ± 2.028 µm2) to the injected eye (Figure 4.3; Kruskal–Wallis, p > .9999). There were also negligible differences in the proportion of synapses on relay cells (ipsilateral 88%; contralateral 87%) and interneurons (ipsilateral 12%; contralateral 13%), or in the proportion of retinogeniculate terminals that contained dendritic protrusions (38.5% of ipsilateral terminals contained protrusions; 34% of contralateral terminals contained protrusions).

Corticogeniculate terminals in WT, math5$^{-/-}$, RBP4-cre, and RBP4-cre/math5$^{-/-}$ mice

Following perinatal monocular enucleation, cortical inputs to the dLGN arise exclusively from V1 (Giasafaki et al., 2022; Grant et al., 2016). Thus, we labeled corticogeniculate terminals via V1 BDA injections in wild-type and *math5*$^{-/-}$ mice. Our injections encompassed all cortical layers to include layer VI neurons that are normally the exclusive source of cortical input to the dLGN (Augustinaite & Kuhn, 2020), as well as layer V neurons, which have been reported to aberrantly innervate the dLGN after early postnatal monocular enucleation

(Giasafaki et al., 2022; Grant et al., 2016). As previously described (Bickford et al., 2015) in wild-type mice, corticogeniculate terminals are small profiles (n = 74 synaptic terminals; 0.178 ± 0.0847 µm2) with densely packed round vesicles (RS profiles; Figure 4.2a). In mice devoid of retinal input (*math5*$^{-/-}$), corticogeniculate terminals labeled via V1 BDA injections were also found to be RS profiles (Figure 4.2b–d; n = 240 synaptic terminals; 0.238 ± 0.123 µm2) that were similar in size to WT corticogeniculate terminals (Figure 4.3; Kruskal–Wallis, p = .0542). In both WT and *math5*$^{-/-}$ mice, corticogeniculate terminals were found to be significantly smaller than retinogeniculate terminals in wild-type mice (Figure 4.3; Kruskal–Wallis, p < .0001). We also found that corticogeniculate terminals in wild-type and *math5*$^{-/-}$ mice contained no dendritic protrusions and dendrites postsynaptic to these terminals contained no detectable levels of GABA (Figure 4.2a–d; green). In the Rbp4-cre line, cre-recombinase is expressed in most layer V cortical neurons, and a subset of layer VI cortical neurons (Adesnik, 2018; Grant et al., 2016; Gensat Brain Atlas, gensat.org). This line has been used to demonstrate changes in cortical innervation of the dLGN following perinatal monocular enucleation (Giasafaki et al., 2022; Grant et al., 2016). Therefore, we also labeled V1 corticogeniculate projections in Rbp4-cre mice and Rbp4-cre/*math5*$^{-/-}$ mice. We placed virus injections in V1 to induce the expression of peroxidase in a cre-dependent manner. These injections resulted in the labeling of a large number of layer V cortical neurons and a small number of layer VI neurons (Figure 4.4a and e). In the injected mice, we found that the majority of labeled profiles in the dLGN of both Rbp4-cre mice and Rbp4-cre/*math5*$^{-/-}$ mice were

myelinated axons that coursed through the dLGN (Figures 4.4b and f and 5c and d). As previously described for monocularly enucleated mice (Grant et al., 2016), in the Rbp4- cre/*math5*$^{-/-}$ mice, we found that many of these axons assumed a more dorsal position, occupying the region of the missing optic tract fibers (wild-type: Figure 4.4b arrow, 5a*; math5*$^{-/-}$: Figure 4.4f arrow; 5b). In the Rbp4-cre and Rbp4-cre/*math5*$^{-/-}$ mice, in addition to labeled myelinated axons, we were able to detect a small number labeled terminals that displayed RS morphology (Figure 4.5e; Rbp4-cre n = 10; Rbp4-cre/*math5*$^{-/-}$ n = 4) as well as unmyelinated axons that contained vesicles (Figure 4.5f).

Tectogeniculate terminals in WT, math5–/–, Rbp4-cre, and Rbp4-cre/*math5*$^{-/-}$ mice

In the Rbp4-cre mouse line, cre-recombinase is also expressed in subsets of subcortical neurons, including areas such as the superior colliculus (SC; Grant et al., 2016; Gensat Brain Atlas, gensat.org), which projects to the shell region of the dLGN (Bickford et al., 2015). The presence of cre-recombinase in SC neurons in Rbp4-cre mice could explain why terminals are detected in the shell of the dLGN in Rbp4-cre mice crossed with reporter mice (Giasafaki et al., 2022; Grant et al., 2016). To test this, we labeled tectogeniculate projections in Rbp4-cre mice and Rbp4-cre/*math5*$^{-/-}$ mice by placing virus injections in the SC to induce the expression of fluorescent proteins in a cre-dependent or non-cre-dependent manner.

Cre-dependent virus injections in the SC of Rbp4-cre mice resulted in the labeling of subsets of neurons in the SC (Figure 4.4c) and sparse axons and

boutons in the shell of the dLGN (Figure 4.4d, arrow). In Rbp4- cre/*math5*$^{-/-}$ mice, cre-dependent injections in the SC also labeled subsets of neurons in the SC (Figure 4.4g) and sparse axons and boutons in the shell of the dLGN (Figure 4.4h, arrow), which were similar in position and density to those labeled in Rbp4-cre mice. Moreover, non-cre-dependent virus injections placed in the SC of Rbp4-cre/*math5*$^{-/-}$ mice resulted in a band of labeled terminals confined to the shell of the dLGN (Figure 4.6b), as in wild-type animals (Figure 4.6a; Bickford et al., 2015).

These results indicate that the SC is one source of terminals labeled in the dLGN of Rbp4-cre mice crossed with reporter mice (Giasafaki et al., 2022; Grant et al., 2016). Tectogeniculate terminals are large “driver-like” terminals (Bickford et al., 2015) and therefore could account for some of the previously noted “retinogeniculate replacement terminals.” However, large terminals are not confined to the dLGN shell in *math5*$^{-/-}$ mice (El-Danaf et al., 2015), while we found that tectogeniculate terminals remain confined to the shell in *math5*$^{-/-}$ mice. Thus, additional sources of input likely contribute to the population of “retinogeniculate replacement terminals” observed in mice lacking retinal input.

Pedunculopontine tegmentum terminals in the dLGN of WT and *math5*$^{-/-}$ mice

Next, to examine the morphology and distribution of terminals that originate from the pedunculopontine tegmentum (PPT), we stained dLGN sections with antibodies against the vesicular acetylcholine transporter (VAChT), which we identified as a specific marker for this projection (Sokhadze et al.,

2022). As illustrated in Figure 4.6c and d, in both wild-type and *math5*$^{-/-}$ mice, the VAChT antibody labels diffusely distributed small puncta. Thus, the PPT is not a source of “retinogeniculate replacement terminals.”

Parabigeminal terminals in the dLGN of WT and *math5*$^{-/-}$ mice

Finally, we explored the parabigeminal nucleus (PBG) as a source of “retinogeniculate replacement terminals” since previous studies of Chat-cre and Chat-cre/*math5*$^{-/-}$ mice indicate significant plasticity in the PBG-dLGN projection (Sokhadze et al., 2018). As described in detail in Sokhadze et al. (2018), virus injections in the PBG of WT mice primarily label terminals in the contralateral dLGN, where they are most densely distributed in the shell; terminals in the ipsilateral dLGN are extremely sparse and confined to a small dorsomedial patch. However, in *math5*$^{-/-}$ mice, the PBG projection expands and both the contralateral and ipsilateral dLGN are filled with a dense distribution of terminals.

At the ultrastructural level, in both wild-type and *math5*$^{-/-}$ mice, labeled PBG terminals engaged in synapses were generally large profiles that often contained dendritic protrusions (Figure 4.7a–c). Indeed, these terminals resembled the previously described “retinogeniculate replacement terminals” observed in anophthalmic, microphthalmic, enucleated, as well as *math5*$^{-/-}$ mice (Cullen & Kaiserman-Abramof, 1976; El-Danaf et al., 2015; Kaiserman-Abramof, 1983; Winkelmann et al., 1985). In fact, labeled PBG terminals in both C57Blk6 mice (Figure 4.7c, contralateral dLGN n = 321; 1.177 ± 0.725 µm2) and *math5*$^{-/-}$ mice (Figure 4.7a, ipsilateral dLGN n = 164; 1.812 ± 1.395 µm2, Figure 4.7b, contralateral dLGN n = 153; 1.381 ± 0.893 µm2) were found to be significantly

larger than corticogeniculate terminals in wild-type and math5–/– mice (Kruskal–Wallis, $p < .0001$).

As a population, PBG terminals were significantly smaller than retinogenicuate terminals (Figure 4.8; Kruskal–Wallis, $p < .0001$). However, there was considerable overlap in the sizes of these terminal populations, with many PBG terminal profiles reaching the size of the largest retinogeniculate terminal profiles and/or exceeding the size of the smaller retinogeniculate terminal profiles. This was especially evident for PBG terminals in *math5*$^{-/-}$ mice (Figure 4.9, ipsilateral and contralateral measurements combined). In addition, a large proportion of PBG terminals in both wild-type (35.8%) and *math5*$^{-/-}$ (55.5%) mice contained dendritic protrusions.

Although there was no significant difference in the sizes of contralateral PBG terminals in the dLGN of wild-type versus *math5*$^{-/-}$ mice (Figure 4.10; Kruskal–Wallis, $p = .1270$), ipsilateral PBG terminals in the dLGN of *math5*$^{-/-}$ mice were found to be significantly larger than contralateral PBG terminals in the dLGN of wild-type mice (Figure 4.10; Kruskal–Wallis, $p < .0001$).

Discussion

To identify the source of “retinogeniculate replacement terminals,” we compared all sources of nonGABAergic input to the dLGN in mice with and without retinofugal input. While previous reports have suggested that layer V cortical neurons provide an anomalous source of input following monocular or binocular enucleation (Frangeul et al., 2016; Giasafaki et al., 2022; Grant et al.,

2016), we found no differences in the ultrastructure of corticogeniculate terminals in wild-type versus *math5*$^{-/-}$ mice. We also found no changes in the overall pattern of tectogeniculate or PPT projections in wild-type versus *math5*$^{-/-}$ mice. In contrast, terminals that originate from the PBG expand their innervation territory in the dLGN of *math5*$^{-/-}$ mice (Sokhadze et al., 2018) and these terminals exhibit characteristics of retinal terminals in both wild-type and *math5*$^{-/-}$ mice; that is, synapses on dendrites that protrude into large terminals filled with round synaptic vesicles and multiple mitochondria. We conclude that projections from the PBG expand to fill the vacancies left by the lack of retinal ganglion cell input in the dLGN of *math5*$^{-/-}$ mice and are the likely source of “retinogeniculate replacement terminals” previously observed in this mouse line (El-Danaf et al, 2015).

Corticogeniculate input in the absence of retinogeniculate input

Previous studies in *math5*$^{-/-}$ mice have indicated that the lack of retinogeniculate input results in changes in the timing of corticogeniculate innervation (Brooks et al., 2013; Seabrook et al., 2013). Normally, corticogeniculate axons begin to innervate the dLGN at P3 and complete their innervation by the second postnatal week, the time of natural eye opening. However, in *math5*$^{-/-}$ mice, corticogeniculate innervation is accelerated, beginning at P0, with completion by the end of the first postnatal week. This effect has been shown to be regulated by the expression of the chondroitin sulfate proteoglycan (CSPG), aggrecan. Aggrecan, a repulsive CSPG, is transiently expressed in the developing dLGN, showing enriched levels at early postnatal ages, and inhibiting cortical axons from prematurely entering. Postnatal

loss of aggrecan from the dLGN coincides with upregulation of aggrecanase expression and the age-related progression of corticogeniculate innervation. However, in the absence of retinal input aggrecan expression is low and aggreganases high, allowing for the accelerated innervation of corticogeniculate input.

Here we found that the change in the timing of corticogeniculate innervation in *math5*$^{-/-}$ mice does not result in any differences in the ultrastructure of corticogeniculate synapses, since we found no difference in the sizes of corticogeniculate terminals in wild-type versus *math5*$^{-/-}$ mice. Moreover, the only changes we observed in V1 projections labeled in a cre-dependent manner in Rbp4-cre and Rbp4- cre/*math5*$^{-/-}$ mice was the change in the position of axons that course through the dLGN en route to other targets.

These results seem at odds with previous studies using Rbp4-cre mice crossed with reporter lines to demonstrate changes in cortical innervation patterns following monocular enucleation (Giasafaki et al., 2022; Grant et al., 2016). Although a subset of tectogeniculate cells contain cre-recombinase in the Rbp4-cre line, we found no apparent expansion of tectogeniculate projections in *math5*$^{-/-}$ mice. Moreover, cre-dependent virus injections in V1 of Rbp4-cre mice that received monocular or binocular enucleation have demonstrated changes in both V1 innervation of the dLGN and activation of dLGN neurons (Frangeul et al., 2016; Giasafaki et al., 2022; Grant et al., 2016). Thus, these discrepancies may pertain to the use of early postnatal enucleation versus the use of *math5*$^{-/-}$ mice as a means to achieve a genetic form of deafferentation. This suggests that

changes in corticogeniculate innervation are not induced by the lack of retinal input per se, but may be caused by other mitigating factors. Indeed, inflammation brought about by retinal degeneration and/or the disruption of genes associated with axon guidance, neuronal migration, and synaptogenesis (Frangeul et al., 2016; Giasafaki et al., 2022) could produce changes in corticogeniculate innervation patterns that are not detected in *math5*$^{-/-}$ mice.

Comparison of synaptic terminals that originate from the retina and the PBG

Besides their size and comparable synaptic arrangements, there are additional similarities between synaptic terminals that originate from the retina and the PBG. First, both projections are bilateral and enter the dLGN via the optic tract. In mice with intact retinofugal projections, the contralateral PBG projection reaches the dLGN via axons that travel rostrally, cross to the contralateral side in the supraoptic decussation, and enter the dLGN via the optic tract (Sokhadze et al., 2018; Watanabe & Kawana, 1979). The ipsilateral PBG projection similarly travels in the optic tract to innervate a small dorsomedial region of the dLGN. Therefore, although the ipsilateral projection from the PBG to the dLGN is normally quite restricted, pathways to access both the ipsilateral and contralateral dLGN are normally present in wild-type mice. In *math5*$^{-/-}$ mice, the PBG axons follow a similar trajectory to cross the midline in the supraoptic decussation, but in the absence of an optic tract they traverse the thalamus to target the dLGN (Sokhadze et al., 2018).

PBG and retinal projections are also similar in that both PBG cells and retinal ganglion cells express the type 2 glutamate transporter (vGLUT2; Steinkellner et al., 2019). Therefore, like retinal terminals, PBG terminals probably release glutamate from the abundant round synaptic vesicles contained within them. PBG innervation may account for at least some of the vGLUT2-positive puncta in the dLGN that remain in *math5*$^{-/-}$ and enucleated mice (Bhandari et al., 2022; El-Danaf et al., 2015). PBG cells also express choline acetyl transferase (ChAT), but do not express the vesicular acetylcholine transporter (VAChT; Sokhadze et al., 2022). Similarly, VAChT mRNA is undetectable in a subdivision of the avian PBG homologue (nucleus isthmi parvocellularis) where ChAT mRNA is colocalized with vGLUT2 mRNA (González-Cabrera et al., 2015). Therefore, it is unclear whether PBG terminals corelease glutamate and acetylcholine.

Interestingly, we found no evidence for plasticity in other brainstem projections. Tectogeniculate projections normally form large “driver-like” terminals that converge with retinal terminals to innervate single neurons in the shell of the ipsilateral dLGN (Bickford et al., 2015). In *math5*$^{-/-}$ mice, tectogeniculate terminals remain confined to the dorsal and lateral regions of the ipsilateral dLGN and do not appear to expand their innervation territory to the dLGN core or the contralateral dLGN. Likewise, we found no differences in PPT projections labeled using immunocytochemistry in wild-type and *math5*$^{-/-}$ mice. Thus, the plasticity of the PBG-dLGN projection appears to be unique.

Implications for retinal reinnervation of the dLGN

The mechanisms underlying the expansion of the PBG pathway are of potential interest for studies interrogating treatments for diseases or trauma that result in retinal degeneration. “Retinal replacement terminals” have been identified in mice enucleated as late as 20 days after birth (Cullen & Kaiserman-Abramof, 1976). Therefore, strategies to regenerate retinal innervation of the dLGN should consider potential competition from remodeled synaptic circuits. On the other hand, it is unknown whether “retinal replacement terminals” are present in other species. In most species, the PBG projections are segregated in discrete regions of dLGN (e.g., C-laminae of carnivores, koniocellular layers of primates; Harting et al., 1991), and it is unclear whether these terminals can expand into other areas of the dLGN following the loss of retinal input.

Implications regarding cross modal plasticity

The function of the expanded PBG-dLGN projection in the absence of retinal input is currently unclear. Normally, the PBG receives all of its input from the visual layers of the superior colliculus (Deichler et al., 2020; Shang et al., 2015; Whyland et al., 2020), and PBG neurons respond to moving visual stimuli (Cui & Malpeli, 2003; Ma et al., 2013; Reinhard et al., 2019). In the absence of retinal input, the superior colliculus could potentially transmit auditory or somatosensory signals to the PBG which could be relayed to the dLGN (Basso et al., 2021; Stevenson & Lund, 1982). The dLGN could then relay these other sensory modalities to the cortex. The transmission of anomalous inputs to the visual cortex in the absence of retinal input has been noted in several previous studies (Izraeli et al., 2002; Kahn & Krubitzer, 2002; Piché et al., 2007; Yaka et

al., 2000), and the identification of the PBG as a source of “retinal replacement terminals” in the dLGN suggests that subcortical pathways may be involved in this transfer of nonvisual sensory signals to the visual cortex.

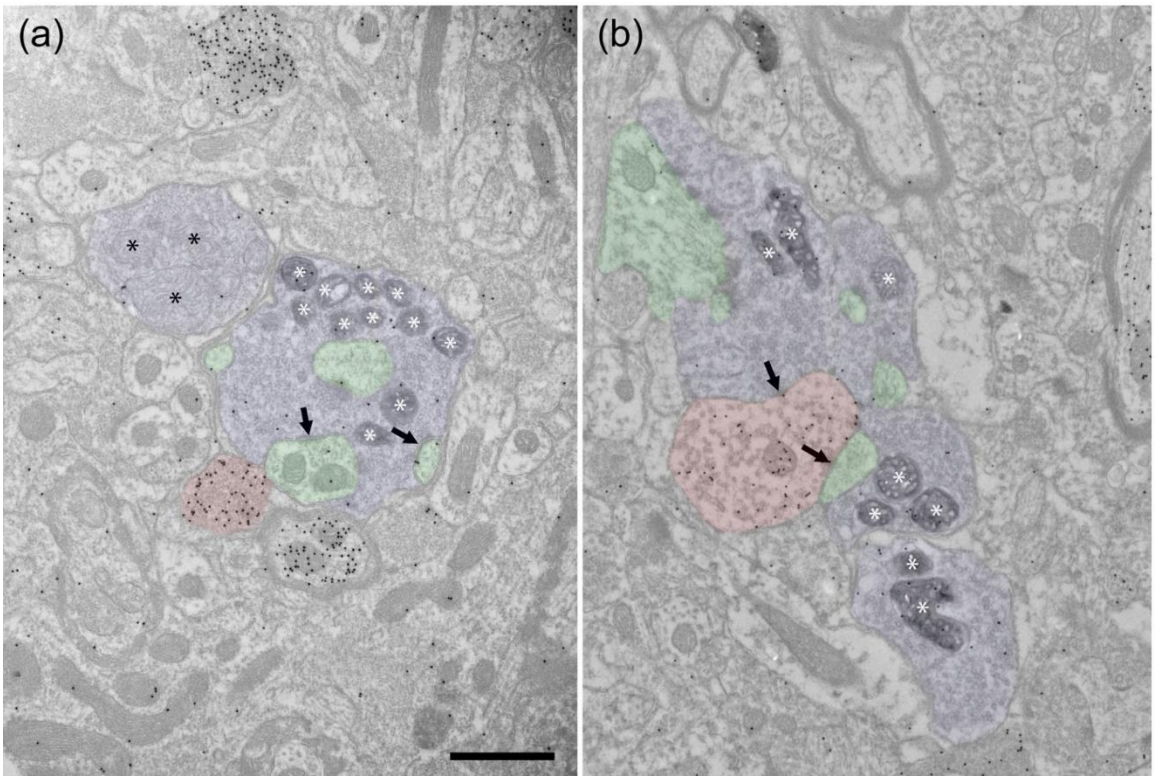

Figure 4.1. Retinogeniculate terminals in WT mice. Electron micrographs illustrate ipsilateral (a) and contralateral (b) retinogeniculate terminals (blue overlay) labeled via monocular virus injections in C57Blk6 mice that induced the expression of peroxidase in mitochondria (white asterisks). The tissue was stained to detect GABA with gold particles. Unlabeled retinogeniculate terminals contain pale mitochondria (black asterisks, a). Retinogeniculate terminals both contain and synapse (black arrows) on the dendrites of nonGABAergic thalamocortical cells (a, green overlay, identified by a low density of gold particles) that often protrude into the terminals. Retinogeniculate terminals also

contact the dendritic terminals of GABAergic interneurons (b, F2 profiles, red overlay, GABA content identified by a high density of overlying gold particles). The illustrated F2 profile synapses (black arrow) on a thalamocortical cell dendrite (green overlay, identified by a low density of overlying gold particles). Scale bar = 1 µm and applies to both panels.

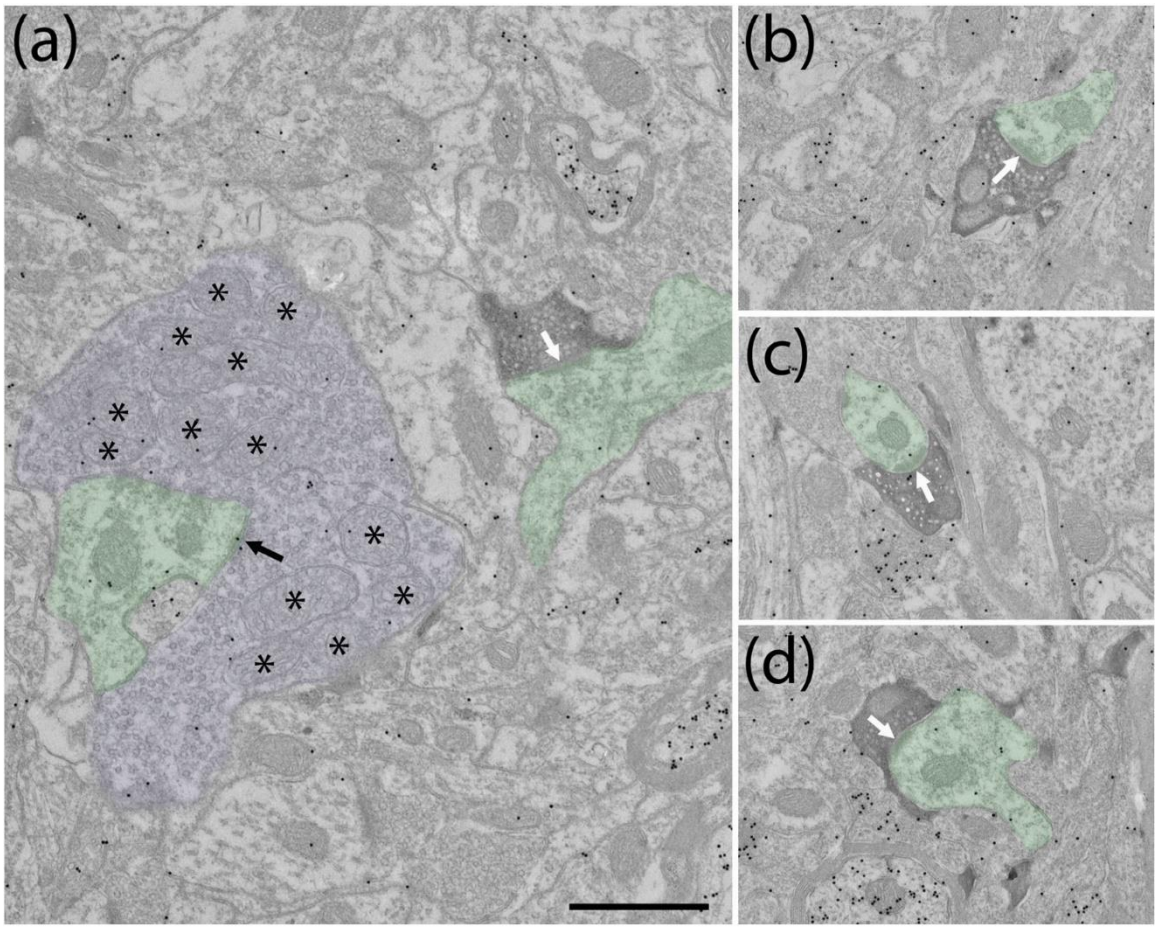

Figure 4.2. Corticogeniculate terminals in WT and *math5*$^{-/-}$ mice. Electron micrographs illustrate corticogeniculate terminals labeled via V1 BDA injections in C57Blk6 (a) and *math5*$^{-/-}$ (b–d) mice. The tissue was stained to detect GABA with gold particles. In both WT and *math5*$^{-/-}$ mice, V1 terminals are small profiles that contain round synaptic vesicles (RS profiles) that synapse (white arrows) on

thalamocortical cell dendrites (green overlay, low density of gold particles). In the electron micrograph illustrating the WT corticogeniculate terminal, an adjacent unlabeled retinal terminal (blue overaly, identified by its pale mitochondria, black asterisks) also contacts (black arrow) a thalamocortical cell dendrite (green overlay). Scale bar = 800 nm and applies to all panels.

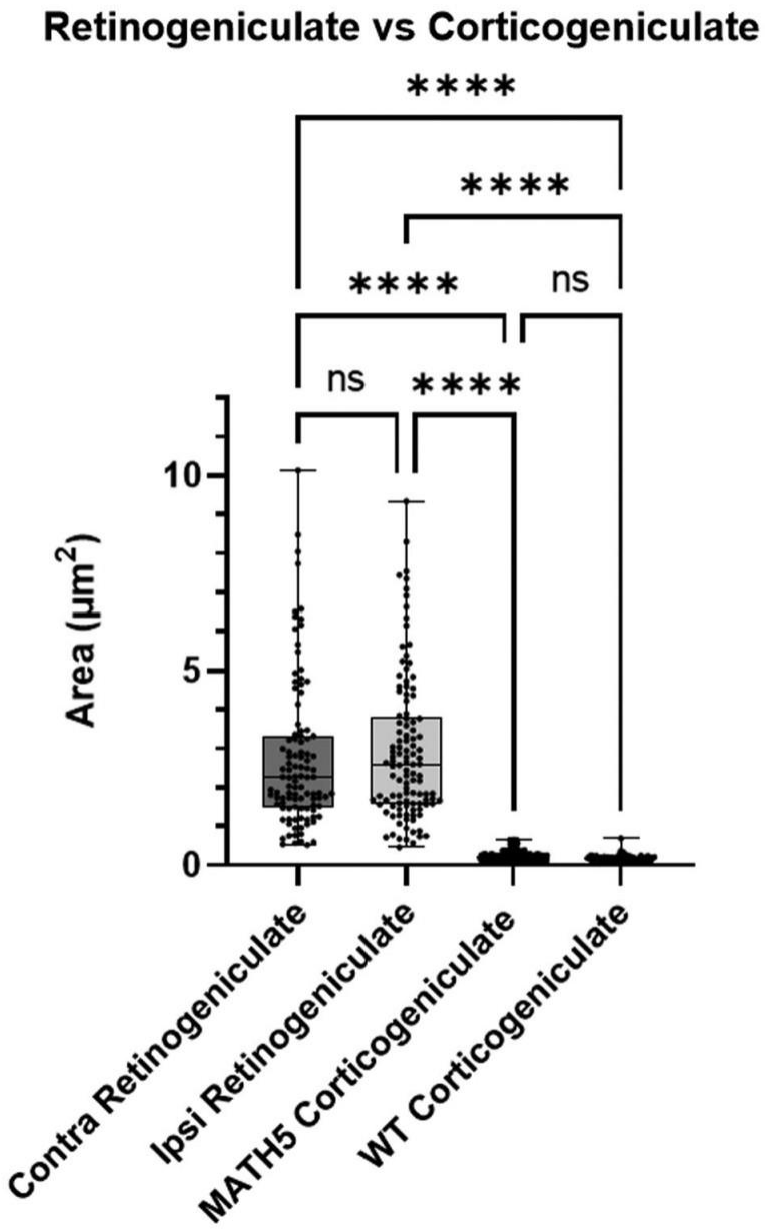

Figure 4.3. (last page): Retinogeniculate terminals in C57Blk6 (WT) mice are significantly larger than corticogeniculate terminals in WT mice and *math5*$^{-/-}$ mice (****p < .0001). There is no significant difference in the size of ipsilateral and contralateral retinogeniculate terminals in WT mice and no significant difference in the sizes of corticogeniculate terminals in WT and *math5*$^{-/-}$ mice (ns).

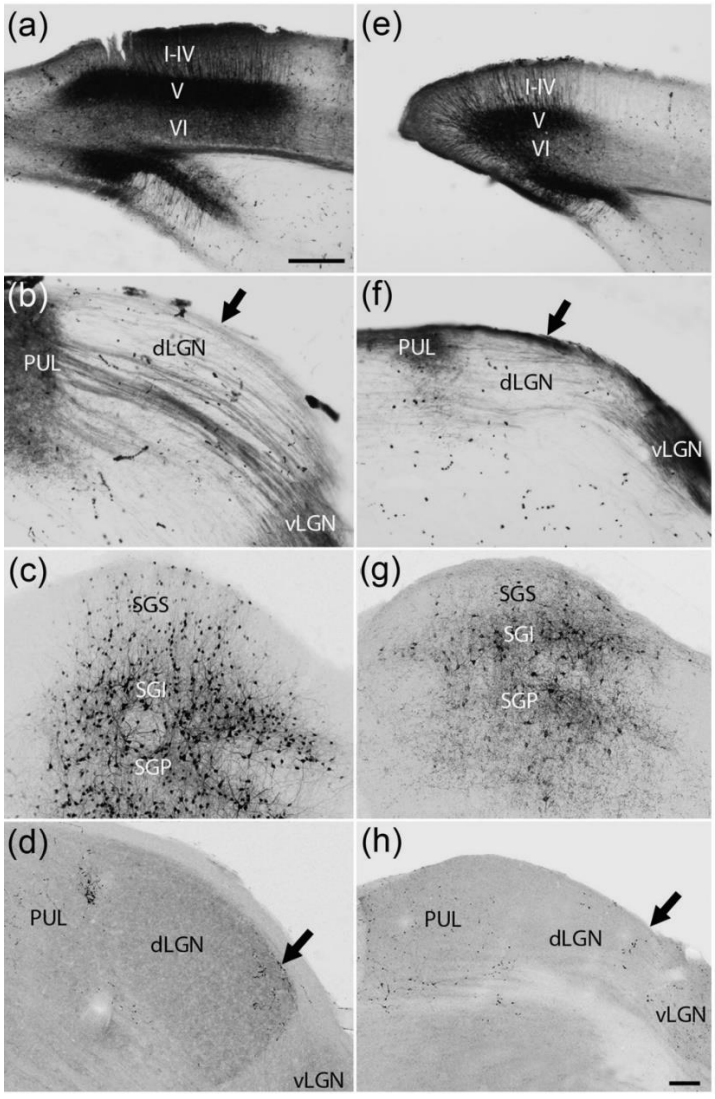

Figure 4.4. Cre-dependent V1 and SC projections to the dLGN of Rbp4-cre and Rbp4-cre/math5–/– mice. Cre-dependent (cell-filling) virus injections in V1 in Rbp4-cre (a, b) and Rbp4-cre/*math5*$^{-/-}$ mice (e, f) labeled a dense population of

cells in layer V that extended dendrites into layers I–IV, a smaller population of cells in layer VI, dense population of terminals in the ipsilateral pulvinar (PUL) and ventral lateral geniculate nucleus (vLGN), and axons that course through the ipsilateral dorsal lateral geniculate nucleus (dLGN). In Rbp4-cre mice, most labeled axons avoid the optic tract (b, arrow). In Rbb4-cre/*math5*$^{-/-}$ mice, the position of many of the labeled axons shifted dorsally to occupy the position of the missing optic tract (f, arrow). Cre-dependent (cell-filling) virus injections in the SC of Rbp4-cre (c, d) and Rbb4-cre/*math5*$^{-/-}$ mice (g, h) labeled subpopulation of cells in the stratum griseum superficiale (SGS), stratum griseum intermediale (SGI), and stratum griseum profundum (SGP) and a sparse population of terminals in the ipsilateral dorsolateral shell of the dLGN (d, h arrows). Scale in a = 500 µm and also applies to e. Scale in h = 100 µm and also applies to (b–d) and (f–g).

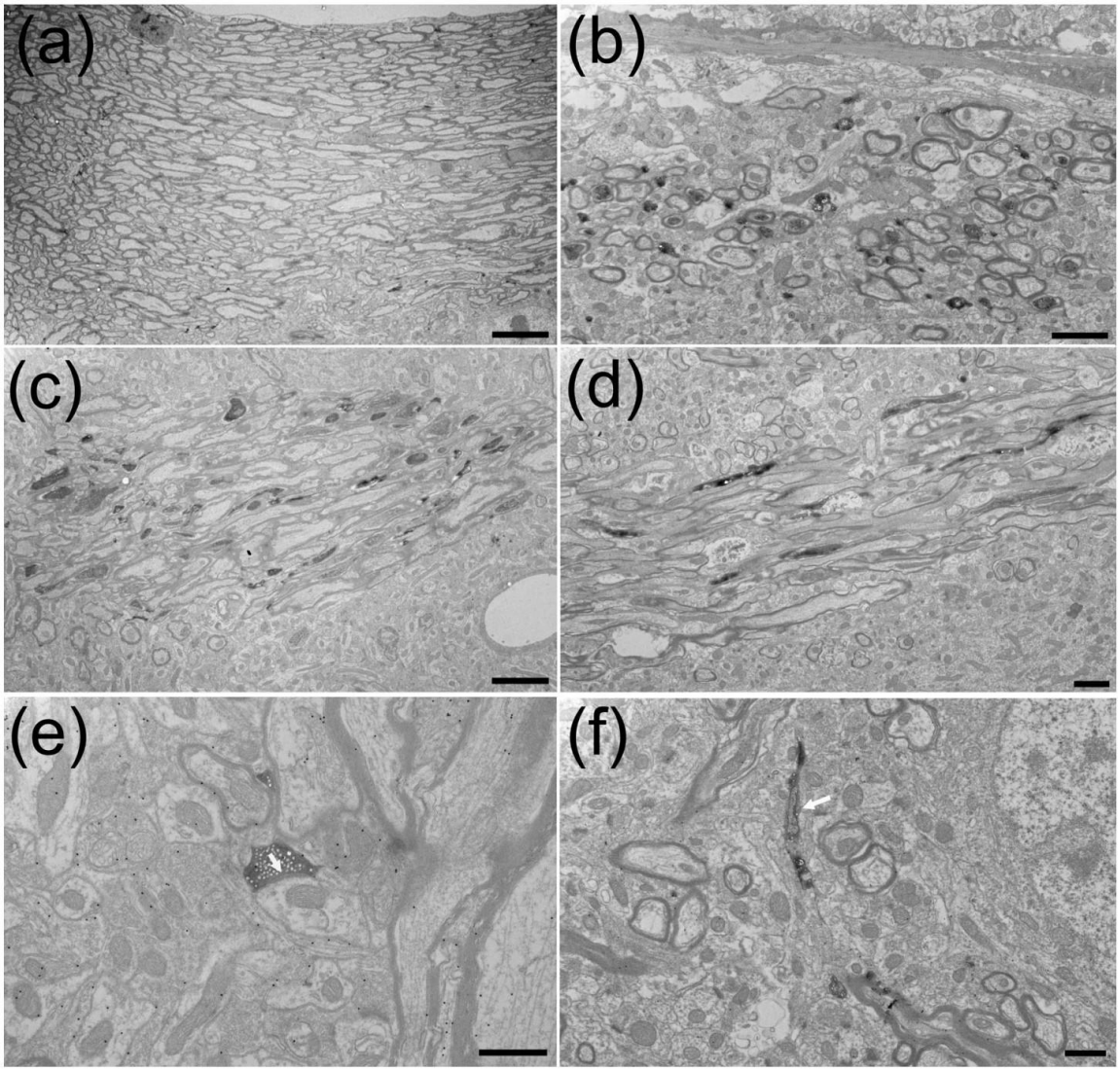

Figure 4.5. Electron micrographs illustrate the ultrastructure of the dLGN in Rbp4-cre mice (a, c, e) and Rbp4-cre/*math5*$^{-/-}$ mice (b, d, f) that received cre-dependent (cell-filling) virus injections in the ipsilateral V1. In Rbp4-cre mice, the optic tract at the dorsal surface of the dLGN is a thick layer of unlabeled myelinated axons (a). In Rbp4/*math5*$^{-/-}$ mice, the dorsal surface of the dLGN contains labeled axons in the location of the missing optic tract (b). Labeled axons course through the body of the dLGN in both Rbp4-cre (c) and Rbp4/*math5*$^{-/-}$ (d) mice. In both Rbp4-cre and Rbp4-cre/*math5*$^{-/-}$ mice, sparse

labeled terminals that displayed RS morphology (e, white arrow indicates synapse, Rbp4-cre) and unmyelinated fibers that contained vesicles (f, white arrow Rbp4-cre/*math5*$^{-/-}$) were occasionally observed. Scale bars: a = 8 µm, b = 2 µm, c = 4 µm, d = 2 µm, e = 800 nm, f = 1 µm.

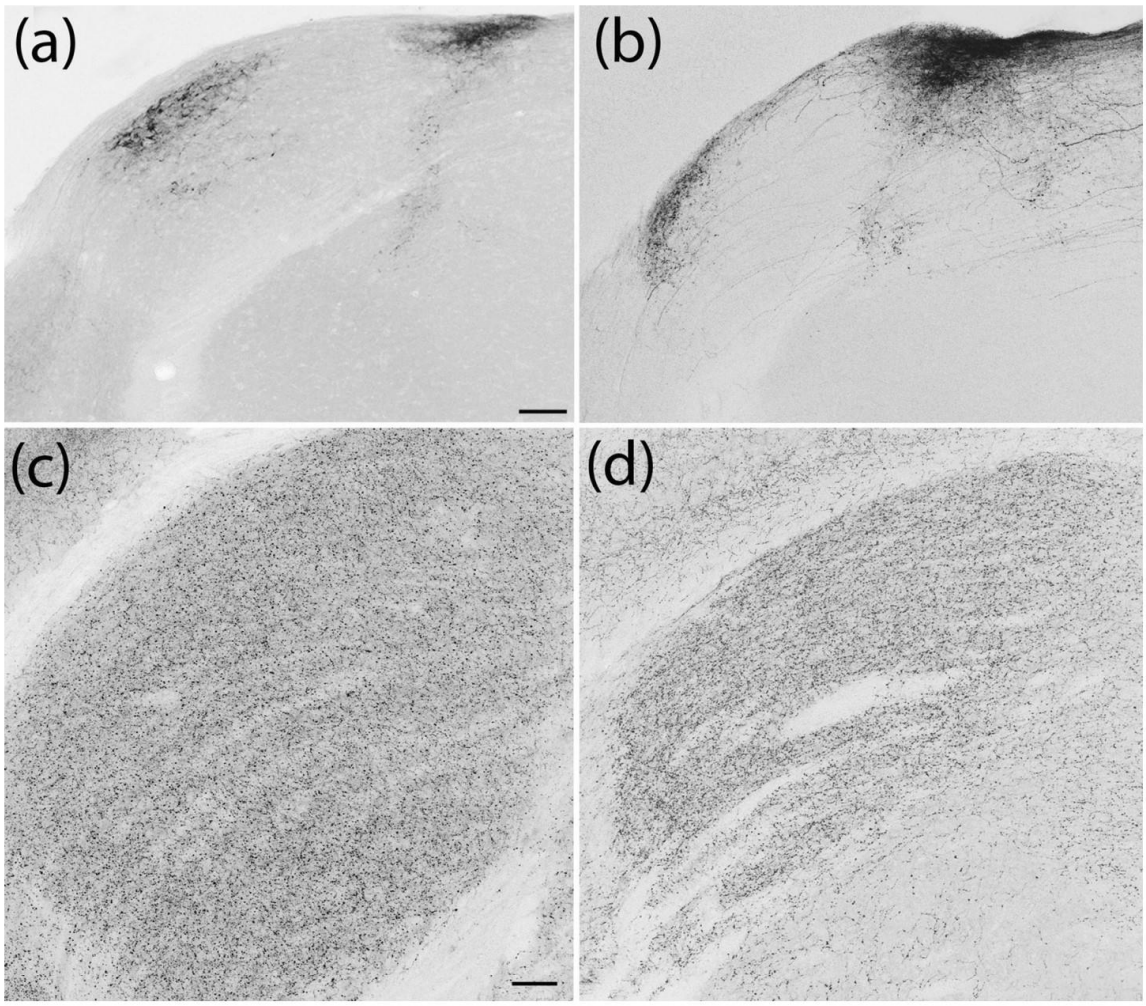

Figure 4.6. SC and PPT projections to the dLGN of WT and *math5*$^{-\backslash -}$ mice. Tectogeniculate projections labeled via virus injections in the ipsilateral SC innervate the dorsolateral shell of the dLGN in WT (a; from Bickford et al., 2015) and *math5*$^{-\backslash -}$ mice (b). An antibody against the vesicular acetylcholine transporter labels small diffusely distributed terminals in both WT (c; from

Sokhadze et al., 2022) and *math5*$^{-\backslash -}$ mice (d). Scale in a = 100 µm and also applies to b. Scale in c = 50 µm and also applies to d.

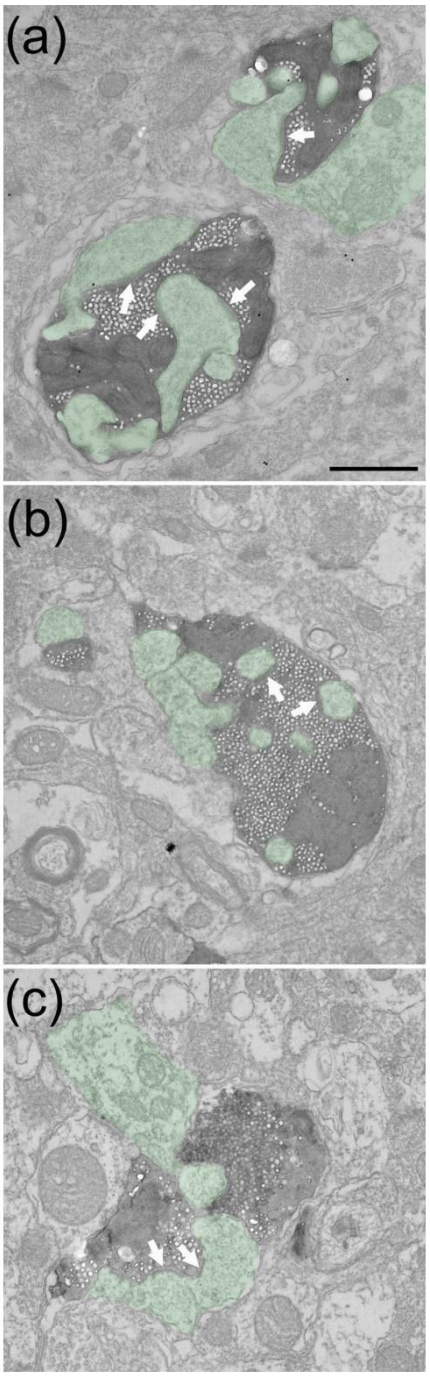

Figure 4.7. PBG terminals in the dLGN of WT and *math5*$^{-/-}$ mice. Electron micrographs illustrate the ulstrastructure of dLGN terminals labeled via unilateral

PBG (cell-filling) virus injections in *math5*$^{-/-}$ (a, ipsilateral dLGN b, contralateral dLGN) and C57Blk6 mice (c, contralateral dLGN). PBG terminals in the dLGN are large profiles that often contain and synapse (white arrows) on dendrites (green overlay) that protrude into the labeled terminals. Scale bar = 800 nm and applies to all panels.

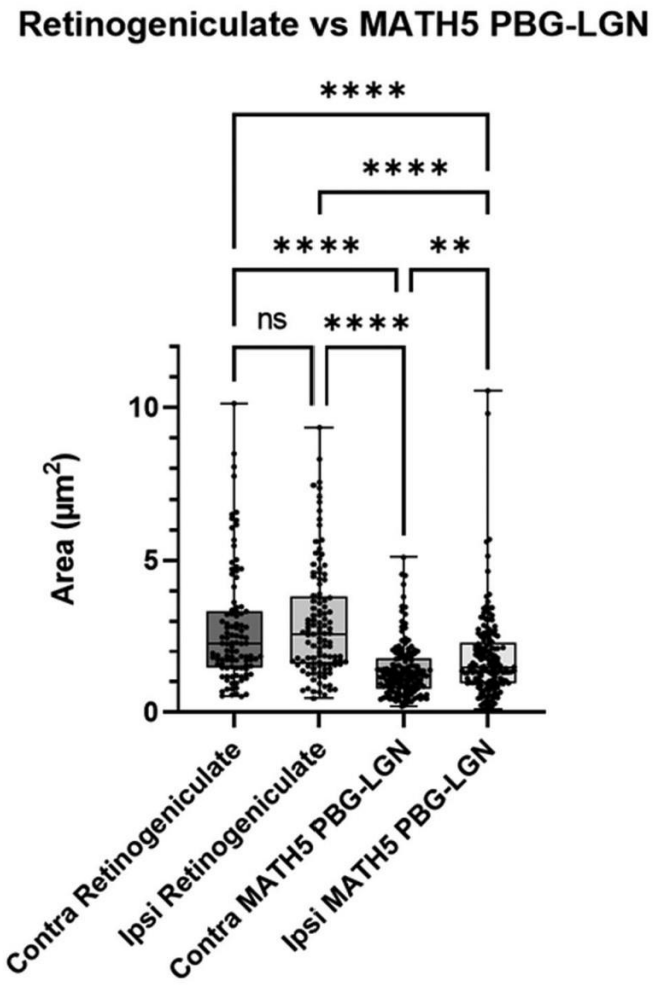

Figure 4.8. Retinogeniculate terminals in C57Blk6 (WT) mice are significantly larger than PBG-dLGN terminals in *math5*$^{-\backslash-}$ mice (****p < .0001). There is no significant difference in the size of ipsilateral and contralateral retinogeniculate

terminals in WT mice (ns). Ipsilateral PBG-dLGN terminals are significantly larger than contralateral PBG-dLGN terminals in *math5*$^{-\backslash -}$ mice (**p = .0083).

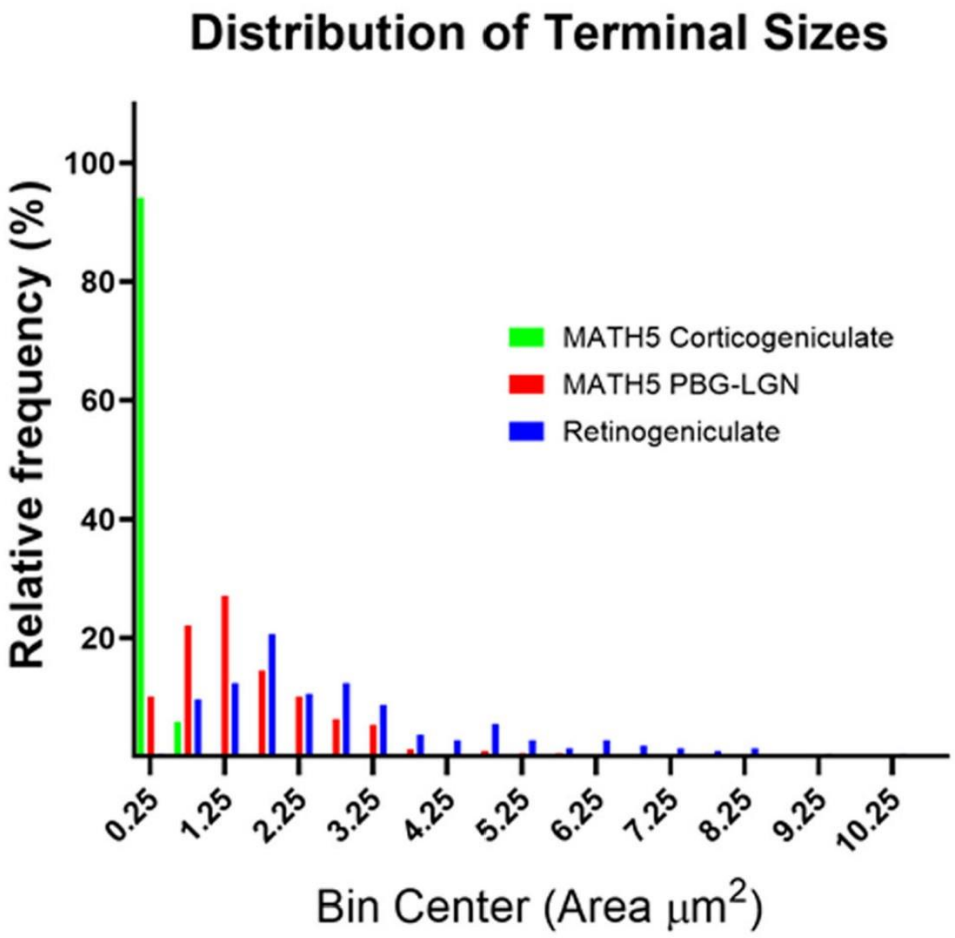

Figure 4.9. There is little overlap in the sizes of retinogeniculate terminals in C75Blk6 mice (blue, ipsilateral and contralateral measurements combined) and corticogeniculate terminals in *math5*$^{-\backslash -}$ mice (green). However, there is considerable overlap in the sizes of retinogeniculate terminals in C57Blk6 mice and PBG-dLGN terminals in *math5*$^{-\backslash -}$ mice (red, ipsilateral and contralateral measurements combined).

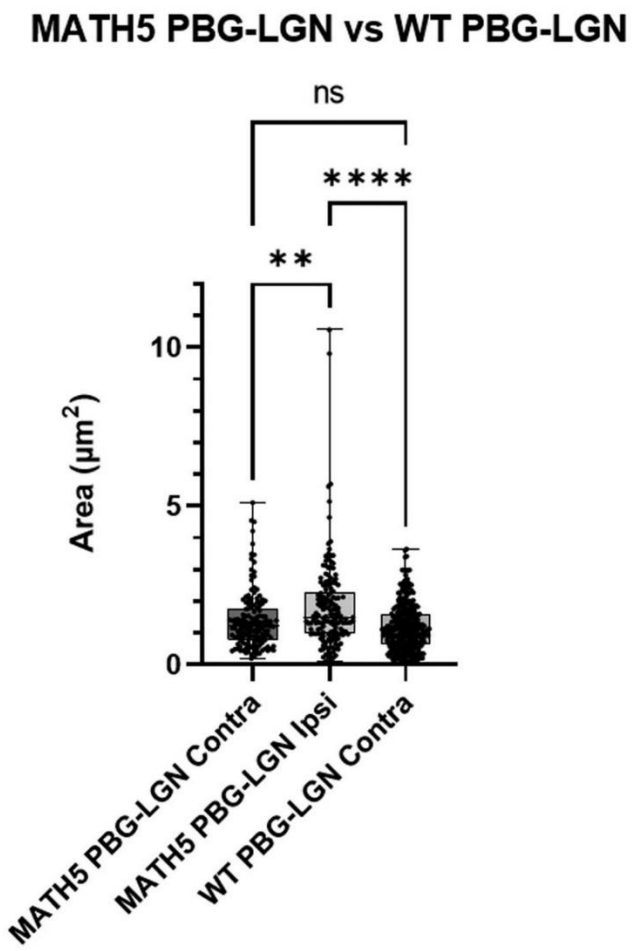

Figure 4.10. Ipsilateral PBG-dLGN terminals in *math5*$^{-}$\$^{-}$ mice are significantly larger than contralateral PBG-dLGN terminals in both C57Blk6 (WT) and *math5*$^{-}$\$^{-}$ mice (**p = .0038; ****p < .0001). There is no significant difference between contralateral PBG-dLGN terminals in WT mice and contralateral PBG-dLGN terminals in *math5*$^{-}$\$^{-}$ mice (ns).

CHAPTER V: SUMMARY AND FUTURE DIRECTIONS

Our anatomical and physiological dissections of the circuits that link the SC, PBG, and LGN detailed in this dissertation yielded several important findings, the highlights of which are summarized by chapter below:

Chapter 1: 1) GABAergic GAD67 neurons of the SC function strictly as interneurons within its superficial layers, and this population makes up approximately two thirds of all the GABAergic cells residing in the visual layers of the SC. 2) GABAergic cells comprise approximately one third of all SGS neurons, and a third of these GABAergic cells are projection neurons that target the LGN, PT, and PBG. 3) PBG projection neurons exhibit NFV, stellate, and horizontal morphologies and can be distinguished from their counterparts that target the LGN and PT by their complete lack of PV expression and their more superficial distribution within the SC's laminae relative to other GABAergic projection populations which frequently reside in the deeper layers. 4) RLPs often form synapses with presynaptic GABAergic dendrites in the SGS and many of these presynaptic dendrites are GAD67 interneurons, forming feedforward inhibitory triads.

Chapter 2: 1) The SC-PBG projection exhibits a coarse topography that preserves the retinotopy of the SC. 2) The PBG can be divided into a "core"

region with densely packed somata and a “shell” region that’s dense with myelinated axons, but both regions have a similar density of synapses. 3) GABAergic SC-PBG neurons inhibit PBG cells and lack PV expression, while PV+ SC-PBG neurons release glutamate and excite PBG neurons. 4) Most PBG neurons receive convergent excitatory and inhibitory inputs from the SC. 5) Approximately 40% of the inputs to the PBG are GABAergic. 6) GAD67 neurons outside the SC provide an additional source of GABAergic input to the PBG.

Chapter 3: 1) Corticogeniculate terminals do not show any ultrastructural changes in MATH5$^{-/-}$ mice that lack retinofugal input relative to their wild-type counterparts and do not possess the characteristics indicative of “retinal replacement terminals”. 2) Tectogeniculate inputs as well as projections from the PPT don’t show any significant changes in how they innervate the LGN in MATH5$^{-/-}$ mice. 3) Terminals in the LGN from the PBG exhibit features characteristic of retinal terminals in both MATH5$^{-/-}$ and wild-type mice and are therefore likely the source of “retinal replacement terminals” observed in previous studies of mice that lack retinofugal input.

Although we took a comprehensive approach to the studies comprising the data chapters of this dissertation, there remain several experiments worth pursuing to help us form a more complete picture of the circuits and cell populations linking our subcortical structures of interest. PV+ neurons of the SGS form a significant subgroup of the excitatory SC-PBG projection population, and our own preliminary retrograde tracing experiments indicate that this population might exhibit unique morphologies and/or physiologies (Figure 5.1). Detailed

retrograde tracing studies targeted to the SC's myriad of postsynaptic partners as well as *in vivo* and/or *in vitro* slice physiology experiments are needed to better characterize the PV projection cells of the SGS in the pursuit of further delineating their role within this structure.

Neurons residing within the PBG don't only exhibit a variety of morphologies, they also form partially overlapping populations of ChAT+ and NTSR1-GN209 (the genetic marker for wide-field vertical cells) cells (Figure 5.2). What role might these NTSR1-GN209 cells play in the PBG? How do cells that express ChAT as well as NTSR1-GN209 differ from those that only express one of these markers? Cre-dependent viral tracer injections as well as optogenetic interrogations are needed to reveal any unique projections and/or physiological properties that might separate these populations into functionally or anatomically distinct groups.

The presence of additional sources of GABAergic input to the PBG is an exciting discovery that could make comparisons of mammalian anatomy with avian brain stem circuits more relevant given GABAergic neurons' important role within the isthmic network. First however, the precise source of these GAD67 terminals within the tegmentum or other brainstem nuclei needs to be identified as well as their physiological effects on their postsynaptic partners in the PBG relative to their tectal inhibitory counterparts.

Clearly terminals in the dLGN originating from the PBG are at least one source (possibly the sole source) of "retinal replacement terminals" in mice that lack retinofugal input, but little is known as to how these terminals might affect

geniculate cells physiologically, especially in animals that lack retinogeniculate inputs. In animals with profound visual deficits, could the PBG terminals in LGN convey auditory signals or information from other sensory modalities? Do enucleation studies or other models of visual deficits produce different effects from the mutant model of vision loss used in our own study of retinal replacement terminals? Only thorough *in vivo* investigations utilizing MATH5$^{-/-}$ and other animal models of profound visual deficits can tell. Lastly, GAD67 interneurons are observed throughout the dLGN, and additionally a subset of these inhibitory cells express BNOS, a marker for cholinergic neurons throughout the brainstem (Figure 5.3). What unique role might these BNOS/GAD67 neurons play in the dLGN? What are their synaptic partners, and could they interact with “retinal replacement” or tectal input to create a unique distribution of convergent inputs? These are just a few of the experiments comprising the obvious next steps in the investigation of these important subcortical visual circuits.

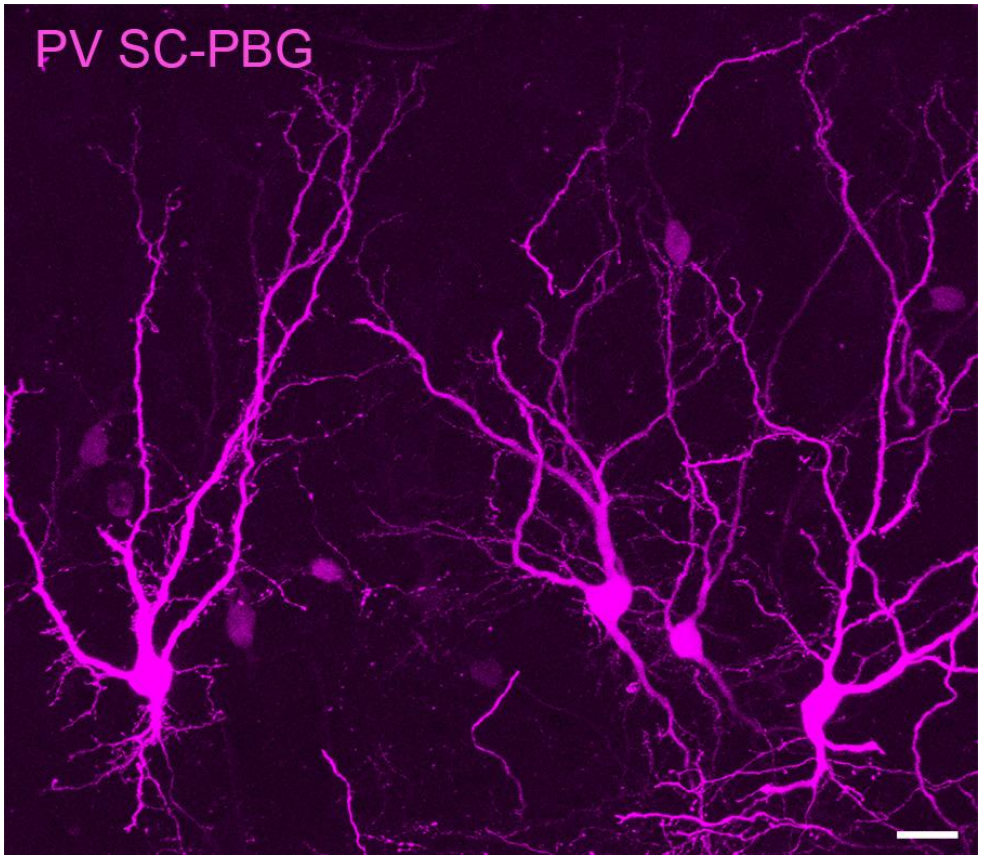

Figure 5.1. PV SC-PBG projection neurons. Injection of a cre-dependent HSV into the PBG of a PV-Cre mouse labels a population of neurons in the SGS (magenta) with unique dendritic morphologies. Scale bar = 20 µm.

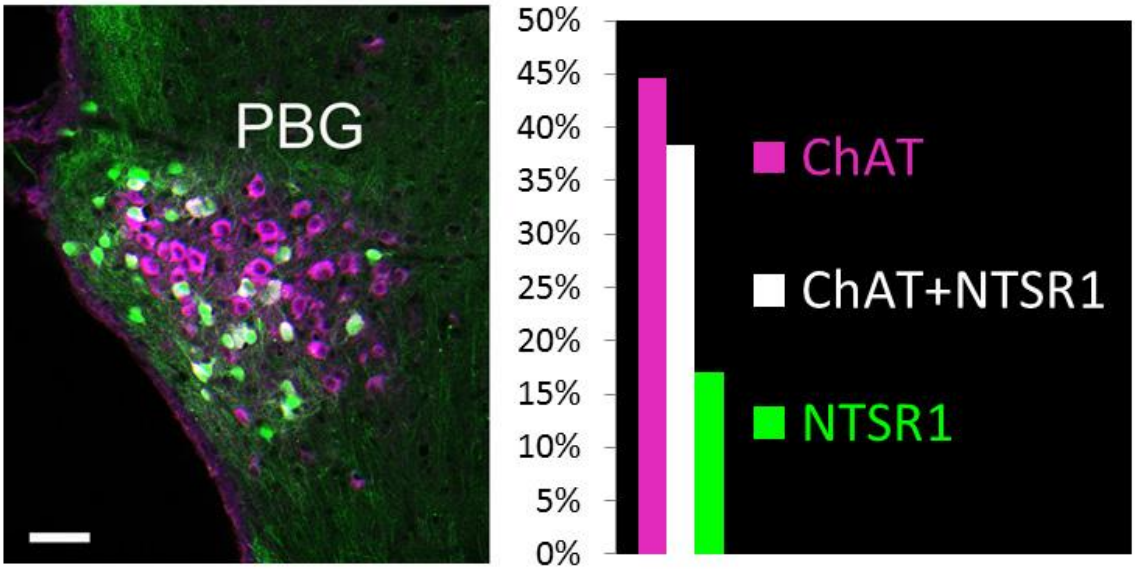

Figure 5.2. ChAT and NTSR1-GN209 expression in the PBG. On the left, the PBG of a NTSR1-GN209 x Ai3 reporter mouse that has been stained with a ChAT antibody shows at least 3 identifiable cell populations based on their expression of NTSR1 (green), ChAT (magenta), or both (white). On the right, a quantification of the proportions of each cell type identified from the confocal stack of the PBG illustrated on the left. Scale bar = 50 µm.

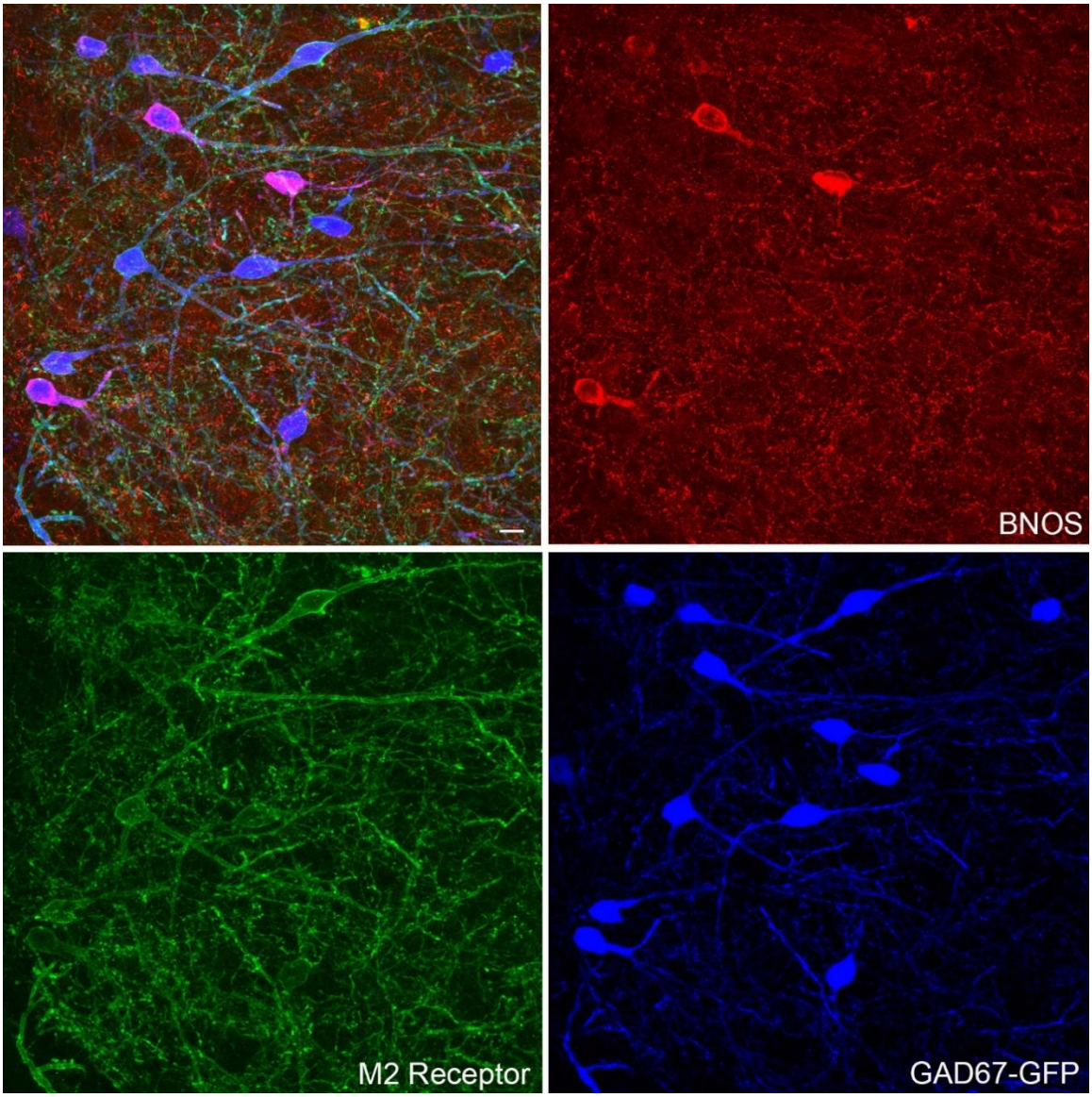

Figure 5.3. BNOS, M2, and GAD67 expression in the dLGN. Fluorescent antibody staining against BNOS (top right, red) and the M2 receptor (bottom left, green) show co-labeling of these markers with GAD67 interneurons (bottom right, blue) shown in the top left panel depicting all three fluorescent labels simultaneously in a high-mag confocal image of the dLGN. Scale bar = 10 µm.

REFERENCES

Abbott, C. W., Kozanian, O. O., & Huffman, K. J. (2015). The effects of lifelong blindness on murine neuroanatomy and gene expression. Frontiers in Aging Neuroscience, 7, (JUL). https://doi.org/10.3389/fnagi.2015.00144

Adesnik, H. (2018). Layer-specific excitation/inhibition balances during neuronal synchronization in the visual cortex. Journal of Physiology, 596(9),1639–1657. https://doi.org/10.1113/JP274986

Ahlsen, G., Lindstrom, S., & Lo, F.-S. (1984). INHIBITION FROM THE BRAIN STEM OF INHIBITORY INTERNEURONES OF THE CAT'S DORSAL LATERAL GENICULATE NUCLEUS. In *J. Physiol* (Vol. 347).

Allen, K., Gonzalez-Olvera, R., Kumar, M., Feng, T., Pieraut, S., & Hoy, J. L. (2022). A binocular perception deficit characterizes prey pursuit in developing mice. *Science*, *25*(11). https://doi.org/10.1016/j.isci.2022.105368

Appell Peter P., and Behan Mary. 1990 "Sources of Subcortical GABAergic Projections to the Superior Colliculus in the Cat." The Journal of Comparative Neurology 302 (1): 143–58. doi:10.1002/cne.903020111. [PubMed: 2086611]

Asadollahi, A., & Knudsen, E. I. (2016). Spatially precise visual gain control mediated by a cholinergic circuit in the midbrain attention network. *Nature Communications*, *7*. https://doi.org/10.1038/ncomms13472

Asadollahi, A., Mysore, S. P., & Knudsen, E. I. (2010). Stimulus-driven competition in a cholinergic midbrain nucleus. *Nature Neuroscience*, *13*(7), 889–895. https://doi.org/10.1038/nn.2573

Asadollahi, A., Mysore, S. P., & Knudsen, E. I. (2011). Rules of competitive stimulus selection in a cholinergic isthmic nucleus of the owl midbrain. *Journal of Neuroscience*, *31*(16), 6088–6097. https://doi.org/10.1523/JNEUROSCI.0023-11.2011

Augustinaite, S., & Kuhn, B. (2020). Complementary Ca2+ activity of sensory activated and suppressed layer 6 corticothalamic neurons reflects behavioral state. Current Biology, 30(20), 3945–3960. e5. https://doi.org/10.1016/j.cub.2020.07.069

Baizer, J. S., Whitney, J. F., & Bender, D. B. (1991). Bilateral projections from the parabigeminal nucleus to the superior colliculus in monkey. *Experimental Brain Research*, *86*(3), 467–470. https://doi.org/10.1007/BF00230521

Baldauf ZB, Wang X-P, Wang S, and Bickford ME. 2003 “Pretectotectal Pathway: An Ultrastructural Quantitative Analysis in Cats.” Journal of Comparative Neurology 464 (2). doi:10.1002/cne.10792.

Barchini, J., Shi, X., Chen, H., & Cang, J. (2018). *Bidirectional encoding of motion contrast in the mouse superior colliculus*. https://doi.org/10.7554/eLife.35261.001

Basso, M. A., Bickford, M. E., & Cang, J. (2021). Unraveling circuits of visual perception and cognition through the superior colliculus. Neuron, 109(6),918–937. https://doi.org/10.1016/j.neuron.2021.01.013

Behan Mary, Steinhacker Kate, Jeffrey-Borger Susan, and Meredith M Alex. 2002 “Chemoarchitecture of GABAergic Neurons in the Ferret Superior Colliculus.” The Journal of Comparative Neurology 452 (4): 334–59. doi:10.1002/cne.10378. [PubMed: 12355417]

Bennett-Clarke C, Mooney RD, Chiaia NL, and Rhoades RW. 1989 “A Substance P Projection from the Superior Colliculus to the Parabigeminal Nucleus in the Rat and Hamster.” Brain Research 500 (1–2): 1–11. http://www.ncbi.nlm.nih.gov/pubmed/2481559. [PubMed: 2481559]

Berson, D. (2021). Keep both eyes on the prize: Hunting mice use binocular vision and specialized retinal neurons to capture prey. *Neuron*, *109*(9), 1418–1420. https://doi.org/10.1016/j.neuron.2021.04.018

Bhandari, A., Ward, T. W., Smith, J., & van Hook, M. J. (2022). Structural and functional plasticity in the dorsolateral geniculate nucleus of mice following bilateral enucleation. Neuroscience, 488, 44–59. https://doi.org/10.1016/j.neuroscience.2022.01.029

Bickford ME, and Hall WC. 1989 “Collateral Projections of Predorsal Bundle Cells of the Superior Colliculus in the Rat.” The Journal of Comparative Neurology 283 (1): 86–106. doi:10.1002/cne.902830108. [PubMed: 2732363]

Bickford, M. E., Slusarczyk, A., Dilger, E. K., Krahe, T. E., Kucuk, C., & Guido,W. (2010). Synaptic development of the mouse dorsal lateral geniculate nucleus. Journal of Comparative Neurology, 518(5), 622–635. https://doi.org/10.1002/cne.22223

Bickford ME, Zhou N, Krahe TE, Govindaiah G, and Guido W. 2015 “Retinal and Tectal ‘Driver-Like’ Inputs Converge in the Shell of the Mouse Dorsal Lateral Geniculate Nucleus.” Journal of Neuroscience 35 (29). doi:10.1523/JNEUROSCI.3375-14.2015.

Binns KE, and Salt TE. 1997 “Different Roles for GABAA and GABAB Receptors in Visual Processing in the Rat Superior Colliculus.” The Journal of Physiology 504

(Pt 3) (11): 629–39. http://www.ncbi.nlm.nih.gov/pubmed/9401970. [PubMed: 9401970]

Boka K, Chomsung R, Li J, and Bickford ME. 2006 “Comparison of the Ultrastructure of Cortical and Retinal Terminals in the Rat Superior Colliculus.” Anatomical Record - Part A Discoveries in Molecular, Cellular, and Evolutionary Biology 288 (8). doi:10.1002/ar.a.20359.

Born Gesche, and Schmidt Matthias. 2007 “GABAergic Pathways in the Rat Subcortical Visual System: A Comparative Study in Vivo and in Vitro.” European Journal of Neuroscience 26 (5): 1183–92. doi:10.1111/j.1460-9568.2007.05700.x. [PubMed: 17767497]

Born Gesche, and Schmidt Matthias. 2008 “A Reciprocal Connection between the Ventral Lateral Geniculate Nucleus and the Pretectal Nuclear Complex and the Superior Colliculus: An in Vitro Characterization in the Rat.” Visual Neuroscience 25 (1): 39–51. doi:10.1017/S0952523808080048. [PubMed: 18282309]

Brooks, J. M., Su, J., Levy, C., Wang, J. S., Seabrook, T. A., Guido, W., & Fox, M.A. (2013). A molecular mechanism regulating the timing of corticogeniculate innervation. Cell Reports, 5(3), 573–581. https://doi.org/10.1016/j.celrep.2013.09.041

Cang Jianhua, Savier Elise, Barchini Jad, andLiu Xiaorong. 2018 “Visual Function, Organization, and Development of the Mouse Superior Colliculus.” Annual Review of Vision Science 4 (1): 239–62. doi: 10.1146/annurev-vision-091517-034142.

Chandrasekaran, A. R., Plas, D. T., Gonzalez, E., & Crair, M. C. (2005). Evidence for an instructive role of retinal activity in retinotopic map refinement in the superior colliculus of the mouse. *Journal of Neuroscience*, *25*(29), 6929–6938. https://doi.org/10.1523/JNEUROSCI.1470-05.2005

Charalambakis, N. E., Govindaiah, G., Campbell, P. W., & Guido, W. (2019). Developmental remodeling of thalamic interneurons requires retinal signaling. Journal of Neuroscience, 39(20), 3856–3866. https://doi.org/10.1523/JNEUROSCI.2224-18.2019

Chaudhry, F. A., Reimer, R. J., Bellocchio, E. E., Danbolt, N. C., Osen, K. K., Edwards, R. H., & Storm-Mathisen, J. (1998). *The Vesicular GABA Transporter, VGAT, Localizes to Synaptic Vesicles in Sets of Glycinergic as Well as GABAergic Neurons*.

Clemente-Perez Alexandra, Makinson Stefanie Ritter, Higashikubo Bryan, Brovarney Scott, Cho Frances S., Urry Alexander, Holden Stephanie S., et al. 2017 “Distinct Thalamic Reticular Cell Types Differentially Modulate Normal and Pathological Cortical Rhythms.” Cell Reports 19 (10): 2130–42. doi: 10.1016/j.celrep.2017.05.044. [PubMed: 28591583]

Cucchiaro JB, Bickford ME, and Sherman SM. 1991 “A GABAergic Projection from the Pretectum to the Dorsal Lateral Geniculate Nucleus in the Cat.”

Neuroscience 41 (1): 213–26. http://www.ncbi.nlm.nih.gov/pubmed/1711649. [PubMed: 1711649]

Cui, H., & Malpeli, J. G. (2003). Activity in the parabigeminal nucleus during eye movements directed at moving and stationary targets. Journal of Neurophysiology, 89(6), 3128–3142. https://doi.org/10.1152/jn.01067.2002

Cullen, M. J., & Kaiserman-Abramof, I. R. (1976). Cytological organization of the dorsal lateral geniculate nuclei in mutant anophthalmic and postnatally enucleated mice. Journal of Neurocytology, 5(4), 407–424. https://doi.org/10.1007/BF01181648

Deichler, A., Carrasco, D., Lopez-Jury, L., Vega-Zuniga, T., Márquez, N., Mpodozis, J., & Marín, G. J. (2020). A specialized reciprocal connectivity suggests a link between the mechanisms by which the superior colliculus and parabigeminal nucleus produce defensive behaviors in rodents. *Scientific Reports*, *10*(1). https://doi.org/10.1038/s41598-020-72848-0

Del Bene, F., Wyart, C., Robles, E., Tran, A., Looger, L., Scott, E. K., Isacoff, E. Y., & Baier, H. (2010). Filtering of visual information in the tectum by an identified neural circuit. *Science*, *330*(6004), 669–673. https://doi.org/10.1126/science.1192949

Diamond, I. T., Fitzpatrick, D., & Conley, M. (1992). A projection from the parabigeminal nucleus to the pulvinar nucleus in Galago. *Journal of Comparative Neurology*, *316*(3), 375–382. https://doi.org/10.1002/cne.903160308

Dossi, R. C., Pare, D., & Steriade, M. (1991). Short-lasting nicotinic and long-lasting muscarinic depolarizing responses of thalamocortical neurons to stimulation of mesopontine cholinergic nuclei. *Journal of Neurophysiology*, *65*(3), 393–406. https://doi.org/10.1152/jn.1991.65.3.393

El-Danaf, R. N., & Huberman, A. D. (2015). Characteristic patterns of dendritic remodeling in early-stage glaucoma: Evidence from genetically identified retinal ganglion cell types. *Journal of Neuroscience*, *35*(6), 2329–2343. https://doi.org/10.1523/JNEUROSCI.1419-14.2015

El-Danaf, R. N., Krahe, T. E., Dilger, E. K., Bickford, M. E., Fox, M. A., & Guido,W. (2015). Developmental remodeling of relay cells in the dorsal lateral geniculate nucleus in the absence of retinal input. Neural Development,10(1), 19. https://doi.org/10.1186/s13064-015-0046-6

Ellis, E. M., Gauvain, G., Sivyer, B., & Murphy, G. J. (2016). Shared and distinct retinal input to the mouse superior colliculus and dorsal lateral geniculate nucleus. *J Neurophysiol*, *116*, 602–610. https://doi.org/10.1152/jn.00227.2016.-The

Endo Toshiaki. 2005 “Nicotinic Acetylcholine Receptor Subtypes Involved in Facilitation of GABAergic Inhibition in Mouse Superficial Superior Colliculus.” Journal of Neurophysiology 94 (6): 3893–3902. doi: 10.1152/jn.00211.2005. [PubMed: 16107532]

Endo Toshiaki, Yanagawa Yuchio, Obata Kunihiko, and Isa Tadashi. 2003 "Characteristics of GABAergic Neurons in the Superficial Superior Colliculus in Mice." Neuroscience Letters 346 (1–2): 81–84. http://www.ncbi.nlm.nih.gov/pubmed/12850553. [PubMed: 12850553]

Fernandes, A. M., Mearns, D. S., Donovan, J. C., Larsch, J., Helmbrecht, T. O., Kölsch, Y., Laurell, E., Kawakami, K., dal Maschio, M., & Baier, H. (2021). Neural circuitry for stimulus selection in the zebrafish visual system. *Neuron*, *109*(5), 805-822.e6. https://doi.org/10.1016/j.neuron.2020.12.002

Fitzpatrick, D., Penny, G. R., & Schmechel, A. D. E. (1984). Glutamic acid decarboxylase-immunoreactive neruons and terminals in the lateral geniculate nucleus of the cat. The Journal of Neuroscience, 4(7),1809–1829.

Frangeul, L., Pouchelon, G., Telley, L., Lefort, S., Luscher, C., & Jabaudon, D. (2016). A cross-modal genetic framework for the development and plasticity of sensory pathways. Nature, 538(7623), 96–98. https://doi.org/10.1038/nature19770

Gale, S. D., & Murphy, G. J. (2014). Distinct representation and distribution of visual information by specific cell types in mouse superficial superior colliculus. *Journal of Neuroscience*, *34*(40), 13458–13471. https://doi.org/10.1523/JNEUROSCI.2768-14.2014

Gale, S. D., & Murphy, G. J. (2016). Active dendritic properties and local inhibitory input enable selectivity for object motion in mouse superior colliculus neurons. *Journal of Neuroscience*, *36*(35), 9111–9123. https://doi.org/10.1523/JNEUROSCI.0645-16.2016

Gale, S. D., & Murphy, G. J. (2018). Distinct cell types in the superficial superior colliculus project to the dorsal lateral geniculate and lateral posterior thalamic nuclei. *Journal of Neurophysiology*, *120*(3), 1286–1292. https://doi.org/10.1152/jn.00248.2018

Giasafaki, C., Grant, E., Hoerder-Suabedissen, A., Hayashi, S., Lee, S., & Molnár, Z. (2022). Cross-hierarchical plasticity of corticofugal projections to dLGN after neonatal monocular enucleation. Journal of Comparative Neurology, 530(7), 978–997. https://doi.org/10.1002/cne.25304

Goddard, C. A., Knudsen, E. I., & Huguenard, J. R. (2007). Intrinsic excitability of cholinergic neurons in the rat parabigeminal nucleus. *Journal of Neurophysiology*, *98*(6), 3486–3493. https://doi.org/10.1152/jn.00960.2007

Goddard, C. A., Mysore, S. P., Bryant, A. S., Huguenard, J. R., & Knudsen, E. I. (2014). Spatially reciprocal inhibition of inhibition within a stimulus selection network in the avian midbrain. *PLoS ONE*, *9*(1). https://doi.org/10.1371/journal.pone.0085865

Goldberg, J. L., Guido, W., Anderson, A., Benowitz, L., Benson, D., Bharti, K., Blumenkranz, M., Smead, H. J., Brooks, B., Constantine-Paton, M., Crair, M., Diamond, J., Dowling, J., Fawcett, J., Feldheim, D., Frishman, L., Goldberg, J.,

Goldman, D., Guido, W., ...Zhou, F. (2016). Report on the national eye institute audacious goals initiative: Regenerating the optic nerve. Investigative Ophthalmology and Visual Science, 57(3), 1201–1205. https://doi.org/10.1167/iovs.15-18500

González-Cabrera, C., Garrido-Charad, F., Roth, A., & Marín, G. J. (2015). The isthmic nuclei providing parallel feedback connections to the avian tectum have different neurochemical identities: Expression of glutamatergic and cholinergic markers in the chick (Gallus gallus). *Journal of Comparative Neurology*, *523*(9), 1341–1358. https://doi.org/10.1002/cne.23739

Grant, E., Hoerder-Suabedissen, A., & Molnár, Z. (2016). The regulation of corticofugal fiber targeting by retinal inputs. Cerebral Cortex, 26(3), 1336–1348. https://doi.org/10.1093/cercor/bhv315

Graybiel, A. M. (1978). A satellite system of the superior colliculus: the parabigeminal nucleus and its projections to the superficial collicular layers. *Brain Research*, *145*(2), 365–374. https://doi.org/10.1016/0006-8993(78)90870-3

Gupta, N., Greenberg, G., de Tilly, L. N., Gray, B., Polemidiotis, M., & Yücel, Y. H. (2009). Atrophy of the lateral geniculate nucleus in human glaucoma detected by magnetic resonance imaging. British Journal of Ophthalmology, 93(1), 56–60. https://doi.org/10.1136/bjo.2008.138172

Hammer, S., Monavarfeshani, A., Lemon, T., Su, J., & Fox, M. A. (2015). Multiple Retinal Axons Converge onto Relay Cells in the Adult Mouse Thalamus. *Cell Reports*, *12*(10), 1575–1583. https://doi.org/10.1016/j.celrep.2015.08.003

Harting, J. K., Huerta, M. F., Hashikawa, T., & Van, D. P. (1991). Projection of the mammalian superior colliculus upon the dorsal lateral geniculate nucleus: organization of tectogeniculate pathways in nineteen species. The Journal of Comparative Neurology, 304.

Helm, J., Akgul, G., & Wollmuth, L. P. (2013). Subgroups of parvalbumin-expressing interneurons in layers 2/3 of the visual cortex. *Journal of Neurophysiology*, *109*(6), 1600–1613. https://doi.org/10.1152/jn.00782.2012

Henriques, P. M., Rahman, N., Jackson, S. E., & Bianco, I. H. (2019). Nucleus Isthmi Is Required to Sustain Target Pursuit during Visually Guided Prey-Catching. *Current Biology*, *29*(11), 1771-1786.e5. https://doi.org/10.1016/j.cub.2019.04.064

Hofbauer, A., & Dräger, U. C. (1985). Depth segregation of retinal ganglion cells projecting to mouse superior colliculus. *Journal of Comparative Neurology*, *234*(4), 465–474. https://doi.org/10.1002/cne.902340405

Houser, C. R., Vaughn, J. E., Barber, R. P., & Roberts, E. (1980). GABA neurons are the major cell type of the nucleus reticularis thalami. Brain Research, 200(2), 341–354. https://doi.org/10.1016/0006-8993(80)90925-7

Hoy, J. L., Bishop, H. I., & Niell, C. M. (2019). Defined Cell Types in Superior Colliculus Make Distinct Contributions to Prey Capture Behavior in the Mouse. *Current Biology*, *29*(23), 4130-4138.e5. https://doi.org/10.1016/j.cub.2019.10.017

Izraeli, R., Koay, G., Lamish, M., Heicklen-Klein, A. J., Heffner, H. E., Heffner, R. S., & Wollberg, Z. (2002). Cross-modal neuroplasticity in neonatally enucleated hamsters: Structure, electrophysiology and behaviour. European Journal of Neuroscience, 15(4), 693–712. https://doi.org/10.1046/j.1460-9568.2002.01902.x

Jen, L. S., Dai, Z. G., & So, K. F. (1984). The connections between the parabigeminal nucleus and the superior colliculus in the Golden hamster. *Neuroscience Letters*, *51*(2), 189–194. https://doi.org/10.1016/0304-3940(84)90549-4

Jiang, Z. D., King, A. J., & Moore, D. R. (1996). Topographic organization of projection from the parabigeminal nucleus to the superior colliculus in the ferret revealed with fluorescent latex microspheres. In *Brain Research* (Vol. 743).

Johnson, K. P., Fitzpatrick, M. J., Zhao, L., Wang, B., McCracken, S., Williams, P. R., & Kerschensteiner, D. (2021). Cell-type-specific binocular vision guides predation in mice. *Neuron*, *109*(9), 1527-1539.e4. https://doi.org/10.1016/j.neuron.2021.03.010

Kahn, D. M., & Krubitzer, L. (2002). Massive cross-modal cortical plasticity and the emergence of a new cortical area in developmentally blind mammals. Proceedings of the National Academy of Sciences of the United States of America, 99(17), 11429–11434. https://doi.org/10.1073/pnas.162342799

Kaiserman-Abramof, I. R. (1983). Intrauterine enucleation of normal mice mimics a structural compensatory response in the geniculate of eyeless mutant mice. Brain Research, 270(1), 149–153. https://doi.org/10.1016/0006-8993(83)90804-1

Kaneda K, and Isa T. (2013). GABAergic Mechanisms for Shaping Transient Visual Responses in the Mouse Superior Colliculus.” Neuroscience 235 (4): 129–40. doi:10.1016/j.neuroscience.2012.12.061. [PubMed: 23337535]

Kardamakis, A. A., Saitoh, K., & Grillner, S. (2015). Tectal microcircuit generating visual selection commands on gaze-controlling neurons. *Proceedings of the National Academy of Sciences of the United States of America*, *112*(15), E1956–E1965. https://doi.org/10.1073/pnas.1504866112

Kasai M, and Isa T. (2016). Imaging population dynamics of surround suppression in the superior colliculus. European J. of Neuroscience 44:2454–2556.

Künzle, H., & Schnyder, H. (1984). The isthmus-tegmentum complex in the turtle and rat: a comparative analysis of its interconnections with the optic tectum. *Experimental Brain Research*, *56*(3), 509–522. https://doi.org/10.1007/BF00237992

Lane RD, Allan DM, Bennett-Clarke C a, Howell DL, and Rhoades RW. 1996 “Projection Status of Calbindin- and Parvalbumin-Immunoreactive Neurons in the

Superficial Layers of the Rat's Superior Colliculus." Visual Neuroscience 14 (2): 277–86. http://www.ncbi.nlm.nih.gov/pubmed/9147480.

Linden, R., & Perry, V. H. (1983). Massive retinotectal projection in rats. *Brain Research*, *272*(1), 145–149. https://doi.org/10.1016/0006-8993(83)90371-2

Ma, R., Cui, H., Lee, S.-H., Anastasio, T. J., & Malpeli, J. G. (2013). Predictive encoding of moving target trajectory by neurons in the parabigeminal nucleus. *J Neurophysiol*, *109*, 2029–2043. https://doi.org/10.1152/jn.01032.2012.-Intercepting

Marín, G., Salas, C., Sentis, E., Rojas, X., Letelier, J. C., & Mpodozis, J. (2007). A cholinergic gating mechanism controlled by competitive interactions in the optic tectum of the pigeon. *Journal of Neuroscience*, *27*(30), 8112–8121. https://doi.org/10.1523/JNEUROSCI.1420-07.2007

Masterson SP, Govindaiah G, Guido W and Bickford ME. 2016 "GABAergic circuit interactions within the mouse dorsal lateral geniculate nucleus." Society for Neuroscience abstract.

Masterson, S. P., Zhou, N., Akers, B. K., Dang, W., & Bickford, M. E. (2019). Ultrastructural and optogenetic dissection of V1 corticotectal terminal synaptic properties. Journal of Comparative Neurology, 527(4), 833–842.https://doi.org/10.1002/cne.24538

Masullo, L., Mariotti, L., Alexandre, N., Freire-Pritchett, P., Boulanger, J., & Tripodi, M. (2019). Genetically Defined Functional Modules for Spatial Orienting in the Mouse Superior Colliculus. *Current Biology*, *29*(17), 2892-2904.e8. https://doi.org/10.1016/j.cub.2019.07.083

May Paul J. 2006 "The Mammalian Superior Colliculus: Laminar Structure and Connections." Progress in Brain Research 151 (1): 321–78. doi:10.1016/S0079-6123(05)51011-2. [PubMed: 16221594]

McCormick, D. A., & Pape, H. C. (1988). Acetylcholine inhibits identified interneurons in the cat lateral geniculate nucleus. *Nature*, *334*(6179), 246–248. https://doi.org/10.1038/334246a0

McCormick, D. A., & Prince, D. A. (1986). Acetylcholine induces burst firing in thalamic reticular neurones by activating a potassium conductance. *Nature*, *319*(6052), 402–405. https://doi.org/10.1038/319402a0

Mccormick, D. A., & Prince, D. A. (1987). ACTIONS OF ACETYLCHOLINE IN THE GUINEA-PIG AND CAT MEDIAL AND LATERAL GENICULATE NUCLEI, IN VITRO. In *J. Phy8iol* (Vol. 392).

Mize RR. 1992 "The Organization of GABAergic Neurons in the Mammalian Superior Colliculus." Progress in Brain Research 90: 219–48. http://www.ncbi.nlm.nih.gov/pubmed/1321459. [PubMed: 1321459]

Mize R. Ranney, Spencer Robert F., and Sterling Peter. 1982 "Two Types of GABA-Accumulating Neurons in the Superficial Gray Layer of the Cat Superior

Colliculus.” The Journal of Comparative Neurology 206 (2): 180–92. doi:10.1002/cne.902060207. [PubMed: 7085927]

Montera, V. M., & Zempel, J. (1985). Evidence for two types of GABA-containing interneurons in the A-laminae of the cat lateral geniculate nucleus: A double-label HRP and GABA-immunocytochemical study. Experimental Brain Research, 60(3), 603–609. https://doi.org/10.1007/BF00236949

Montero, V. M., & Singer, W. (1984). Ultrastructure and synaptic relations of neural elements containing glutamic acid decarboxylase (GAD) in the perigeniculate nucleus of the cat—A light and electron microscopic immunocytochemical study. Experimental Brain Research, 56(1),115–125. https://doi.org/10.1007/BF00237447

Morgan, J. L., & Lichtman, J. W. (2020). An individual interneuron participates in many kinds of inhibition and innervates much of the mouse visual thalamus. Neuron, 106(3), 468–481. e2. https://doi.org/10.1016/j.neuron.2020.02.001

Mysore, S. P., & Knudsen, E. I. (2013). A shared inhibitory circuit for both exogenous and endogenous control of stimulus selection. *Nature Neuroscience*, *16*(4), 473–478. https://doi.org/10.1038/nn.3352

Nasirova, N., Quina, L. A., Agosto-Marlin, I. M., Ramirez, J. M., Lambe, E. K., & Turner, E. E. (2020). Dual recombinase fate mapping reveals a transient cholinergic phenotype in multiple populations of developing glutamatergic neurons. *Journal of Comparative Neurology*, *528*(2), 283–307. https://doi.org/10.1002/cne.24753

Olivier E, Corvisier J, Pauluis Q, and Hardy O. 2000 “Evidence for Glutamatergic Tectotectal Neurons in the Cat Superior Colliculus: A Comparison with GABAergic Tectotectal Neurons.” The European Journal of Neuroscience 12 (7): 2354–66. http://www.ncbi.nlm.nih.gov/pubmed/10947814. [PubMed: 10947814]

Piché, M., Chabot, N., Bronchti, G., Miceli, D., Lepore, F., & Guillemot, J. P. (2007). Auditory responses in the visual cortex of neonatally enucleated rats. Neuroscience, 145(3), 1144–1156. https://doi.org/10.1016/j.neuroscience.2006.12.050

Piscopo, D. M., El-Danaf, R. N., Huberman, A. D., & Niell, C. M. (2013). Diverse visual features encoded in mouse lateral geniculate nucleus. *Journal of Neuroscience*, *33*(11), 4642–4656. https://doi.org/10.1523/JNEUROSCI.5187-12.2013

Ptito, M., Paré, S., Dricot, L., Cavaliere, C., Tomaiuolo, F., & Kupers, R. (2021). A quantitative analysis of the retinofugal projections in congenital and late-onset blindness. NeuroImage: Clinical, 32, 102809. https://doi.org/10.1016/j.nicl.2021.102809

Ranney Mize R 1988 “Immunocytochemical Localization of Gamma-Aminobutyric Acid (GABA) in the Cat Superior Colliculus.” The Journal of Comparative Neurology 276 (2): 169–87. doi:10.1002/cne.902760203. [PubMed: 3220979]

Reinhard, K., Li, C., Do, Q., Burke, E. G., Heynderickx, S., & Farrow, K. (2019). A projection specific logic to sampling visual inputs in mouse superior colliculus. ELife, 8. https://doi.org/10.7554/eLife.50697

Robinson, D. A. (1972). Eye movements evoked by collicular stimulation in the alert monkey. *Vision Research*, *12*(11), 1795–1808. https://doi.org/10.1016/0042-6989(72)90070-3

Runyan, C. A., Schummers, J., van Wart, A., Kuhlman, S. J., Wilson, N. R., Huang, Z. J., & Sur, M. (2010). Response Features of Parvalbumin-Expressing Interneurons Suggest Precise Roles for Subtypes of Inhibition in Visual Cortex. *Neuron*, *67*(5), 847–857. https://doi.org/10.1016/j.neuron.2010.08.006

Rupert, D. D., & Shea, S. D. (2022). Parvalbumin-Positive Interneurons Regulate Cortical Sensory Plasticity in Adulthood and Development Through Shared Mechanisms. In *Frontiers in Neural Circuits* (Vol. 16). Frontiers Media S.A. https://doi.org/10.3389/fncir.2022.886629

Sahibzada N, Dean P, Redgrave P. Movements resembling orientation or avoidance elicited by electrical stimulation of the superior colliculus in rats. J Neurosci. 1986 Mar;6(3):723-33. doi: 10.1523/JNEUROSCI.06-03-00723.1986. PMID: 3958791; PMCID: PMC6568468.

Schiller, P. H., & Stryker, M. (1972). Single-unit recording and stimulation in superior colliculus of the alert rhesus monkey. *Journal of Neurophysiology*, *35*(6), 915–924. https://doi.org/10.1152/jn.1972.35.6.915

Schryver, H. M., & Mysore, S. P. (2019). Spatial dependence of stimulus competition in the avian nucleus isthmi pars magnocellularis. In *Brain, Behavior and Evolution* (Vol. 93, Issues 2–3, pp. 137–151). S. Karger AG. https://doi.org/10.1159/000500192

Seabrook, T. A., El-Danaf, R. N., Krahe, T. E., Fox, M. A., & Guido, W. (2013). Retinal input regulates the timing of corticogeniculate innervation. Journal of Neuroscience, 33(24), 10085–10097. https://doi.org/10.1523/JNEUROSCI.5271-12.2013

Sefton, A. J., & Martin, P. R. (1984). Relation of the parabigeminal nucleus to the superior colliculus and dorsal lateral geniculate nucleus in the hooded rat. *Experimental Brain Research*, *56*(1), 144–148. https://doi.org/10.1007/BF00237450

Shang, C., Chen, Z., Liu, A., Li, Y., Zhang, J., Qu, B., Yan, F., Zhang, Y., Liu, W., Liu, Z., Guo, X., Li, D., Wang, Y., & Cao, P. (2018). Divergent midbrain circuits orchestrate escape and freezing responses to looming stimuli in mice. *Nature Communications*, *9*(1). https://doi.org/10.1038/s41467-018-03580-7

Shang, C., Liu, Z., Chen, Z., Shi, Y., Wang, Q., Liu, S., Li, D., & Cao, P. (2015). A parvalbumin-positive excitatory visual pathway to trigger fear responses in mice. *Science*, *348*(6242), 1472–1477. https://doi.org/10.1126/science.aaa8694

Sherk, H. (1978). Visual response properties and visual field topography in the cat's parabigeminal nucleus. *Brain Research*, *145*(2), 375–379. https://doi.org/10.1016/0006-8993(78)90871-5

Sherk, H. (1979a). A comparison of visual-response properties in cat's parabigeminal nucleus and superior colliculus. *Journal of Neurophysiology*, *42*(6), 1640–1655. https://doi.org/10.1152/jn.1979.42.6.1640

Sherk, H. (1979b). Connections and Visual-Field Mapping in Cat's Tectoparabigeminal Circuit. In *JOURNALOF NEUROPHYSIOLOGY* (Vol. 42, Issue 6). www.physiology.org/journal/jn

Sokhadze, G., Seabrook, T. A., & Guido, W. (2018). The absence of retinal input disrupts the development of cholinergic brainstem projections in the mouse dorsal lateral geniculate nucleus 11 Medical and Health Sciences 1109 Neurosciences. Neural Development, 13(1). https://doi.org/10.1186/s13064-018-0124-7

Sokhadze, G., Whyland, K. L., Bickford, M. E., & Guido, W. (2022). The organization of cholinergic projections in the visual thalamus of the mouse. Journal of Comparative Neurology, 530(7), 1081–1098. https://doi.org/10.1002/cne.25235

Sparks, D. L. (1978). Functional properties of neurons in the monkey superior colliculus: Coupling of neuronal activity and saccade onset. *Brain Research*, *156*(1), 1–16. https://doi.org/10.1016/0006-8993(78)90075-6

Sparks, D. L., & Mays, L. E. (1980). Movement fields of saccade-related burst neurons in the monkey superior colliculus. *Brain Research*, *190*(1), 39–50. https://doi.org/10.1016/0006-8993(80)91158-0

Steinkellner, T., Yoo, J. H., & Hnasko, T. S. (2019). Differential expression of VGLUT2 in mouse mesopontine cholinergic neurons. ENeuro, 6(4). https://doi.org/10.1523/ENEURO.0161-19.2019

Stevenson, J. A., & Lund, R. D. (1982). A crossed parabigemino-lateral geniculate projection in rats blinded at birth. Experimental Brain Research, 45(1–2), 95–100. https://doi.org/10.1007/BF00235767

Tokunaga, A., & Otani, K. (1978). Neuronal organization of the corpus parabigeminum in the rat. *Experimental Neurology*, *58*(2), 361–375. https://doi.org/10.1016/0014-4886(78)90147-4

Tokuoka, K., Kasai, M., Kobayashi, K., & Isa, T. (2020). Anatomical and electrophysiological analysis of cholinergic inputs from the parabigeminal nucleus to the superficial superior colliculus. *Journal of Neurophysiology*, *124*(6), 1968–1985. https://doi.org/10.1152/jn.00148.2020

Triplett Jason W, Wei Wei, Gonzalez Cristina, Sweeney Neal T, Huberman Andrew D, Feller Marla B, and Feldheim David A. 2014 "Dendritic and Axonal Targeting Patterns of a Genetically-Specified Class of Retinal Ganglion Cells That

Participate in Image-Forming Circuits.” Neural Development 9 (1): 2. doi: 10.1186/1749-8104-9-2. [PubMed: 24495295]

Usunoff, K. G., Itzev, D. E., Rolfs, A., Schmitt, O., & Wree, A. (2006). Brain stem afferent connections of the amygdala in the rat with special references to a projection from the parabigeminal nucleus: A fluorescent retrograde tracing study. *Anatomy and Embryology*, *211*(5), 475–496. https://doi.org/10.1007/s00429-006-0099-8

Usunoff, K. G., Schmitt, O., Itzev, D. E., Rolfs, A., & Wree, A. (2007). Efferent connections of the parabigeminal nucleus to the amygdala and the superior colliculus in the rat: A double-labeling fluorescent retrograde tracing study. *Brain Research*, *1133*(1), 87–91. https://doi.org/10.1016/j.brainres.2006.11.073

Vaney, D. I., Peichl, L., Wässle, H., & Illing, R. B. (1981). Almost all ganglion cells in the rabbit retina project to the superior colliculus. *Brain Research*, *212*(2), 447–453. https://doi.org/10.1016/0006-8993(81)90476-5

Villalobos, C. A., Wu, Q., Lee, P. H., May, P. J., & Basso, M. A. (2018). Parvalbumin and GABA microcircuits in the mouse superior colliculus. *Frontiers in Neural Circuits*, *12*. https://doi.org/10.3389/fncir.2018.00035

Wang, J., Qian, L., Wang, S., Shi, L., & Wang, Z. (2022). Directional Preference in Avian Midbrain Saliency Computing Nucleus Reflects a Well-Designed Receptive Field Structure. *Animals*, *12*(9). https://doi.org/10.3390/ani12091143

Wang Siting, Eisenback Michael, Datskovskaia Aygul, Boyce Martin, and Bickford Martha E. 2002 “GABAergic Pretectal Terminals Contact GABAergic Interneurons in the Cat Dorsal Lateral Geniculate Nucleus.” Neuroscience Letters 323 (2): 141–45. http://www.ncbi.nlm.nih.gov/pubmed/11950513. [PubMed: 11950513]

Wang, S. W., Kim, B. S., Ding, K., Wang, H., Sun, D., Johnson, R. L., Klein, W. H., & Gan, L. (2001). Requirement for math5 in the development of retinal ganglion cells. Genes and Development, 15(1), 24–29. https://doi.org/10.1101/gad.855301

Wang, Y. Q., Takatsuji, K., Kiyama, H., Yamano, M., & Tohyama, M. (1988). Localization of neuroactive substances in the rat parabigeminal nucleus: an immunohistochemical study. *Journal of Chemical Neuroanatomy*, *1*(4), 195–204. https://doi.org/10.1016/0921-8696(88)90305-2

Watanabe, K., & Kawana, E. (1979). Efferent projections of the parabigeminal nucleus in rats: A horseradish peroxidase (HRP) study. *Brain Research*, *168*(1), 1–11. https://doi.org/10.1016/0006-8993(79)90123-9

Wei Haiyang, Bonjean Maxime, Petry Heywood M, Sejnowski Terrence J, and Bickford Martha E. 2011 “Thalamic Burst Firing Propensity: A Comparison of the Dorsal Lateral Geniculate and Pulvinar Nuclei in the Tree Shrew.” The Journal of Neuroscience : The Official Journal of the Society for Neuroscience 31 (47): 17287–99. doi: 10.1523/JNEUROSCI.6431-10.2011. [PubMed: 22114295]

Wei, P., Liu, N., Zhang, Z., Liu, X., Tang, Y., He, X., Wu, B., Zhou, Z., Liu, Y., Li, J., Zhang, Y., Zhou, X., Xu, L., Chen, L., Bi, G., Hu, X., Xu, F., & Wang, L. (2015). Processing of visually evoked innate fear by a non-canonical thalamic pathway. *Nature Communications*, *6*. https://doi.org/10.1038/ncomms7756

Winkelmann, E., Garey, L. J., & Brauer, K. (1985). Ultrastructural development of the dorsal lateral geniculate nucleus of genetically microphthalmic mice. *Experimental Brain Research*, *60*(3), 527–534. https://doi.org/10.1007/BF00236938

Whyland KL, Hernandez Y, Slusarczyk AS, Guido W, Bickford ME. The parabigeminal nucleus is a source of "retinogeniculate replacement terminals" in mice that lack retinofugal input. J Comp Neurol. 2022 Dec;530(18):3179-3192. doi: 10.1002/cne.25401. Epub 2022 Sep 6. PMID: 36066425; PMCID: PMC9588688.

Whyland, K. L., Slusarczyk, A. S., & Bickford, M. E. (2020). GABAergic cell types in the superficial layers of the mouse superior colliculus. *Journal of Comparative Neurology*, *528*(2), 308–320. https://doi.org/10.1002/cne.24754

Xu Hong-ping, Furman Moran, Mineur Yann S., Chen Hui, King Sarah L., Zenisek David, Zhou Z. Jimmy, et al. 2011 “An Instructive Role for Patterned Spontaneous Retinal Activity in Mouse Visual Map Development.” Neuron 70 (6): 1115–27. doi: 10.1016/j.neuron.2011.04.028. [PubMed: 21689598]

Yaka, R., Yinon, U., Rosner, M., & Wollberg, Z. (2000). Pathological and experimentally induced blindness induces auditory activity in the cat primary visual cortex. Experimental Brain Research, 131(1), 144–148. https://doi.org/10.1007/s002219900295

Zhang Ze, Liu Wen-Ying, Diao Yu-Pu, Xu Wei, Zhong Yu-Heng, Zhang Jia-Yi, Lazarus Michael, Liu Yuan-Yuan, Qu Wei-Min, and Huang Zhi-Li. 2019 “Superior Colliculus GABAergic Neurons Are Essential for Acute Dark Induction of Wakefulness in Mice.” Current Biology, 1, doi: 10.1016/j.cub.2018.12.031.

Zhao, X., Chen, H., Liu, X., & Cang, J. (2013). Orientation-selective responses in the mouse lateral geniculate nucleus. *Journal of Neuroscience*, *33*(31), 12751–12763. https://doi.org/10.1523/JNEUROSCI.0095-13.2013

Zhou NA, Maire PS, Masterson SP, and Bickford ME. 2017 “The Mouse Pulvinar Nucleus: Organization of the Tectorecipient Zones.” Visual Neuroscience 34. doi: 10.1017/S0952523817000050.

Zhou, N., Masterson, S. P., Damron, J. K., Guido, W., & Bickford, M. E. (2018). The mouse pulvinar nucleus links the lateral extrastriate Cortex, Striatum, and Amygdala. Journal of Neuroscience, 38(2), 347–362. https://doi.org/10.1523/JNEUROSCI.1279-17.201

Zhu, J. J., & Heggelund, P. (2001). *Muscarinic Regulation of Dendritic and Axonal Outputs of Rat Thalamic Interneurons: A New Cellular Mechanism for Uncoupling Distal Dendrites*.

Zhu, J. J., & Uhlrich, D. J. (1997). Nicotinic receptor-mediated responses in relay cells and interneurons in the rat lateral geniculate nucleus. *Neuroscience*, *80*(1), 191–202. https://doi.org/10.1016/S0306-4522(97)00095-X

Zhu, J. J., & Uhlrich, D. J. (1998). Cellular mechanisms underlying two muscarinic receptor-mediated depolarizing responses in relay cells of the rat lateral geniculate nucleus. *Neuroscience*, *87*(4), 767–781. https://doi.org/10.1016/S0306-4522(98)00209-7

Zhu, J. J., Uhlrich, D. J., & Lytton, W. W. (1999). Properties of a hyperpolarization-activated cation current in interneurons in the rat lateral geniculate nucleus. *Neuroscience*, *92*(2), 445–457. https://doi.org/10.1016/S0306-4522(98)00759-3

Zingg, B., Chou, X. lin, Zhang, Z. gang, Mesik, L., Liang, F., Tao, H. W., & Zhang, L. I. (2017). AAV-Mediated Anterograde Transsynaptic Tagging: Mapping Corticocollicular Input-Defined Neural Pathways for Defense Behaviors. *Neuron*, *93*(1), 33–47

CURRICULUM VITA

NAME: Kyle L. Whyland

ADDRESS: 411 Merryman Drive

Jeffersonville, IN 47130

DOB: Louisville, KY - January 21, 1991

EDUCATION & TRAINING:

B.S., Psychology

Indiana University 47401–47408

M.S., Neuroscience

University of Louisville 40202

AWARDS: Ruth L. Kirschstein Predoctoral Individual National Research Service Award (F31)

Best Graduate Student Poster Award at Research! Louisville (2019)

PUBLICATIONS: “The parabigeminal nucleus is a source of ‘retinogeniculate replacement terminals’ in mice that lack retinofugal input”. *The Journal of Comparative Neurology*, 2022 Dec; 530(18), 3179-3192.

“GABAergic cell types in the superficial layers of the mouse superior colliculus”. *The Journal of Comparative Neurology*, 528(2), 308–320.

“The organization of cholinergic projections in the visual thalamus of the mouse.” *The Journal of Comparative Neurology*, 530(7), 1081–1098.